Co-RICH Fe-Mn CRUSTS FROM THE MARSHALL ISLANDS (LEG 1) AND HYDROTHERMAL AND HYDROGENETIC Fe-Mn DEPOSITS FROM MICRONESIA (LEG 2), KODOS 98-3 CRUISE, WEST PACIFIC

By

James R. Hein[1], Jai-Woon Moon[2], Kyeong-Yong Lee[2], Jennifer S. Dowling[1], Ki-Hyune Kim[2], Malia Burrows[1], Sung Hyun Park[2], Youn-ji Choi[2], Anthony A. Schuetze[1], Hoi Soo Jung[2], Hyun-Sub Kim[2], Gun Chang Lee[2], Cheong-Kee Park[2], Seung Kyu Son[2], *and* Chan Young Park[2]

Open-File Report 99-412

1999

This report is preliminary and has not been reviewed for conformity with U.S. Geological Survey editorial standards or with the North American Stratigraphic Code. Any use of trade, product, or firm names is for descriptive purposes only and does not imply endorsement by the U.S. Government

[1]U.S. Geological Survey, 345 Middlefield Rd., MS 999, Menlo Park, CA, 94025, USA

[2]Korea Ocean Research and Development Institute, P.O. Box 29, Ansan, 425-6000, Seoul, Korea

INTRODUCTION

The KODOS 98-3 cruise took place 13-28 August 1998 aboard the R.V. Onnuri and was divided into two legs. Leg 1 operations included mapping and sampling Litakpooki Ridge and mapping Lomilik Seamount, both within the Exclusive Economic Zone (EEZ) of the Republic of the Marshall Islands (RMI) (Figs. 1-3). Leg 2 operations included mapping and sampling a corridor of the Yap convergent margin (YCM) extending from the southwestern margin of the West Caroline Ridge west to the Yap back-arc region in the EEZ of the Federated States of Micronesia (FSM) (Figs. 4, 5). Members of the KODOS 98-3 cruise (Table 1) participated in this second cruise of a renewed effort by the Korea Ocean Research and Development Institute (KORDI) and the U.S. Geological Survey (USGS) to study seamount mineral deposits. Earlier efforts included three USGS-KORDI cooperative cruises aboard the R.V. Farnella, one each in the years 1989-1991, and more recently cruise KODOS 97-4 in 1997.

The first set of objectives of the KODOS 98-3 cruise was to map the distribution of thick ferromanganese oxyhydroxide crusts (Fe-Mn crusts) on Lomilik Seamount and Litakpooki Ridge and to determine the geologic and oceanographic conditions that promoted growth of thick Fe-Mn crusts. Reconnaissance sampling and mapping of Lomilik Seamount were completed in 1989 during the first cooperative USGS-KORDI cruise aboard the R.V. Farnella (F10-89-CP; Hein, Kang, et al., 1990) and both Lomilik and Litakpooki were studied during the KODOS 97-4 cruise (Hein, Moon, et al., 1998). Lomilik was chosen for detailed work because during the 1989 cruise, the thickest (180 mm) shallow-water Fe-Mn crust ever recovered from the ocean basins was collected from its summit; thick Fe-Mn crusts (up to 130 mm) were also collected in 1997. Thick Fe-Mn crusts up to 154 mm thick were collected on Litakpooki Ridge during cruise KODOS 98-3, which are described here.

The second set of objectives of the KODOS 98-3 cruise was sampling and mapping of the YCM. Reconnaissance sampling and mapping of that region was completed in 1990 and 1991 during the second and third cooperative USGS-KORDI cruises (F11-90-CP and F7-91-WP) aboard the R.V. Farnella (Hein, Ahn, et al., 1992). During the 1990 cruise, hydrothermal stratabound Mn-oxide deposits were recovered from the crest of Yap arc, along with hydrothermally altered rocks, serpentinite, blue-serpentinite muds, and abundant vein quartz. Additional hydrothermal deposits were collected during leg 2 of KODOS 98-3.

Representative Fe-Mn crust samples, hydrothermal stratabound Mn oxides, and substrate rock samples from the dredge hauls taken from those areas during KODOS 98-3 were analyzed for this study, which extends our previous work on Fe-Mn crusts collected in and around RMI and FSM (Hein et al., 1988; Hein, Kang, et al., 1990; Hein, Ahn, et al., 1992; Hein et al., 1997a; Hein, Moon, et al., 1998). This report presents data for all dredge hauls, including sample descriptions, detailed chemical (major, minor, platinum group, and rare earth elements) and mineralogical analyses of bulk Fe-Mn crusts, individual crust layers, hydrothermal Mn, and substrate rocks collected during KODOS 98-3. Correlation coefficients and Q-mode factor analysis are used to determine relationships between and among elements and associations of elements with mineralogical phases.

Shipboard Operations

Shipboard operations on Litakpooki Ridge included four dredge hauls, two piston cores, two CTD casts, and 534 km of SeaBeam bathymetric lines including 152 km of 12-channel airgun lines (Tables 2-5; Figs. 1-3). Operations on Lomilik Seamount included 279 km of SeaBeam bathymetric lines. Operations on the YCM included five dredge hauls, two piston cores, two box cores, two multiple cores, nine CTD casts, one deep-sea camera-video survey, and 737 km of SeaBeam bathymetric lines and 12-channel airgun lines (Tables 2-5; Figs. 4-5). Of the nine dredge hauls attempted, six provided usable samples, one contained mostly pumice, and two had no recovery (Tables 5, 6).

Bathymetry and Seafloor Descriptions

Litakpooki Ridge is located at the southwestern margin of the RMI EEZ (Fig. 1). The bathymetry of the central part of the ridge shows a relatively flat top at 2000-2800 m water depth dotted with small hills that rise as shallow as about 1600 m depth (Fig. 2). The ridge summit narrows and extends to the northeast to the edge of the survey area. A rift zone is defined by a ridge that extends to the northwest from the summit. The base of the Litakpooki ridge is at about 5000 m water depth. Channels characterize the very steep northern slope. Slope angles on the summit are mostly less than 5°, whereas those on the flanks are up to 30°, with an average slope angle of about 11° (KODOS, 1999a).

Foraminiferal sediment fills some lows and forms a thin blanket over the central and northeast parts of the summit where dredges D3 and D4 encountered only sediments (Fig. 2). Seismic-reflection profiles (KODOS, 1999a) show that much of the summit is underlain by sedimentary rocks, with protruding volcanic hills composed of basalt. Dredges D1 and D2 and dredges D14 and D15 from KODOS 97-4 (Hein, Moon, et al., 1998) show that those sedimentary rocks consist of bioclastic and foraminiferal limestones, breccia composed of mostly volcanic and phosphorite clasts in a carbonate fluorapatite cement, phosphorite, and minor ironstone. Most thick crusts were collected from saddles between summit hills.

Lomilik Seamount is located among a large group of seamounts to the west of Anewetak Atoll in the western Marshall Islands. The bathymetry reveals a flat-topped edifice with a summit at about 1500 m water depth and small hills rising to about 1350 m (Fig. 3). A broad, gently sloping summit terrace occurs on the NE flank down to about 2400 m which steepens in slope on the SE flank, but does not exist on the north, west, and south flanks. The terrace is separated from the summit by a 200-250 m-high scarp. Many volcanic pinnacles occur on the east, southeast, and west flanks of the seamount (Fig. 3). Lomilik Seamount is connected to Lami Seamount (Fig. 1) by a ridge on its NW flank (Fig. 3). A large landslide likely created the notch in the south flank which begins where the summit narrows before changing trend to the northwest along the ridge that connects with Lami Seamount. The seamount base is at about 4600 m water depth. The summit region slopes at less than 5° and the flanks up to 20°, with an average slope of Lomilik of about 11° (KODOS, 1999a).

The terrace and summit support a thin blanket of foraminiferal ooze between outcrops of basalt, volcaniclastic rocks, and foraminiferal and bioclastic limestones (Hein, Moon, et al., 1998). Most thick crusts were collected from the terrace and the scarp that separates the terrace from the summit, whereas the thinnest crusts were collected from the middle and upper steep flanks of the seamount; the lowermost flanks were not sampled.

YCM bathymetry from east to west is characterized by a gently dipping summit of the southwestern margin of West Caroline Ridge at about 1500-2200 m water depth (Fig. 5). West from the summit, the outer trench slope is characterized by an upper steep wall; rough, central ridge and valley topography; and a lower steep, irregular slope showing block faulting that bottoms at about 8600 m. The trench axis deepens to the south. The inner trench wall is more uniform in topography than the outer trench wall and rises through a series of thrust faults to a summit ridge at about 1500 m. A summit seamount shallows to about 500 m water depth (Fig. 5). Most sampling was completed on the west side of the summit ridge in the back-arc area at water depths of 1750-2800 m. Seismic-reflection profiles (KODOS, 1999b) show that most of the region supports thin sediment cover, with basement highs cropping out in the arc and back-arc regions.

CTD Data

Water temperatures measured in CTD-1 (Litakpooki Ridge; Fig. 2) and CTD-2 (open-ocean between Litakpooki Ridge and Lomilik Seamount; Fig. 1) profiles range from 2.2° to 29.2° C and salinities from 34.4 to 34.9 psu, defining high temperature and low salinity surface waters and a seasonal thermocline at about 100 m water depth (KODOS, 1999a). Dissolved oxygen contents range from 1.3 to 4.3 ml/l, with maximum values occurring at about 100 m water depth and minimum values at about 300 m (Table 4). The depth to the top of the oxygen-minimum zone

(OMZ) is about the same (280 and 275 m), although the depth to the lowest oxygen content is 36 m deeper at the more northerly site. The 5° and 10° isotherms are also deeper at the more northerly site (Table 4).

Nine CTD profiles were taken at the YCM, where the lowest oxygen content at each site is very uniform at 2.00±0.08 ml/l. These values show that primary productivity in surface waters is not as high in this region as in the western RMI, where minimum values are 1.3 ml/l, indicating greater amounts of oxygen consumption during degradation of organic matter. Indications of hydrothermal activity were not seen in water column properties at any of the sites.

METHODS

X-ray diffraction was completed on a Philips diffractometer using Cukα radiation and a curved-crystal carbon monochromator. Abundances of the 10 major oxides and Cr, Ba, Sr, Y, Zr, Nb, and Rb in substrate rocks were determined by X-ray fluorescence spectroscopy (XRF; Taggart et al., 1987); Fe(II) by colorimetric titration (Peck, 1964); CO_2 by coulometric titration (Engleman et al., 1985); H_2O^+ by water evolved at 925°C as determined coulometrically by Karl-Fischer titration (Jackson et al., 1987); H_2O^- by sample weight difference at 110°C for greater than one hour (Shapiro, 1975); F and Cl by specific ion electrode, S by combustion and infrared spectroscopy (Jackson et al., 1987), and C by induction furnace; Y, U, Th, and rare earth elements (REEs) by inductively coupled plasma-atomic emission spectrometry-mass spectrometry (ICP-MS; Aruscavage et al., 1989; Lichte et al., 1987a,b); and Au, As, Sb, and W by neutron activation analysis (NAA; McKown and Millard, 1987). Low totals for the phosphorite sample occurs because of typically high F, Cl, and S contents, which are not included in the total.

For Fe-Mn crusts and hydrothermal stratabound Mn, the concentrations of Mn, Fe, Si, Al, Mg, Ca, Na, K, Ti, P, Ba, Nb, Rb, Zr, and Y were determined by XRF; Be, B, Co, Cu, Ge, Li, Mo, Ni, Pb, Sc, Sr, V, Zn, and Ag were determined by ICP; Bi, Cd, Ga, In, Sn, Tl, Y, Au, REEs, and platinum group elements (PGEs) by ICP-MS; As, Au, Br, Cr, Cs, Hf, Sb, Se, Ta, Th, U, and W by NAA; Te by graphite furnace atomic-absorption spectroscopy; Hg by wet chemical techniques; S by combustion and infrared spectroscopy; and Cl by specific ion electrode. REEs in plots are normalized to both chondrites (Anders and Grevesse, 1989) and shale (PAAS, Post-Archean Australian Shale; McLennan, 1989).

The usual Pearson product moment correlation coefficient was used to calculate the correlation coefficient matrices. For Q-mode factor analysis, each variable percentage was scaled to the percent of the maximum value before the values were row normalized and the cosine theta coefficients calculated. The factors were derived from orthogonal rotations of the principal component eigenvectors using the Varimax method (Klovan and Imbrie, 1971). Communalities for all samples are ≥0.97.

Growth rates of non-phosphatized crusts were determined using the empirical equations of Puteanus and Halbach (1988): $GR = 1.28/Co-0.24$, with cobalt content in weight percent; and Manheim and Lane-Bostwick (1988): $Co^n = Co-0.0012\%$, $GR = 0.68/(Co^n)^{1.67}$.

LITAKPOOKI RIDGE SUBSTRATE ROCKS

Descriptions

Substrate rocks based on dredges D1 and D2 as well as dredges D14 and D15 from KODOS 97-4, in decreasing order of abundance include limestone, breccia, phosphorite, basalt, and ironstone (Tables 5, 6; Hein, Moon, et al., 1998). As seen in hand samples, most limestones from KODOS 98-3 Litakpooki dredges are either friable to well-lithified foraminiferal limestone or bioclastic limestone composed of shell hash and foraminifera. Limestones are pale-brown to off-white, yellow-brown, or brown. They are commonly peppered with Fe-Mn oxyhydroxide grains,

contain Mn dendrites, or have vugs lined with Fe-Mn oxyhydroxides. Some limestone samples are partly phosphatized, which grade into phosphorites. Phosphorites are massive, vuggy, or pebbly. Pebbly phosphorite contains sparse, brown basalt clasts commonly coated with Fe-Mn oxyhydroxides, and yellow-green altered hyaloclastite clasts. Vugs in vuggy phosphorites are lined with Mn oxides. Carbonate fluorapatite (CFA) veins and Mn-oxide dendrites are common in all three types. Most of the phosphorite is CFA-replaced limestone, more rarely CFA-replaced basalt.

Breccias most commonly consist of white to brown phosphorite, brown basalt, and brown ironstone clasts in cream to pinkish CFA cement, rarely Fe-Mn oxyhydroxide cement. CFA veins are common and Fe-Mn oxyhydroxide veins also occur. Volcanogenic clasts are commonly partly to completely replaced by smectite. Basalt is altered, brown to red-brown, and may be laced with CFA and Fe-Mn oxyhydroxides and contain large yellow-green amygdules. Sample D2-2E consists solely of smectite, yet maintains relict volcanic textures.

Ironstone samples are brown to dark brown, massive, and dense. Ironstone also occurs as clasts in breccia and pebbly limestone and formed by replacement of basalt. Ironstone most likely formed from hydrothermal processes related to formation of the volcanic edifice during the Cretaceous (Hein et al., 1994).

X-ray Diffraction Mineralogy

For the four samples for which minerals were identified by X-ray diffraction, primary volcanogenic and sedimentary minerals include plagioclase and calcite; and secondary minerals include CFA and smectite (Table 7). Secondary CFA is the most abundant mineral in these samples and occurs in three of the four samples as a major or moderate constituent, regardless of rock type (Table 7).

Fresh basalt was not recovered in dredges D1 and D2. Altered basalt consists of plagioclase and various amounts (up to 100%) of smectite and CFA. The most altered basalts lack all primary minerals, but maintain volcanic textures. CFA replaces basalt and fills vesicles and fractures.

Limestones are composed chiefly of calcite, with various amounts of CFA, showing all gradations from limestone (only calcite) to phosphorite (only CFA). Most phosphorites have relict limestone textures, especially that of foraminiferal sand.

Chemistry

The most P_2O_5 rich CFA-replaced sedimentary rock has a CaO/P_2O_5 ratio of 1.63 (Table 8), whereas theoretical compositions for CFA produce ratios that range from 1.5 to 1.6 (Manheim and Gulbrandsen, 1979). The very slight excess Ca over P in some KODOS 98-3 samples may be due to additional Ca associated with minor contamination by volcanogenic plagioclase, phillipsite cement (an alteration product of volcanic debris), or to relict calcite in the phosphatized limestone. However, Hein, Moon, et al. (1998) showed that, CaO/P_2O_5 ratios between 1.60 and 1.66 characterize chemically very pure phosphorites, indicating that CaO/P_2O_5 ratios between 1.58 and 1.66 are characteristic of uncontaminated marine CFA. Ratios in that range have been found in many of our previous studies (e.g., Hein, Kang, et al., 1990; Hein, Ahn, et al., 1992; Hein et al., 1993). The CaO/P_2O_5 ratio of 1.63 is very near the most cation- and anion-substituted francolite (1.62) end of the fluorapatite (1.32)-CFA range (Manheim and Gulbrandsen, 1979; McClellan and van Kauwenbergh, 1990). The Sr content for the phosphorite sample is 1260 ppm, near the middle of the range (900-1600 ppm) found for other central Pacific phosphorite samples (Hein et al., 1993). Normalized REE plots of phosphatic limestone (Table 9) show a seawater-type pattern with large negative Ce anomaly, small positive Gd anomaly, and heavy REE enrichment (Fig. 6). These identical patterns indicate that the CFA as well as the calcite were derived from seawater.

Smectite occurs in major to moderate amounts in two of the four samples analyzed, and is especially abundant in the strongly altered basalts. The pure smectite sample (D2-2E) has relatively

high Si, Al, Fe, and Zr contents and low Mg content, indicative of an iron-rich montmorillonite (Tables 7, 8).

Most samples of basalt and basalt clasts in breccia are altered to smectite and goethite and are rarely replaced by phosphorite and phillipsite. Alteration is best characterized by increases in Fe_2O_3 and water and decreases in FeO and K_2O contents (Table 8). Volcaniclastic mudstone and hyaloclastite have compositions comparable to highly altered basalts.

SOUTHWEST CAROLINE RIDGE SUBSTRATE ROCKS

Dredge D7 was taken on southwest Caroline Ridge and consists of pillow basalt wedges, limestone, and breccia in that order of abundance (Table 6). The basalt is gray (relatively fresh) to brown (altered), massive, and variably vesicular with a red-brown alteration rind underlain by a black basaltic glass rind. Small vesicles occur in the basalt below the glass rind, which grades into massive basalt. The basalt is composed of primary plagioclase, pyroxene, magnetite, and secondary smectite and hematite.

Foraminiferal limestone is white, friable, massive, and one sample contains a gray volcanic ash layer. The limestone is composed solely of calcite.

Breccias are composed of basalt, basaltic glass, and limestone clasts in (1) calcite cement; (2) calcite-phillipsite cement, with fine-grained volcanogenic minerals; (3) calcite-smectite-phillipsite cement; (4) phillipsite cement, with fine-grained plagioclase and smectite. The limestone clasts consist of foraminiferal limestone and reef fossils such as coral, bryozoans, and benthic foraminifera.

YAP ARC SUBSTRATE ROCKS

Descriptions and Composition

Substrate rocks based on dredges D5, D6, D8, and D9, in decreasing order of abundance are limestone, andesite and basalt, breccia, sandstone, serpentinite, and hydrothermal stratabound Mn deposits (Tables 5, 6). Carbonates consist of white to brown foraminiferal ooze; pale-brown, friable, burrowed, sandy foraminiferal limestone; pale-brown, argillaceous, burrowed micritic limestone with Mn veinlets interbedded with sandy foraminiferal limestone. Sand grains are basalt. A small amount of reef limestone and sandy chalk were also recovered. Foraminiferal sediment also comprise the matrix of some breccia samples. The limestones are composed of calcite and various amounts of volcanogenic minerals, chiefly plagioclase, and their alteration products, chiefly smectite (Table 7).

Volcanic rocks consist mainly of andesite, dacite, and basalt (Tables 6, 7, 10; KODOS, 1999b). Basalts are brown, mottled greenish-pale brown, and gray-brown, altered, commonly plagioclase phyric, and show a brown, altered chill margin. Some samples are amygdaloidal, have calcite veins, or disseminated sulfides. Basalts consist chiefly of plagioclase and pyroxene, with minor amounts of magnetite, smectite, and hematite. Vesicles are lined with phillipsite or filled with smectite. A large hydrofracture vein in basalt sample D9-8D is composed of altered glassy basalt fragments in Mn oxide, smectite, and phillipsite cement with small grains of disseminated amphibole. Andesites are fresh to mildly altered (Table 10), gray, massive, vesicular, and plagioclase phyric; or black, plagioclase phyric, andesite glass with an altered, soft, gray rind. Andesite from dredge D5 is composed chiefly of plagioclase and pyroxene, with minor tridymite and quartz and the secondary minerals calcite and smectite. Andesite from dredge D7 is composed chiefly of tridymite, cristobalite, plagioclase, and pyroxene, with minor hematite and smectite. Phillipsite is abundant and magnetite occurs in moderate amounts in the alteration rind of andesite glass (Table 7, sample D9-6-2).

Breccia in dredge D5 is matrix supported and consists of clasts of volcaniclastic sandstone, andesite, breccia, and rarely hydrothermal(?) quartz in a fine-grained matrix of plagioclase, pyroxene, tridymite, smectite, and calcite (Table 6). Fe-Mn-oxide cement occurs near the contact with crusts. Two fragments of breccia consisting of serpentinite clasts in a quartz-calcite cement were also recovered. Breccia sample D5-2B is enriched in Au about 4 times over its earth's crust mean content of 4 ppb (Govett, 1983; Table 10). Breccia in dredge D8 is matrix supported and consist of altered brown basalt clasts in a pale-brown matrix of carbonate with blue serpentine grains, Mn oxides, and metamorphic rock fragments. Three types of breccia occur in dredge D9: 1. Andesite and altered basalt clasts in clast-supported fine-grained volcaniclastic matrix; 2. Black andesite glass, andesite, and altered basalt in brown to yellow-green smectite matrix; 3. Gray, aphyric to feldspar phyric basalt and andesite clasts in yellow-green smectite matrix, phillipsite cement and veinlets, and Mn veinlets and grains.

Reworked pyroclastic rocks were recovered in dredge D9 and consist predominantly of sandstone, siltstone, and mudstone, which are commonly interbedded. Primary grains and glass have been completely replaced by phillipsite and smectite (Table 7). Different beds are black, brown, and yellow-green, display soft-sediment deformation and burrowing, and are peppered with Mn-oxide grains that also form laminae and graded beds. Smectite veins are also present. Gold is enriched about 4 times over its earth's crust mean content in some beds (Table 10). Volcaniclastic sandstone and siltstone consist of black glassy andesite grains with Fe-oxide and minor Mn-oxide cements (Fe_2O_3 is 19.5%, MnO is 0.88%, Table 10). The sandstone is composed of plagioclase, smectite, and X-ray amorphous Fe-oxide. Volcaniclastic siltstone and mudstone are pale-brown, yellow-green, and greenish, with Fe-Mn veinlets, dendrites, and grains. Those rocks are completely altered to smectite. The sandstone is enriched in Au about 6.5 times over its earth's crust mean content (Table 10).

Serpentinite from dredge D5 is partly replaced gabbro that is mottled white, dark-gray, blue-gray, green, and yellow-brown, and is dense and heavy. The serpentinite is composed of serpentine (probably lizardite), pyroxene, plagioclase, and minor smectite, talc, tridymite, and magnetite as determined by XRD and also minor brucite, tremolite, chlorite, and hornblende as determined by thin-section petrography. The dominant replacement texture is bastite, indicating that pyroxene (less commonly amphibole) was the dominant mineral that was replaced (Wicks et al., 1977). Minor mesh texture also occurs, indicating replacement of minor olivine. Some replaced grains are laced with magnetite, which also forms veins, surrounds the margin of grains, and is disseminated. Serpentinite from dredge D8 is nearly completely replaced peridotite(?) that is brown with black patches and contains Mn dendrites, large lizardite plates, and extensive magnetite veins. Coarse-grained magnetite and lizardite indicate that the serpentinite is at a mature stage of development. The mineral composition is lizardite, magnetite, and chromite. The replacement texture is approximately 70% mesh and 30% bastite, indicating replacement predominantly of olivine and secondarily of pyroxene (Wicks and Whittaker, 1977; Wicks et al., 1977). Compared to other serpentinites (Faust and Fahey, 1962), serpentinites from dredges D5 and D8 have high Cr (to 3560 ppm) and Fe (to 10.3% Fe_2O_3) contents, reflecting their high contents of magnetite and chromite (Tables 7, 10).

LITAKPOOKI RIDGE FERROMANGANESE CRUSTS

Description

Fe-Mn crusts collected during KODOS 98-3 vary in thickness from a patina to 154 mm (Tables 5, 6). Dredge D1 had a maximum crust thickness of 120 mm and an average crust thickness of 80 mm. Dredge D2 has a maximum crust thickness of 154 mm and an average crust thickness of 48 mm. Thicker crusts are composed of two or more layers, five being the maximum and three and four layers being the most common. The typical bedding sequence is an uppermost massive black layer (layer 1); which is underlain by a black, porous to vuggy layer that is stained reddish (layer 2); which in turn is underlain by a dense, massive, black, phosphatized layer (layer 3). Layer 3

may contain CFA-filled veins and lenses in addition to being impregnated by CFA. Layer 3 can be sub-divided into as many as four layers based on content and form of CFA and degree and orientation of fractures. All crusts greater than 60 mm thick have a phosphatized older crust generation. CFA in the 32-mm-thick crust D2-6A results from contamination from the substrate phosphorite, which has a gradational contact with the crust.

The growth rates and ages of nonphosphatized, or very mildly phosphatized bulk crusts and crust layers were determined using the empirical equation of Puteanus and Halbach (1988), which is based on Co contents and assumes a constant flux of Co in space and time, and that of Manheim and Lane-Bostwick (1988) (Table 11). The Puteanus and Halbach (1988) equation produces growth rates that range from 2.7 to 9.3 mm/Ma (mean 5.8 mm/Ma) for bulk crusts and 1.5 to 7.5 mm/Ma (mean 4.0 mm/Ma) for crust layers. In contrast, growth rates determined by the Manheim and Lane-Bostwick (1988) equation are much slower, with a range for bulk crusts of 1.2 to 3.5 mm/Ma (mean 2.4 mm/Ma) and for crust layers a range of 0.6-3.0 mm/Ma (mean 1.7 mm/Ma). The latter growth rates are much more in line with those determined by U-series and Be isotopes, which range from <1-10 mm/Ma, but mostly fall within the range of 1-3 mm/Ma (Hein et al., 1999). Using the slower growth rates, the age range for the beginning of growth of bulk crusts is 16.0-30.3 Ma. The 30.3 Ma age for the 100-mm-thick crust D1-1A is probably much too young and that age needs to be confirmed with Be isotope dating. The ages for initiation of crust growth are much younger than the age of the volcanic edifices on which they grew. Marshall Islands seamounts range in age from about 76-138 Ma old, ages of 76-86 Ma being most common (Davis et al., 1989; Lincoln et al., 1993). The fast growth rates determined by the Puteanus and Halbach (1988) equation produce unreasonably young ages for initiation of crust growth, especially for the thick crusts. Analytical precision in the chemical composition of the crusts produces growth rates and resulting crust ages with relative differences that range from 6-13%.

X-Ray Diffraction Mineralogy

Great care was taken in sampling crusts for chemical and mineralogical analyses. Contamination from recent sediments was removed, which was especially critical in porous crust layers. Also, special attention was paid to obtaining a clean separation of the lowest crust layer from the substrate; however, that was not possible with crust D2-6A where the contact was gradational. Any minerals or elements determined to exist in the various crust layers were incorporated into those layers during deposition or diagenesis and are not due to sampling procedures or post-depositional infiltration of sediment. Finally, encrusting organisms and other debris were cleaned from the crust surfaces before subsampling. Bulk always refers to the entire crust thickness, whether composed of layers or not.

δ-MnO_2 (vernadite) contents of bulk crusts and crust layers range from 69% to 100% (Table 12). δ-MnO_2 has only two X-ray reflections at about 2.42Å and 1.41Å. X-ray amorphous Fe oxyhydroxide epitaxially intergrown with the δ-MnO_2 is also a dominant phase in these crusts, but is not included with the crystalline phases listed in Table 12. Part of this X-ray amorphous iron phase crystallized to goethite in 56% of the layers analyzed. CFA occurs in 78% of the bulk crusts and 44% of the layers analyzed. Crust layer samples contain up to 26% CFA, always within the lowermost one or two layers of the crust. CFA is not found in the outer layers of thick crusts or in thin crusts. CFA is found in such a high percentage of the bulk crusts because most of the crusts analyzed are thick.

Quartz occurs in 24% of the samples analyzed; it was detected in 11% of the bulk crusts and 31% of the crust layers (Table 12). Quartz contents are less than or equal to about 1%. Plagioclase (<1 to 7%) was found in six samples and K-feldspar in one sample. The quartz and some of the plagioclase are of eolian origin, carried by the westerlies from Asia, as there is no local or regional source for quartz in the west-central Pacific. The Marshall Islands are south of the main westerly wind belt which is reflected in lower quartz contents compared to crusts from higher latitudes (Hein et al., 1985, 1987; Hein, Kang, et al., 1990). The remainder of the plagioclase, as well as the smectite, phillipsite, K-feldspar, and calcite were reworked from local outcrops and

incorporated into the crusts during precipitation of the Fe-Mn oxyhydroxides. Smectite occurs in about 24% of the samples.

Calcite occurs in two crust layers. The outermost layer of crust D2-1B contains calcite that probably resides in the outermost few millimeters of that layer. Calcite is replaced by Fe-Mn oxyhydroxides after burial by more than a couple of millimeters of crust. Calcite in the inner layer (25-55 mm) of crust D1-2 is probably the result of contamination.

Chemistry

Twenty-five Fe-Mn crust samples (9 bulk crusts and 16 crust layers) were analyzed for chemical composition (Tables 13-18). Data are presented including hygroscopic water (Table 13) and on a hygroscopic water-free basis--that is normalized to 0% H_2O^- (Tables 14-17). Hygroscopic water varies from about 6% to 19% (to 30% in other samples from the region) and consequently can significantly affect the contents of all other elements. Sample compositions normalized to 0% H_2O^- can be more meaningfully compared and also more closely represent the grade of the potential ore. The following discussion is confined to hygroscopic water-free compositional data.

Bulk Crusts: The mean Fe and Mn contents of the 9 bulk crusts are 20.1% and 25.2%, respectively (Tables 14, 16). The mean Fe/Mn ratio (0.8) is higher than the mean ratio for the entire central Pacific region (0.72; Hein et al., 1992), the ratio for the entire Marshall Islands EEZ (0.64; Hein et al., 1999), and the ratio for the area to the northwest of the Marshall Islands EEZ (0.76; Hein et al., 1997a). For the entire Marshall Islands EEZ, the mean Mn content is more (26.3%), while the Fe content is less (16.9%) compared to bulk crusts from this study. The mean contents of the economically important metals Co (0.48%), Ni (0.34%), and Pt (0.54 ppm) are less than the mean contents of 0.79%, 0.57%, and 0.63 ppm, respectively, for the entire Marshall Islands EEZ (Hein et al., 1999). The mean Co and Ni contents are less and Pt about the same compared to mean contents for crusts from the entire equatorial Pacific region. Phosphorus, a potential byproduct of mining crusts for Co and Ni, has a mean value of 2.2%, higher than the central Pacific mean of about 1%, and the mean content of 1.8% for crusts from the entire Marshall Islands EEZ. Analysis of a large number of thick crusts lowers the mean contents of many metals, and that is probably why this study shows mean concentrations below the regional and Marshall Islands means for Co, Ni, and other metals. Studies that include only analyses of thin crusts yield mean concentrations higher than those of regional means (for example, Pichocki and Hoffert, 1987; see Hein et al., 1992 for discussion). The Co+Ni+Cu mean content for all bulk crusts is 0.92% and the maximum mean percent is 1.40%. If Pb is added to that group of elements, the mean content is 1.07% and the maximum mean content is 1.57%. The mean content of Co+Ni+Cu decreases with increasing crust thickness, for example the mean is 1.22% for crusts <60 mm thick, and 0.83% for crusts >60 mm thick. That decrease in metals is controlled by Co and Ni contents because Cu contents increase in thick crusts, 0.07% for <60 mm-thick crusts versus 0.11% for crusts >60 mm thick. Mean Pb contents are about the same in thin and thick crusts. The relationship of Co+Ni+Cu to Fe and Mn contents can be seen on a Bonatti et al. (1972) diagram (Fig. 7), on which the KODOS 98-3 data fall in the range typical for central Pacific Fe-Mn crusts (Halbach et al., 1982; De Carlo et al., 1987; Hein et al., 1992).

Other metals of potential economic interest that are concentrated in the Fe-Mn crusts include Zr (535 ppm), Tl (121 ppm), Te (95 ppm), Bi (mean 52 ppm), W (~36 ppm), and Pt (0.5 ppm). Only recently have crusts been analyzed for Tl, Te, and Bi. Te contents are remarkably high compared to its earth's crust mean content of about 1 ppb--95,000 times enrichment for the Fe-Mn crust mean of 95 ppm and 145,000 times enrichment for the maximum Te content of 145 ppm in bulk crusts. However, the mean Te content of the earth's crust is poorly known and some estimates have placed it as high at 10 ppb, which would lower those enrichments by a factor of 10. The interesting aspect is that the mean content of two of those elements, Bi and Te increase in thick crusts, while Tl , Zr, and W decrease in thick crusts, that is, they are 39, 80, 159, 569, and 44 ppm in <60 mm-thick crusts and 58, 102, 102, 519, and 32 ppm, respectively, in >60 mm-thick

crusts. Mean contents of Ca, P, S, As, Cr, Cu, Mo, Pb, Sr, Th, U, V, Y, and Pt increase in thick crusts, whereas the other elements decrease except for Be, Ga, Hf, Rb, Sb, Sc, Sn, Rh, and Os, which are about the same in both crust thickness groups. This means that the ore grade for some rare metals (Bi, Te, Pt) increases with tonnage (thickness), the reverse of the situation for Co in crusts, the chief metal of economic interest. This decrease in grade with increase in tonnage is typical for metals of interest in most types of ore deposits. The increases in Ca and P contents are the result of phosphatization of the older generation of thick crusts.

Crust Layers: Individual layers from five crusts were analyzed: Two crusts were split into four layers, two crusts into three layers, and one crust into two layers (Tables 14, 17). Crust D2-5 was divided into two layers and the change in element contents is controlled by the high content of detritus in the inner layer. Therefore, Si, Al, and other aluminosilicate-associated elements are higher in the inner layer and Fe and Mn oxide-associated elements are higher in the outer layer (Table 14). For the crusts divided into three layers, D1-1 shows uniform increases toward the substrate for Ca, P, Ba, Cu, (CFA associated elements) and Te and uniform decreases in Mn, B, Cd, Co, Ga, Ni, Tl, Hg, Ru, mostly Mn oxyhydroxide-associated elements. Aluminosilicate-associated elements are highest in the middle layer and residual biogenic-associated elements are lowest in the middle layer. For crust D2-2, there are uniform increases toward the substrate for Ca, P, Ba, Be, and Sr (CFA-associated elements), similar to D1-1, and uniform decreases in Fe and Mn oxyhydroxide-associated elements. Aluminosilicate-associated elements are lowest in the middle layer and residual biogenic-associated elements are highest in the middle layer. For the crusts divided into four layers, D1-2 shows uniform decreases to the substrate of Mn, B, Co, Tl, and Hg and a uniform increase in Cu. Only the lowermost layer of the crust is phosphatized. All other elements have maximum values in one of the four layers, with variable distributions in the other layers. For crust D2-1, there are uniform decreases to the substrate only for Cd and uniform increases for Be, Bi, and Sr. The lower two layers are phosphatized with layer 3 having the highest P content; consequently, most other elements have their highest contents in layer 1, 2, or 4. Platinum typically increases with depth in thick crusts, although here it increased in one crust and decreased in another. In general, the trends indicate that there is a decrease of manganophile elements with depth in the crusts accompanied by increases in elements characteristic of the residual biogenic phase. Non-phosphatized crust layers generally have higher trace metal contents relative to Fe and Mn contents than do phosphatized crust layers.

Platinum Group Elements and Gold

Four bulk crusts and six crust layers were analyzed for PGEs, and nine bulk crusts and 12 crust layers for Au (Table 14). Mean palladium (mean 8 ppb), Os (2 ppb), and Au (~5 ppb) contents are roughly at their earth's crust mean content. One high Au outlier (54 ppb) raises the mean Au content to its earth's crust mean, otherwise it would be lower than its earth's crust mean. Two samples analyzed from the KODOS 97-4 cruise had high Au contents of 543 and 51 ppb, but overall crusts from that cruise had a mean Au content about at its earth's crust mean. The other PGEs are enriched over their earth's crust mean content by 7 times for Ir (Fe-Mn crust mean of 7 ppb), 20 times for Ru (mean 20 ppb), 30 times for Rh (mean 31 ppb), and 130 times for Pt with a mean content of 648 ppb. Crust layer D2-2B has an uncommonly high Pt content of 1930 ppb, the maximum measured content being 2650 ppb (Hein et al., 1997a). The high content in D2-2B is especially unusual in that it occurs in the outermost layer of the crust rather than the innermost phosphatized layer, which is more common. That same layer has the highest Mn, Ti, Te, Sn, As, Sb, Nb, Au, Ir, Rh, and Ru contents measured in this study, all of which decrease toward the substrate; Co has its second highest content. These element enrichments are likely associated with the high Mn content, that is with the δ-MnO_2 phase. There is also an uncommonly low Pt content of 151 ppb for the outermost layer of crust D1-1B. The mean Pt content of 648 ppb is comparable to the mean for the entire RMI EEZ (634 ppb; Hein et al., 1999) and lower than the mean content for a large area of the northwest Pacific, 777 ppb (Usui and Someya, 1997).

Enrichment of PGEs in the inner parts of crusts is common for central Pacific crusts. The highest Pd and Ru concentrations occur in crusts from the Yap and Mariana arcs, as do other

elements indicative of clastic input. As shown in previous studies, Pt, Ir, and Rh are derived predominantly from seawater, whereas Pd and much of the Ru are derived from clastic debris, the remainder of the Ru being derived from seawater. The extraterrestrial component (meteorite debris) in the bulk crusts is small. However, meteorite debris may be concentrated locally in the crusts by formation of dissolution unconformities, or by proximity of the crust to meteorite fallout during formation of the layer. Localized extraterrestrial debris-rich horizons, however, do not alter the overall hydrogenetic signature of the PGEs. In addition, the PGE ratios are non-chondritic, with Fe-Mn crust compositions showing more than an order of magnitude more Pt relative to Ir and Rh relative to Ir. More likely, Pt is a redox sensitive element and its changing concentration reflects changing redox conditions, and diagenesis in the inner parts of the crusts (see Hein et al., 1997b).

Rare Earth Elements

For 7 bulk crusts and 6 crust layers, total REEs vary from about 0.15% to 0.27% (Table 18). For bulk crusts, total REE contents range from 0.15% to 0.24%, with a mean of 0.20%. The range and mean for individual crust layers are somewhat higher than for bulk crusts, 0.15%-0.27% and 0.21%, respectively. Mean total REE content differences between thick and thin crusts is 0.22% and 0.18%, respectively. The two samples for which layers were analyzed show different patterns of REE concentrations with depth in the crusts. The three layers of crust D1-1 generally show a decrease of light REEs (La to Gd) from the innermost layer 3 to the outer two layers, which have similar contents; the heavy REEs (Gd-Lu) have their highest content in the outermost layer, next highest in the innermost layer and lowest content in the middle layer. Total REEs and the Ce anomalies follow the pattern of the light REEs. The three layers of crusts D2-2 show the highest content of each element in the middle layer (except La), the next highest content in the lowermost layer, and lowest content in the uppermost layer. Total REEs follow the same pattern, but the Ce anomalies decrease from the surface to the substrate. These two trends are not related to degree of phosphatization of the crust layers. For crusts from the area northwest of the RMI, 11 of 13 crusts analyzed showed decreases in REE contents from the substrate to the crust surface (Hein et al., 1997a), as did total REEs for crust D1-1 here.

Chondrite-normalized REE patterns show moderate to large positive Ce anomalies, small positive Gd anomalies, light REE enrichments, and slight decreases in heavy REEs with increasing atomic number, or flat heavy REE patterns (Figs. 8-10). PAAS shale-normalized REE patterns show nearly flat heavy REEs, light REE depletion, and positive Ce and Gd anomalies. A small positive Gd anomaly is typical of hydrogenetic Fe-Mn crusts and of seawater (Hein et al., 1988). In crust D1-1, the Ce anomalies increase through the crust from the surface to the substrate, where as the opposite trend in seen in crust D2-2.

Element Associations

Correlation coefficients and Q-mode factor analysis coupled with X-ray diffraction mineralogy can be used to interpret which elements are associated with the mineral phases that make up Fe-Mn crusts. We analyzed correlation coefficient matrices and Q-mode factor analyses for three data sets including nine bulk crusts from Table 14 (Table 19; Fig. 11), four bulk crusts ≤62 mm (Table 20), and five bulk crusts ≥85 mm (Table 21; Fig. 12). We interpret the data for bulk crusts to indicate that the following elements are associated with the following phases. **Detrital** (aluminosilicate) phase: Si, Al, Fe, Ti, K, Na, Zr, B, Nb, Hf, Li, Y; **Mn-oxyhydroxide** phase: Mn, Tl, Co, Ni, Pb, Ga, Mo, Cd, Na, Bi; **Fe-oxyhydroxide** phase: Fe, As; **CFA** phase: Ca, P, S, Sr, As, Te, Bi, Ba, Be, Cu, Sn, Hf, Pb, Sc; **residual-biogenic** phase: Sr, Ba, Cu, W, Zn, As, V, Bi.

Only minor differences exist between the data sets of bulk crusts ≤62 mm thick and all bulk crusts, but significant differences exist for crusts ≥85 mm thick. It has been shown that element associations for very thick crusts do not follow those typical of Fe-Mn crusts because of extensive phosphatization and remobilization of elements (e.g. Hein, Kang, et al., 1990; Koschinsky et al., 1997; Hein and Morgan, 1999). The detrital phase shows minor differences but the other three

phases are mixed (Table 21; Fig. 12): **Mn-oxyhydroxide plus residual biogenic** phase includes Mn, W, As, Sr, Bi, Cu, Zn, V, Ca, P, Ba, Pb, Ni; the **CFA-diagenetic** phase includes Te, Sn, P, Tl, Ca, Co, Nb, Pb, Ti, Bi. This latter phase contains those elements that are known to be, or thought to be, incorporated into Fe-Mn crusts through an oxidation reaction (Co, Pb, Te, Tl, Bi, Ti, Sn).

Element associations indicate that the rare metals (Te, Tl, W, Bi, Hf, Zr, Nb, Sn) are associated with several phases. Tl is clearly associated solely with the Mn-oxyhydroxide phase. Te may be associated primarily with the CFA phase, secondarily with the residual biogenic phase, and possible also with the Mn phase. Hf, Zr, and Nb are predominantly part of the detrital phase, but Hf may also, in part, be associated with the CFA phase, Zr with the residual biogenic phase, and Nb with each of the other three phases. Bi appears to be associated predominantly with the CFA phase and secondarily with the residual biogenic and Mn phases. W may be associated with the residual biogenic phase and secondarily with the Mn oxyhydroxide phase. Sn may be predominantly associated with the CFA phase and, in part, with each of the other three phases. Tl, Hf, and Zr associations are very consistent among the various data sets analyzed here, but the other rare metals need to be analyzed in greater detail with a larger data set.

Correlation coefficients also show that the following elements increase with increasing crust thickness: Ba, S, Bi, Ca, P, Be, and Sr, whereas Si, Cd, B, Al, and K decrease with increasing crust thickness. These relationships indicate that the CFA and residual biogenic phases increase and the detrital phase decreases with increasing crust thickness. It has been noted many times that Co contents, the most important metal of economic interest, decreases with increasing crust thickness, but that correlation is not seen here at the 95% confidence level.

YAP CONVERGENT MARGIN FERROMANGANESE CRUSTS AND STRATABOUND MANGANESE DEPOSITS

Description

Fe-Mn crusts collected on the YCM during KODOS 98-3 are thin and vary in thickness from a patina to 15 mm for Yap Arc samples (D5, D6, D8-, D9) and a patina to 10 mm for dredge D7 from southwest Caroline Ridge (Tables 5, 6). The Fe-Mn crusts are composed of one or two layers. Crust layers are black, massive, and porous and rarely dendritic or acicular. Crust surfaces are granular to smooth and rarely botryoidal. None of the crusts have been phosphatized.

Stratabound hydrothermal deposits consists of Mn oxyhydroxide-cemented volcaniclastic sandstone (D5) composed of medium sand-sized grains in gray to black cement; and a 15 mm-thick, submetallic, gray layer of Mn oxyhydroxide with adjacent layers of Mn-cemented volcaniclastic sandstone (D8). The submetallic luster and gray color is a hallmark of hydrothermal Mn deposits.

Growth rates of the Fe-Mn crusts based on the Manheim and Lane-Bostwick (1988) equation (3.1-6.1 mm/Ma) are typical of hydrogenetic precipitation. Based on those growth rates, the oldest crust began forming only 2.6 Ma ago. The growth rate of the stratabound hydrothermal Mn layer is about 38 mm/Ma, which is slow compared to other hydrothermal Mn deposits (e.g. Hein, Ahn, et al., 1992). That relatively slow growth rate is the result of an anomalously high Co content for hydrothermal Mn. The ages for initiation of crust growth are much younger than the age of the volcanic edifices on which they grew, which is Oligocene for southwest Caroline Ridge and Oligocene and Miocene for Yap Arc (Hein, Ahn, et al., 1992).

X-Ray Diffraction Mineralogy

δ-MnO_2 (vernadite) contents of bulk crusts range from 91% to 95% (Table 12). X-ray amorphous Fe oxyhydroxide epitaxially intergrown with the δ-MnO_2 is also a dominant phase in these crusts, but is not included with the crystalline phases listed in Table 12. Quartz, plagioclase,

and calcite occur as accessory minerals. Hydrothermal birnessite cements the volcaniclastic sandstone, which is composed of plagioclase, serpentine, pyroxene, amphibole, and quartz. The hydrothermal Mn layer is predominantly birnessite, with moderate smectite and quartz (Table 12). It is difficult to distinguish δ-MnO_2 in the presence of birnessite because of overlapping peaks, so it is possible that δ-MnO_2 occurs in addition to the birnessite.

Chemistry

Three bulk Fe-Mn crust samples, one Mn-cemented sandstone, and one stratabound Mn layer were analyzed for chemical composition (Tables 22-24).

Bulk Crusts: The mean Fe and Mn contents of the 3 bulk crusts are 22.2% and 22.6%, respectively (Tables 23, 24). The mean Fe/Mn ratio (1.0) is higher than the mean ratio for the entire central Pacific region (0.72; Hein et al., 1992), the Marshall Islands EEZ (0.64; Hein et al., 1999), the area to the northwest of the Marshall Islands EEZ (0.76; Hein et al., 1997a), and Fe-Mn crusts from Litakpooki Ridge from this study; but is about the same as the ratio for the FSM EEZ, 1.02 (Hein et al., 1999). Generally, island-arc Fe-Mn crusts form by both hydrogenetic and hydrothermal input and have Fe/Mn ratios greater than 1.0. However, only the bulk crust from southwest Caroline Ridge (D7) has more Fe than Mn. The Co contents, Fe/Mn ratios, and growth rates indicate that the YCM crusts are solely of hydrogenetic origin. The southwest Caroline Ridge crust is similar in composition to the Yap Arc crusts, but with somewhat higher Fe, Cl, Nb, Rb, and Zr contents and lower Al and Ba contents. The Caroline Ridge crust has an unusually high Si/Al ratio (>645) indicating a low detrital component and likely a high biogenic silica content.

Mean contents of the economically important metals Co (0.34%) and Ni (0.34%) are less than their mean contents (0.79% and 0.57%, respectively) for the RMI EEZ crusts (Hein et al., 1999). The Co+Ni+Cu mean content for bulk crusts is 0.75% and the maximum mean content is 0.86%. If Pb is added to that group of elements, the mean content is 0.86% and the maximum mean content is 0.98%. The relationship of Co+Ni+Cu to Fe and Mn (Fig. 7), show that the YCM samples have relatively less trace metals and more Fe compared to Litakpooki Ridge samples.

Other metals of potential economic interest that are concentrated in the YCM Fe-Mn crusts include Zr (554 ppm), Tl (98 ppm), Te (37 ppm), and Bi (mean 14 ppm). Zr is somewhat more, Tl somewhat less, and Bi and Te much lower that mean contents from Litakpooki Ridge crusts. The recovery of only thin crusts from the YCM limits their economic potential.

Stratabound deposits: The hydrothermal stratabound Mn-oxide layer (D8-1A) has very high Mn (44%), Ba (1.18%), Ni (0.64%), and copper (0.2%) contents, as well as moderately high Zn (0.16%), Cd (16 ppm), and Li (179 ppm) contents, with an Fe/Mn ratio of 0.03 (Table 23). The high Mn and low Fe/Mn ratio are characteristic of hydrothermal Mn deposits. The high trace-metal contents are found in some hydrothermal Mn deposits (Hein et al., 1997b). Previously analyzed hydrothermal Mn samples (n=7) from Yap Arc also had high Mn (44%), Ni (0.45%), Ba (0.31%), Cu (0.26%), Zn (0.16%), Cd (44 ppm), and Cr (436 ppm) contents (Hein, Ahn, et al., 1992), although the sample from this study has much higher Ni and Ba contents. Yap Arc hydrothermal Mn deposits have higher trace metal contents than similar deposits from other regions (Hein et al., 1997b), which may be the result of intensive leaching of ultramafic rocks by the hydrothermal fluids and the lack of precipitation of sulfides at depth, or the leaching of sulfides that formed at depth in the hydrothermal system. A high serpentinite content (Table 12) in the Mn-cemented sandstone (D5-16A) attests to the ubiquitous occurrences of ultramafic and mafic rocks in the Yap Arc, which had previously been dredged from outcrops and collected as blue-green muds that formed from serpentinite diapers (Hein, Ahn, et al., 1992).

Rare Earth Elements

Total REE contents for the 3 bulk crusts vary from 0.14% to 0.16%, with a mean of 0.15%; whereas the total REE contents for the hydrothermal deposits are very low, 130 ppm for the Mn-cemented sandstone and 34 ppm for the stratabound Mn layer (Table 18).

Chondrite-normalized REE patterns for the Fe-Mn crusts show small positive Ce and Gd anomalies, light REE enrichments, and decreases in heavy REEs with increasing atomic number (Fig. 13). These characteristics are typical of west Pacific hydrogenetic Fe-Mn crusts (Hein, Ahn, et al., 1992). PAAS shale-normalized REE patterns show nearly flat heavy REEs, light REE depletion, convex up middle REEs, and small positive Ce and Gd anomalies. The stratabound Mn layer shows a strong negative Ce anomaly, typical of hydrothermal Mn deposits, and a positive Eu anomaly, which reflects weathering of the basement rock and sediments by the mineralizing fluids (Fig. 14). The REE pattern for the Mn-cemented sandstone is very similar to those of the Fe-Mn crusts, but with an order of magnitude less enrichment relative to chondrites and shale. This indicates that there is a hydrogenetic component in the hydrothermal Mn-cemented sandstone. The negative Yb anomaly probably results from analytical error because of the very low contents of the heaviest REEs.

RESOURCE CONSIDERATIONS

The commonly cited cut-off grade for potential economic development is 0.8% Co and the cut-off thickness is 40 mm. On a water-free basis, KODOS 98-3 samples have moderate mean Pt (0.54 ppm), Mn (25.2%), Co (0.48%), Ni (0.34%), and Cu (0.10%) contents, with a mean Co+Ni+Cu content of 0.92%. The mean crust thickness is >40 mm for dredge hauls from Litakpooki Ridge, with one being 80 mm; none of the dredge hauls from the YCM yielded thick crusts. It is not known whether ultimately grade or tonnage (thickness) will be the most important factor in choosing a potential mine site, but if it is tonnage, then both Litakpooki Ridge and Lomilik Seamount in the RMI EEZ are excellent sites for additional work.

It is important that several very rare metals, such as the PGEs, Te, and Bi increase in grade with increasing crust thickness in the RMI crusts. Te contents are especially interesting because its earth's crust abundance may be as much as 5 times less than that of Pt, but its concentration in Fe-Mn crusts is about 200 times greater than that of Pt. Te, Bi, Nb, Tl, W, and Zr need to be looked at in detail in terms of their resource potential in Fe-Mn crusts. Elevated gold contents in some of the dredged Yap Arc rocks indicate that epithermal gold deposits like those that occur on nearby Gagil-Tamil and Maap Islands may also occur offshore.

ACKNOWLEDGMENTS

We thank the captain, crew, and scientific staff of the R.V. Onnuri cruise KODOS 98-3 for excellent support while at sea. We thank Jane Reid, U.S. Geological Survey (USGS), for reviewing this report, and C. Degnan, D. Mosier, and F. Wong of the USGS for help with the maps.

REFERENCES

Anders, E. and Grevesse, N., 1989, Abundances of the elements: Meteoritic and solar. Geochimica et Cosmochimica Acta, v. 53, p. 197-214.

Aruscavage, P.J., Kirschenbaum, H., and Brown, F., 1989, Analytical methods: The determination of 27 elements in ferromanganese materials: *in* Manheim, F.T. and Lane-Bostwick, C.M. (eds.), Chemical Composition of Ferromanganese Crusts in the World Ocean: A Review and Comprehensive Database. U.S. Geological Survey Open File Report 89-020, 200 p. plus 3 appendices.

Bonatti, E., Kraemer, T., and Rydell, H., 1972, Classification and genesis of submarine iron-manganese deposits: in Horn, D.R. (ed.), Ferromanganese Deposits On the Ocean Floor. Washington, D.C., National Science Foundation, p. 149-166.

Chase, T.E., Seekings, B.A., and Young, J.D., 1988. Marine topography of the Republic of the Marshall Islands, Federated States of Micronesia, Republic of Palau, Commonwealth of the Northern Mariana Islands, and Territory of Guam. U.S. Geological Survey unpublished map that was modified from Chase, T.E. and Menard, H.W. (compilers), 1973. Bathymetric atlas of the North Pacific Ocean. U.S. Naval Oceanographic Office, Washington, D.C., Publication 1301-2-3. .

Cook, H.E., Johnson, P.D., Matti, J.C., and Zemmels, I., 1975, Methods of sample preparation and X-ray diffraction data analysis (X-ray mineralogy laboratory, Deep Sea Drilling Project, University of California Riverside): *in* Hays, D.E., Frakes. L.A., et al., Initial Reports of the Deep Sea Drilling Project, U.S. Government Printing Office, Washington, D.C., v. 28, p. 999-1007.

Davis, A.S., Pringle, M.S., Pickthorn, L-B.G., Clague, D.A., and Schwab, W.C., 1989, Petrology and age of alkalic lava from the Ratak Chain of the Marshall Islands. Journal of Geophysical Research, v. 94, p. 5757-5774.

De Carlo, E.H., McMurtry, G.M., and Kim, K.H., 1987, Geochemistry of ferromanganese crusts from the Hawaiian Archipelago--I. Northern survey areas. Deep-Sea Research, v. 34, p. 441-467.

Engleman, E.E., Jackson, L.L., and Norton, D.R., 1985, Determination of carbonate carbon in geological materials by coulometric titration. Chemical Geology, v. 53, p. 125-128.

Faust, G.T. and Fahey, J.J., 1962. The serpentine-group minerals. U.S. Geological Survey Professional Paper 384-A, 92 pp.

Govett, G.J.S., 1983, Rock Geochemistry in Mineral Exploration. Elsevier, Amsterdam, 461 pp.

Halbach, P., Manheim, F.T., and Otten, P., 1982, Co-rich ferromanganese deposits in the marginal seamount regions of the central Pacific basin--results of the Midpac '81. Erzmetall, v. 35, p. 447-453.

Hein, J.R. and Morgan, C.L., 1999, Influence of substrate rocks on Fe-Mn crust composition. Deep-Sea Research I, v. 46, p. 855-875.

Hein, J.R., Manheim, F.T., Schwab, W.C., and Davis, A.S., 1985, Ferromanganese crusts from Necker Ridge, Horizon Guyot, and S.P. Lee Guyot: Geological considerations. Marine Geology, v. 69, p. 25-54.

Hein, J.R., Morgenson, L.A., Clague, D.A., and Koski, R.A., 1987, Cobalt-rich ferromanganese crusts from the Exclusive Economic Zone of the United States and nodules from the oceanic Pacific: *in* Scholl, D.W., Grantz, A., and Vedder, J.G. (eds.), Geology and Resource Potential of the Continental Margin of Western North America and Adjacent Ocean Basins-Beaufort Sea to Baja California. Circum-Pacific Council for Energy and Mineral Resources, Earth Science Ser., Houston, TX, v. 6, p. 753-771.

Hein, J.R., Schwab, W.C. and Davis, A.S., 1988, Cobalt and platinum-rich ferromanganese crusts and associated substrate rocks from the Marshall Islands. Marine Geology, v. 78, p. 255-283.

Hein, J.R., Kang, J.-K., Schulz, M.S., Park, B.-K., Kirschenbaum, H., Yoon, S.-H., Olson, R.L., Smith, V.K., Park., D.-W., Riddle, G.O., Quinterno, P.J., Lee, Y.-O., Davis, A.S., Kim, S.R., Pringle, M.S., Choi, D.-L., Pickthorn, L., Schlanger, S.O., Duennebier, F.K., Bergersen, D.D. and Lincoln, J.M., 1990, Geological, geochemical, geophysical, and oceanographic data and interpretations of seamounts and Co-rich ferromanganese crusts from the Marshall Islands, KORDI-USGS R.V. Farnella Cruise F10-89-CP. U.S. Geological Survey Open File Report 90-407, 246 p.

Hein, J.R., Ahn, J.-H., Wong, J.C., Kang, J-K., Smith, V.K., Yoon, S-H., d'Angelo, W.M., Yoo, S-O., Gibbs, A.E., Kim, H-J., Quinterno, P.J., Jung, M.-Y., Davis, A.S., Park, B.-K., Gillison, J.R., Marlow, M.S., Schulz, M.S., Siems, D.F., Taggart, J.E., Rait, N., Gray, L., Malcolm, M.J., Kavulak, M.G., Yeh, H.-W., Mann, D.M., Noble, M., Riddle, G.O., Roushey, B.H., and Smith, H., 1992, Geology, geophysics, geochemistry, and deep-sea mineral deposits, Federated States of Micronesia: KORDI-USGS R.V. Farnella cruise F11-90-CP. U.S. Geological Survey Open File Report 92-218, 191 pp.

Hein, J.R., Schulz, M.S., and Gein, L.M., 1992, Central Pacific cobalt-rich ferromanganese crusts: Historical perspective and regional variability. in Keating, B. H. and Bolton, B. R. (eds.), Geology and Offshore Mineral Resources of the Central Pacific Basin, Springer-Verlag, New York, p. 261-283.

Hein, J.R., Yeh, H.-W., Gunn, S.H., Sliter, W.V., Benninger, L.M., and Wang, C.-H., 1993, Two major Cenozoic episodes of phosphogenesis recorded in equatorial Pacific seamount deposits. Paleoceanography, v. 8, p. 293-311.

Hein, J.R., Yeh, H.-W., Gunn, S.H., Gibbs, A.E., and Wang, C.-H., 1994, Composition and origin of hydrothermal ironstones from central Pacific seamounts. Geochimica et Cosmochimica Acta, v. 57, p. 179-189.

Hein, J.R., Zielinski, S.E., Staudigel, H., Chang, S.-W., Greene, M., and Pringle, M.S., 1997a, Composition of Co-rich ferromanganese crusts and substrate rocks from the NW Marshall Islands and international waters to the north, Tunes 6 cruise. U.S. Geological Survey Open File Report 97-482, 65 pp.

Hein, J.R., Koschinsky, A., Halbach, P., Manheim, F.T., Bau, M., Kang, J.-K., and Lubick, N., 1997b, Iron and manganese oxide mineralization in the Pacific: *in* Nicholson, K., Hein, J.R., Bühn, B., and Dasgupta, S. (eds.) Manganese Mineralization: Geochemistry and Mineralogy of Terrestrial and Marine Deposits. The Geological Society Special Publication No. 119, London, p. 123-138.

Hein, J.R., Moon, J.-W., Lee, K.-Y., Kim, K.-H., Roberts, L., Burrows, M., Park, S.H., Dowling, J., Choi, Y.-J., Zielinski, S.E., Chi, S.-B., Benninger, L., Kim, H.-S., and Park, C.-K., 1998. Composition of Co-rich ferromanganese crusts and substrate rocks from the Marshall Islands, cruise KODOS 97-4. U.S. Geological Survey Open File Report 98-375, 71 pp.

Hein, J.R., Koschinsky, A., Bau, M., Manheim, F.T., Kang, J.-K., and Roberts, L., 1999, Cobalt-rich ferromanganese crusts in the Pacific. In, CRC Handbook of Marine Minerals, Cronan, D.S. (Ed.), CRC Press, Boca Raton (in press).

Jackson, L.L., Brown, F.W., and Neil, S.T., 1987, Major and minor elements requiring individual determination, classical whole rock analysis, and rapid rock analysis: *in* Baedecker, P.A. (ed.) Methods for Geochemical Analysis. U.S. Geological Survey Bulletin 1770, p. G1-G23.

Klovan, J.E. and Imbrie, J., 1971, An algorithm and FORTRAN-IV program for large-scale Q-mode factor analysis and calculation of factor scores. Mathematical Geology, v. 3, p. 61-77.

KODOS, 1999a, Distribution and genesis of Co-rich crusts in the Marshall Islands, Western Pacific. Korea Ocean Research and Development Institute, Technical Report Number BSPE 98729-00-1172-7, 205 pp (in Korean with English summary).

KODOS, 1999b, A geochemical study for the submarine hydrothermal mineralization. Korea Ocean Research and Development Institute, Technical Report Number BSPE 98712-00-1162-7, 271 pp (in Korean with English summary).

Koschinsky, A., Stascheit, A., Bau, M., and Halbach, P., 1997. Effects of phosphatization on the geochemical and mineralogical composition of marine ferromanganese crusts. Geochimica et Cosmochimica Acta, v. 61, p. 4079-4094.

Lichte, F.E., Golightly, D.W., and Lamothe, P.J., 1987a, Inductively coupled plasma-atomic emission spectrometry: *in* Baedecker, P.A. (ed.), Methods for Geochemical Analysis. U.S. Geological Survey Bulletin 1770, p. B1-B10.

Lichte, F.E., Meier, A.L., and Crock, J.G., 1987b, Determination of the rare earth elements in geological materials by inductively coupled plasma-mass spectrometry. Analytical Chemistry, v. 59, p. 1150-1157.

Lincoln, J.M., Pringle, M.S., and Silva, I.P., 1993, Early and Late Cretaceous volcanism and reef-building in the Marshall Islands. In, The Mesozoic Pacific: Geology, Tectonics, and Volcanism, Pringle, M.S., Sager, W.W., Sliter, W.V., and Stein, S. (Eds.), American Geophysical Union Geophysical Monograph 77, Washington, D.C., p. 279-305.

Manheim, F.T. and Gulbrandsen, R.A., 1979, Marine phosphorites. *in* Burns, R.G. (ed.), Marine Minerals. Mineralogical Society of America Short Course Notes, v. 6, p. 151-173.

Manheim, F.T. and Lane-Bostwick, C.M., 1988, Cobalt in ferromanganese crusts as a monitor of hydrothermal discharge on the Pacific sea floor. Nature, v. 335, p. 59-62.
McClellan, G.H. and van Kauwenbergh, S.J., 1990, Mineralogy of sedimentary apatites. In, Phosphorite Research and Development, Notholt, A.J.G. and Jarvis, I. (Eds.), The Geological Society, London, p. 23-31.
McKown, D.M. and Millard, H.T., Jr., 1987, Determination of uranium and thorium by delayed neutron counting. *in* Baedecker, P.A. (ed.), Methods for Geochemical Analysis. U.S. Geological Survey Bulletin 1770, p. I1-I12.
McLennan, S.M., 1989, Rare earth elements in sedimentary rocks: Influence of provenance and sedimentary processes: *in* Lipin, B.R. and McKay, G.A. (eds.) Geochemistry and Mineralogy of Rare Earth Elements. Mineralogical Society of America's Reviews in Mineralogy, v. 21, Washington D.C.
Peck, L.C., 1964, Systematic analysis of silicates. U.S. Geological Survey Bulletin 1170, 89 p.
Pichocki, C. and Hoffert, M., 1987, Characteristics of Co-rich ferromanganese nodules and crusts sampled in French Polynesia. Marine Geology, v. 77, p. 109-119.
Puteanus, D. and Halbach, P., 1988, Correlation of Co concentration and growth rate: A method for age determination of ferromanganese crusts. Chemical Geology, v. 69, p. 73-85.
Shapiro, L., 1975, Rapid analysis of silicate, carbonate, and phosphate rocks--revised edition. U.S. Geological Survey Bulletin 1401, 76 p.
Taggart, J.E., Lindsay, J.R., Scott, B.A., Vivit, D.V., Bartel, A.J., and Stewart, K.C., 1987, Analysis of geologic materials by wavelength-dispersive X-ray fluorescence spectrometry: *in* Baedecker, P.A. (ed.), Methods for Geochemical Analysis. U.S. Geological Survey Bulletin 1770, p. E1-E19.
Usui, A. and Someya, M., 1997, Distribution and composition of marine hydrogenetic and hydrothermal manganese deposits in the northwest Pacific, in Manganese Mineralization: Geochemistry and Mineralogy of Terrestrial and Marine Deposits, Nicholson, K., Hein, J. R., Bühn, B., and Dasgupta, S. Eds., Geological Society Special Publication No. 119, London, p. 177-198, 1997.
Wicks, F.J. and Whittaker, E.J.W., 1977. Serpentine textures and serpentinization. Canadian Mineralogist, v. 15, p. 459-488.
Wicks, F.J., Whittaker, E.J.W., and Zussman, J., 1977. An idealized model for serpentine textures after olivine. Canadian Mineralogist, v. 15, p. 446-458.

Table 1. Scientific personnel on R.V. *Onnuri* cruise KODOS 98-3

Jai Woon Moon	Co-chief scientist	KORDI[1]
Kyeong Young Lee	Co-chief scientist	KORDI
James R. Hein	Geochemistry	USGS[2]
Malia Burrows	Sampling	USGS
Youn-ji Choi	CTD[4]	KORDI
Jennifer S. Dowling	Sampling	USGS
Raymond Freeman-Lynde	Sedimentology	UGA[3]
Young Geun Jin	Airgun Seismic	KORDI
Hoi Soo Jung	Sampling	KORDI
Hyun Sub Kim	SBP, PDR	KORDI
Duk Kee Lee	Airgun Seismic	KORDI
Gun Chang Lee	Sampling DSC	KORDI
Sang Heon Nam	Airgun Seismic	KORDI
Chan Young Park	Data Processing	KORDI
Cheong Kee Park	SeaBeam Bathymetry	KORDI
Sung Hyun Park	Sampling	KORDI
Seung Kyu Son	CTD	KORDI
In Sung Yoo	Airgun Seismic	KORDI

[1]Korea Ocean Research and Development Institute
[2]United States Geological Survey
[3]University of Georgia, Athens
[4]CTD = conductivity, temperature, density; SBP= sub-bottom profiler; PDR = precision depth recorder; DSC = deep sea camera

Table 2. Station locations and operations for cruise KODOS 98-3

Station	Operation[1]	Location
Marshall Islands Fe-Mn crust leg		
SB 1	CTD1	Litakpooki Ridge
SB 2	PC1	Litakpooki Ridge
SB 3	PC2	Litakpooki Ridge
SB 4	D1	Litakpooki Ridge
SB 5	D2	Litakpooki Ridge
SB 6	D3	Litakpooki Ridge
SB 7	D4	Litakpooki Ridge
SB 8	CTD2	SW of Litakpooki
FSM Hydrothermal leg		
H 1	CTD3	Yap Arc
H 2	CTD4	Yap Arc
H 3	CTD5	Yap Arc
H 4	BC1, 2	Yap Arc
H 5	PC3	Yap Arc
H 6	MC1	Yap Arc
H 7	D5	Yap Arc
H 8	D6	Yap Arc
H 9	DSC1	Yap Arc
H 10	CTD6	Yap Arc
H 11	CTD7	Yap Trench
H 12	CTD8	W. Caroline Ridge
H 13	CTD9	W. Caroline Ridge
H 14	MC2	W. Caroline Ridge
H 15	D7	W. Caroline Ridge
H 16	PC4	Yap Trench
H 17	CTD10	Yap Arc
H 18	D8	Yap Arc
H 19	D9	Yap Arc
H 20	CTD11	Yap Arc

[1]CTD = conductivity, temperature, density, and oxygen profile; PC = piston core; D = dredge; BC = box core; MC = multiple core; DSC = deep-sea camera

Table 3. Twelve channel, two-150 in^3 airgun lines (AG); 3.5kHz and 12 kHz bathymetry lines (3.5, 12); and SeaBeam lines (SB) (see Figures 2, 3, and 5)

Location	Line Number	Operation	Nautical Miles	Kilometers
Marshall Islands Fe-Mn crust leg				
Litakpooki Ridge	SB 1	3.5, 12, SB	23.78	44.04
Litakpooki Ridge	SB 1-1	3.5, 12	4.98	9.22
Litakpooki Ridge	SB 2	3.5, 12, SB	23.79	44.05
Litakpooki Ridge	SB 2-1	3.5, 12	4.98	9.22
Litakpooki Ridge	SB 3	3.5, 12, SB	23.79	44.06
Litakpooki Ridge	SB 3-1	3.5, 12	2.49	4.61
Litakpooki Ridge	SB 4	3.5, 12, SB	16.85	31.21
Litakpooki Ridge	SB 5	3.5, 12, SB	7.47	13.83
Litakpooki Ridge	SB 6	3.5, 12, SB	23.80	44.07
Litakpooki Ridge	SB 6-1	3.5, 12	4.98	9.22
Litakpooki Ridge	SB 7	3.5, 12, SB	23.80	44.08
Litakpooki Ridge	SB 8	3.5, 12, SB	25.79	47.76
Litakpooki Ridge	SB 9	AG, 3.5, 12, SB	28.21	52.25
Litakpooki Ridge	SB 10	AG, 3.5, 12, SB	23.29	43.14
Litakpooki Ridge	SB 11	AG, 3.5, 12, SB	30.41	56.31
Litakpooki Ridge	SB 12	3.5, 12, SB	3.67	6.8
Litakpooki Ridge	SB 13	3.5, 12, SB	7.07	13.09
Litakpooki Ridge	SB 14	3.5, 12, SB	9.35	17.31
Lomilik Seamount	SB 15	3.5, 12, SB	26.41	48.91
Lomilik Seamount	SB 16	3.5, 12, SB	4.35	8.06
Lomilik Seamount	SB 17	3.5, 12, SB	11.73	21.72
Lomilik Seamount	SB 17-1	3.5, 12, SB	3.24	6.00
Lomilik Seamount	SB 17-2	3.5, 12, SB	11.40	21.11
Lomilik Seamount	SB 18	3.5, 12, SB	2.8	5.18
Lomilik Seamount	SB 19	3.5, 12, SB	26.32	48.74
Lomilik Seamount	SB 20	3.5, 12, SB	14.41	26.68
Lomilik Seamount	SB 21	3.5, 12, SB	17.38	32.19
Lomilik Seamount	SB 22	3.5, 12, SB	26.23	48.57
Lomilik Seamount	SB 23	3.5, 12, SB	6.65	12.31
Subtotal	--		439.42	813.74
FSM Hydrothermal leg				
Across Convergent Margin	H 1	AG, 3.5, 12, SB	78.9	146.1
Yap Arc	H 1-1	AG, 3.5, 12, SB	5.1	9.4
Across Convergent Margin	H 2	AG, 3.5, 12, SB	78.9	146.1
W. Caroline Ridge	H 2-1	AG, 3.5, 12, SB	8.2	15.2
Across Convergent Margin	H 3	AG, 3.5, 12, SB	78.8	146
Yap Arc	H 3-1	AG, 3.5, 12, SB	3.0	5.6
Yap Arc	H 4a	AG, 3.5, 12, SB	10.2	18.8
Yap Arc	H 4b	AG, 3.5, 12, SB	5.6	10.3
Yap Arc	H 4c	AG, 3.5, 12, SB	4.8	8.9
Yap Arc	H 4d	AG, 3.5, 12, SB	8.6	16
Yap Arc	H 4e	AG, 3.5, 12, SB	7.6	14.1
Yap Arc	H 5	AG, 3.5, 12, SB	20.3	37.6
Yap Arc	H 5-1	AG, 3.5, 12, SB	5.6	10.3
Yap Arc	H 6a	AG, 3.5, 12, SB	17.8	33.0
Yap Arc	H 6b	AG, 3.5, 12, SB	2.5	4.6
Yap Arc	H 6c	AG, 3.5, 12, SB	2.1	3.9
Yap Arc	H 6d	AG, 3.5, 12, SB	2.0	3.7
Yap Arc	H 6e	AG, 3.5, 12, SB	2.2	4.0
Yap Arc	H 6f	AG, 3.5, 12, SB	4.9	9.0
Yap Arc	H 6g	AG, 3.5, 12, SB	12.7	23.5
W. Caroline Ridge	H 7a	AG, 3.5, 12, SB	4.9	9.0
W. Caroline Ridge	H 7b	AG, 3.5, 12, SB	7.3	13.5
W. Caroline Ridge	H 7c	AG, 3.5, 12, SB	2.2	4.0
W. Caroline Ridge	H 7d	AG, 3.5, 12, SB	3.0	5.6
W. Caroline Ridge	H 7e	AG, 3.5, 12, SB	3.0	5.5
W. Caroline Ridge	H 7f	AG, 3.5, 12, SB	3.8	7.0
W. Caroline Ridge	H 7g	AG, 3.5, 12, SB	4.1	7.5
W. Caroline Ridge	H 7h	AG, 3.5, 12, SB	10.0	18.5
Subtotal	--	--	397.8	736.7
Total	--	--	837.2	1550.4

Table 4. Preliminary oxygen and temperature data from CTD casts, cruise KODOS 98-3 (see Figures 2 and 5)

	Latitude (N)	Longitude (E)	Station Number	Julian Day	Greenwich Mean Time[1]	Lowest O_2 Content (ml/l)	Water Depth at minimum O_2 (m)	Water Depth at Top of OMZ[2] (m)	Water Depth at 10°C Isotherm (m)	Water Depth at 5°C Isotherm (m)
Marshall Islands Fe-Mn crust leg										
Litakpooki Ridge										
CTD 1	8°09.15'N	160°32.02'E	1	226	1327-1457	1.34	307	280	279	890
CTD2	10°24.31'N	161°9.61'E	8	227	0827-1010	1.33	343	275	308	919
FSM Hydrothermal leg										
Yap Arc										
CTD 3	8°58.21'N	137°28.67'E	9	234	0942-1216	2.01	406	350	301	887
CTD 4	8°55.25'N	137°32.04'E	10	234	1310-1510	1.98	440	350	285	886
CTD 5	8°54.64'N	137°37.73'E	11	235	1354-1600	2.03	467	340	315	878
CTD 6	8°57.03'N	137°40.96'E	18	236	2145-2335	2.07	479	300	279	910
CTD 10	8°57.58'N	137°41.05'E	25	237	0958-1200	2.06	482	360	313	913
CTD 11	8°57.39'N	137°34.94'E	28	238	0202-0418	1.94	419	275	270	903
Yap Trench										
CTD 7	8°46.23'N	138°08.15'E	19	236	0208-0651	2.04	434	310	288	904
W. Caroline Ridge										
CTD 8	8°35.07'N	138°45.07'E	20	236	1200-1325	2.08	450	300	287	948
CTD 9	8°31.75'N	138°36.57'E	21	237	1423-1618	1.92	421	275	285	953

[1]Local Time equals GMT plus eleven hours for CTD 1 and 2 and GMT plus ten hours for CTD 3-11
[2]OMZ = oxygen minimum zone

Table 5. Dredge summary for cruise KODOS 98-3 (see Figures 2 and 5)

Dredge number	Location	Water depth on-off bottom (m)	Water depth corrected (m)[1]	Recovery (kg)	Max. crust thickness (mm)	Mean crust thickness (mm)	Dominant substrate	Comments
Marshall Islands Fe-Mn crust leg								
D1	Litakpooki	2058-1893	2040-1900	55	120	80	Breccia	Ironstone, phosphorite
D2A[2]	Litakpooki	1862-1680	1840-1770	145	154	48[3]	Basalt, limestone	Megacrusts
D2B[2]	Litakpooki	1610-1468	1600-1500	75	1	<1	Foram limestone	Large boulders
D3	Litakpooki	2200-1850	--	--	--	--	--	No recovery
D4	Litakpooki	2700-2388	--	--	--	--	--	No recovery
FSM Hydrothermal leg								
D5	Yap Arc	2757-2250	2600-2350	3.2	11	3	Breccia	Serpentinite, hydrothermal Mn
D6	Yap Arc	2720-1779	2720-1779	1.3	<1	<1	Pumice	1 breccia fragment
D7	W. Caroline Ridge	2280-1778	2250-1950	122	10	1	Basalt	Foraminiferal limestone
D8	Yap Arc	2672-1778	2600-2350	150	6	<1	Foram limestone	Serpentinite, hydrothermal Mn
D9	Yap Arc	2676-2223	2650-2450	81	15	3	Micritic limestone	Andesite, sandstone

[1]Depth interval from which samples were likely recovered
[2]Dredge repositioned because of ship's drift off station, clear change in rock types from lower to upper dredged samples
[3]Average for basalt substrate is 95 mm and for limestone substrate is 19 mm

Table 6. Location and description of dredge hauls, Marshall Islands Fe-Mn crust and FSM hydrothermal legs, KODOS 98-3 cruise

Dredge number	Latitude (°N)[1]	Longitude (°E)	Total recovery (kg)	Broken from outcrop (%)	Talus (%)	Fe-Mn encrusted rock (%)	Description of ferromanganese oxides	Description of substrate rocks
D1	08°13.97' 08°13.42'	160°35.97' 160°35.46'	55	100	0	100	Botryoidal surface, rarely granular to smooth, granular on sides; Thick crusts with 3 or 4 layers: 1. massive black, 2. porous to vuggy, 3. massive dense black, 4. where present, an uppermost <10 mm massive layer; layer 3 may be subdivided into up to 4 layers by bedding parallel fractures & occurrence of CFA veins and blebs; thinner crusts are missing layer 3; 2 nodules with large nuclei; some breccia with Fe-Mn cement; thickness: max=120 mm, av=80mm	70% breccia with white to brown phosphorite, brown basalt, & brown ironstone clasts in cream to pinkish CFA cement laced with Mn dendrites and cut by CFA veins; more rarely Fe-Mn oxide cement; 20% pebbly phosphorite with sparse brown basalt (some coated with Fe-Mn crust) & yellow-green altered hyaloclastite pebbles; CFA veins & Mn dendrites; 5% basalt, brown, altered; 5% ironstone, brown, oolitic to massive, replaced basalt
D2	08°11.79' 08°10.77'	160°34.48' 160°34.59'	220	99	1	66	Thick crusts on basalt+phosphorite: Small/medium botryoids on surface, granular on sides; 3 to 4 layers: 1. black massive, 2. porous to vuggy & columnar, Fe stained, 3. massive, dense, black, disseminated CFA & veins; layer 3 may be divided into an upper layer without apparent CFA and a lower layer with much CFA &/or fractures; 4. Where present, an uppermost <10mm massive layer; Thin crusts on limestone & phosphorite: Large to modified botryoids on surface, granular on thin crusts; 1-3 layers: 1. massive black, 2. porous, few vugs, 3. porous & vuggy, impregnated limestone or phosphorite; 1 completely encrusted cobble with 3 layers: 1. acicular black, 2. black, massive, fractured, 3. massive, CFA veins and vug fill; sparse granular crusts on friable foram limestone; thickness on basalt: max=154mm, av=95mm; on limestone: max=35mm, av=19mm; on friable limestone: av=<1mm	Rocks are divided into two groups--D2A, encrusted & D2B not encrusted--because ship was repositioned during operation & samples were collected from two places on a small hill at the summit of the guyot. D2A: 65% limestone & differentially CFA-replaced limestone, yellow-brown to brown, foraminiferal, hard to soft depending on degree of phosphatization, massive to vuggy, laced with Mn dendrites, blebs, & vein & vug fill. 35% basalt, brown to red-brown, altered, large yellow-green amygdules, laced with CFA and Fe-Mn oxides. D2B: 100% foraminiferal limestone, friable, pale brown to off white, large vugs lined with granular Fe-Mn oxides

Table 6 continued

D3	08°19.12' 08°19.01'	160°43.42' 160°42.55'	0	–	–	–	No recovery	No recovery
D4	08°22.10' 08°23.06'	160°49.19' 160°44.45'	0	–	–	–	No Recovery	No Recovery
D5	08°56.67' 08°54.38'	137°40.74' 137°41.17'	3.2	80	20	50	Smooth, granular, and microbotryoidal surfaces; 1 or 2 layers: 1. black very porous, 2. black, porous, dendritic; for one layer=black, porous, massive; 1 sample of sandstone cemented by hydrothermal Mn oxide; thickness: max=11mm, av=3mm	60% breccia: gray volcaniclastic sandstone, volcanic, & breccia clasts in greenish-brown volcaniclastic matrix; matrix supported; Fe-Mn oxide cement near surface with Fe-Mn crusts; rarely hydrothermal(?) quartz clasts and cement; 2 samples with serpentinite clasts in quartz-calcite cement; 21% serpentinite, mottled white, dark-gray, blue-gray, green, and yellow-brown, dense and heavy; 8% altered basalt, mottled greenish tan to gray, some with sulfides, calcite veins, chill margin, &/or amygdaloidal; 4% gray volcaniclastic sandstone, calcite &/or quartz cement, quartz crystals in vugs; 1 sample cemented by Fe-Mn oxides; 5% reef limestone & sandy chalk; 1% crust fragments without substrate; pumice pebble & golden coral
D6	08°53.53' 08°51.81'	137°37.02' 137°41.36'	1.3	<1	>99	<1	Sparse, patchy, granular patina on breccia fragment; none on pumice	98% gray pumice; 2% breccia, brown volcanic clasts altered to clay minerals in gray-green matrix of clay minerals; veins of quartz & hydrothermal(?) Mn oxides

Table 6 continued

D7	08°43.42' 08°42.69'	138°44.86' 138°45.24'	122	100	–	75	Granular to smooth surfaces; patchy crust with 1 layer, black, porous, in places capped by limestone; foraminiferal limestone boulders with sparse, patchy, granular crust; some vesicles in basalt may be filled with hydrothermal boxwork, Mn oxides; thickness: max=10mm, av=1mm	68% pillow basalt wedges: 1. gray, massive, variably vesicular, 1-2 mm red-brown alteration rind underlain by 10-12 mm black glass rind variably altered, underlain by 10-13 mm of small vesicles in the basalt; aphyric to plagioclase &/or olivine phyric; 2. same as #1, but basalt is altered brown; 3. massive, gray basalt; 4. amygdaloidal basalt; limestone encloses many basalt fragments; 31% white, friable, massive foraminiferal limestone, 1 sample with a gray calcareous ash layer; 1% 1. breccia with basaltic glass, basalt, and limestone, clasts in calcite cement, grain supported; 2. large tabular basaltic glass clasts in yellow-white to greenish carbonate +smectite matrix, matrix supported; 3. gray basalt clasts in greenish soft smectite matrix, matrix supported, zeolite vug fill
D8	08°55.05' 08°53.71'	137°39.97' 137°42.54'	150	95	5[2]	<1	Granular to smooth surfaces on mostly patchy patina or thin crust; 1 layer, massive, black, porous, rarely acicular; 1 piece of hydrothermal Mn oxide, stratabound, submetallic gray to black, massive to porous; crust thickness: max=6mm, av=<1mm	60% foraminiferal ooze, white to brown; 32% foraminiferal limestone, friable, extensively burrowed, pale brown, silt- & sand-sized grains of basalt; 4% serpentinite, brown, altered, mottled black with Mn oxides & Mn dendrites, large serpentine flakes, soft; 2% breccia, altered volcanic rock clasts in pale brown carbonate matrix with blue serpentine grains, Mn oxides, and metamorphic rock fragments, matrix supported; 1% gray, plagioclase-phyric andesite; 1% hydrothermal Mn, submetallic gray to black, massive

Table 6 continued

D9	08°50.18' 08°48.32'	137°35.07' 137°35.10'	81	90	10	60	Granular, smooth, & botryoidal surfaces on mostly patchy patina or thin crusts; 1 layer, massive, black, porous, rarely dendritic & acicular; 1 cobble of andesite with 20 mm thick vein of hydrofractured andesite clasts in hydrothermal Mn oxide, smectite, and phillipsite cement; crust thickness: max=15mm, av=<3mm	38% limestone, muddy, micritic, pale brown, variable amounts of smectite, Mn veinlets, extensively burrowed, interbedded with foraminiferal limestone with basalt grains; 26% andesite, 1. mildly altered, gray, massive, highly vesicular, feldspar phyric; 2. fresh glassy black, highly vesicular with gray rind altered to phillipsite, both feldspar phyric; 17% breccia, 1. andesite clasts as in #1 under andesite & yellow-brown, gray, brown altered volcanic clasts in clast supported silt & clay volcaniclastic matrix; 2. black glassy andesite clasts, as in #2 under andesites, & other volcanic rock clasts in brown to yellow-green smectite matrix, some yellow-green smectite clasts; 3. dark gray to pale gray aphyric to feldspar phyric basalt & andesite clasts in yellow-green matrix of smectite & phillipsite cement & veinlets, Mn veinlets & grains; 17% tuff or tuffaceous sandstone-siltstone-mudstone, black, brown, yellow-green, dark brown layers deformed by soft sediment deformation & burrowing, peppered with Mn oxide grains that also form laminae, graded beds, clay veins, mostly smectite; 2% volcaniclastic sandstone: 1. sandstone with grains of black glassy andesite; 2. medium to dark gray massive, Fe-oxide cement & fine-grained volcaniclastic matrix; pumice pebble

[1]Latitudes and longitudes for on and off bottom
[2]Pumice

Table 7. X-ray diffraction mineralogy of substrate rocks from KODOS 98-3 cruise

Sample	Major[1]	Moderate	Minor/Trace	Rock/Sediment
Marshall Islands Fe-Mn crust leg				
D1-5A	CFA[2], plagioclase	Smectite	–	Phosphatized basalt clast from breccia[3]
D1-5B	CFA, plagioclase	–	Smectite	Phosphatized hyaloclastite clast
D1-10A	Calcite	CFA	–	Pebbly phosphatic limestone
D2-2E	Smectite	–	Halite	Highly altered basalt
D2-4B	CFA	–	–	Phosphorite (Foraminiferal limestone)[4]
FSM Hydrothermal leg				
D5-2B-C	Plagioclase, pyroxene	Tridymite	Smectite	Volcaniclastic sandstone clast from breccia
D5-2B-M	Plagioclase, pyroxene	Tridymite	Smectite, calcite	Altered clay matrix of D5-2B-C
D5-4A	Lizardite, pyroxene	Plagioclase	Smectite, magnetite, talc, tridymite	Serpentinite
D5-7A	Plagioclase	Pyroxene	Tridymite, calcite, quartz, smectite	Amygdaloidal andesite
D7-2-1A	Plagioclase, pyroxene	–	Magnetite, smectite, hematite	Pillow basalt with chill margins
D7-4-1A	Plagioclase, pyroxene	–	Magnetite, hematite, smectite	Altered pillow basalt
D7-6-1A	Plagioclase, pyroxene	–	Magnetite, smectite, hematite	Vesicular pillow basalt fragment
D7-8-1A	Calcite	–	–	Breccia matrix
D7-9-1A	Calcite	Plagioclase, phillipsite	Smectite, hematite	Breccia matrix
D7-10-1A	Phillipsite, plagioclase	Smectite	–	Dark green matrix in breccia
D7-10-2A	Calcite	–	Smectite	White matrix in breccia
D7-10-2B	Calcite	Smectite	Phillipsite	Green matrix in breccia
D7-10-2C	Phillipsite	Calcite	Smectite	Brown-rind on clast from breccia
D7-13A	Amorphous, plagioclase	Calcite	Smectite	Volcanic ash bed in limestone
D8-2A	Lizardite	Magnetite	Chromite	Serpentinite
D8-4A	Lizardite	Magnetite	Chromite, smectite	Serpentinite
D9-3-1A	Phillipsite	Magnetite	Plagioclase, smectite	Sandy layer in bedded tuff
D9-3-1B	Smectite, phillipsite	–	–	Mudstone layer in bedded tuff
D9-3-2A	Smectite, phillipsite	–	–	Pale brown mudstone layer in bedded tuff
D9-3-2B	Smectite	Phillipsite	–	Green-gray sandstone layer in bedded tuff
D9-3-2C	Smectite, phillipsite	–	–	Pale brown mudstone layer in bedded tuff
D9-3-2D	Phillipsite, smectite	–	–	Brown sandstone layer in bedded tuff
D9-3-2E	Smectite, phillipsite	–	–	Mottled brown siltstone layer in bedded tuff
D9-4A	Tridymite, cristobalite	Plagioclase, pyroxene	Hematite, smectite	Andesite
D9-6-2A	Cristobalite, plagioclase	Pyroxene	Smectite	Black glassy andesite
D9-6-2B	Phillipsite, plagioclase	Pyroxene, magnetite	–	Gray rind on glassy andesite
D9-8C	Smectite, phillipsite	Plagioclase	–	Yellow and white vein in basalt
D9-8D	Plagioclase	Pyroxene	Hematite, smectite	Basalt
D9-8E	Phillipsite, plagioclase	–	Amphibole	Vein in basalt
D9-11-1A	Smectite, plagioclase	–	–	Volcaniclastic sandstone
D9-14A	Calcite	Plagioclase	High-Mg calcite, smectite	Limestone and micritic limestone

[1]Major: >25%, Moderate: 5-25%, Minor: <5%; [2]CFA is carbonate fluorapatite; [3]All breccias are sedimentary, and most are volcaniclastic; [4]Rock type in parentheses is replaced by CFA

Table 8. Chemical composition of substrate rocks from Litakpooki Ridge, Marshall Islands Fe-Mn crust leg, KODOS 98-3 cruise

	D1-10A	D1-10A[1]	D2-2E	D2-2E[1]	D2-4B
SiO_2 wt%	0.78	0.78	43.0	42.8	4.45
Al_2O_3	0.24	0.24	18.0	18.0	1.87
FeO	--	--	<0.1	<0.1	<0.1
Fe_2O_3	0.22	0.22	12.4	12.5	1.73
MgO	0.34	0.34	1.91	1.90	0.62
CaO	54.2	54.1	6.42	6.41	48.7
Na_2O	0.21	0.22	2.28	2.27	1.27
K_2O	0.05	0.05	1.61	1.62	0.13
TiO_2	0.024	0.024	2.490	2.498	0.169
P_2O_5	10.0	10.0	2.98	2.99	29.8
MnO	0.09	0.09	0.03	0.03	0.50
LOI[2]	33.0	33.1	7.10	7.05	7.80
Total	99.2	99.2	98.3	98.2	97.1
H_2O^+	0.6	0.6	6.6	6.4	2.4
H_2O^-	0.20	0.20	4.50	4.40	0.60
CO_2	32.4	32.3	0.44	0.42	4.92
C_{total}	9.00	9.01	--	--	--
S_{total}	0.20	0.19	--	--	--
F	0.918	0.931	--	--	--
Cl	0.051	0.050	--	--	--
Ba ppm	44	45	78	77	162
Cr	<68	<68	340	340	<68
Nb	<2	2	14	13	5
Rb	<2	<2	30	29	3
Sr	650	653	248	249	1260
Y	16	17	147	147	254
Zr	8	7	186	185	91
Th	0.4	0.4	--	--	--
U	1.7	1.6	--	--	--
CaO/P_2O_5	5.42	5.41	2.15	2.14	1.63
Rock type	Phosphatic limestone	Phosphatic limestone	Altered basalt	Altered basalt	Phosphorite

[1]Duplicate analysis
[2]LOI = loss on ignition at 925° C; dash means not analyzed

Table 9. Yttrium and rare earth element contents (in ppm) of a partly phosphatized limestone, Marshall Islands Fe-Mn crust leg, KODOS 98-3 cruise

	D1-10A	D1-10A[1]
Y	16	17
La	8.7	8.9
Ce	5.7	6.0
Pr	1.3	1.3
Nd	5.8	5.7
Sm	1.4	1.4
Eu	0.38	0.38
Gd	1.7	1.6
Tb	0.2	0.2
Dy	1.5	1.5
Ho	0.37	0.35
Er	1.2	1.1
Tm	0.2	0.2
Yb	1.3	1.3
Lu	0.22	0.22
∑REEs	30.0	30.2
Ce*	0.4	0.4
Y/Ho	43	49

[1]Duplicate analysis;
Ce* is Ce anomaly = chondrite-normalized 2Ce/La+Pr

Table 10. Chemical composition of substrate rocks from FSM hydrothermal leg, KODOS 98-3 cruise

	D5-2B	D5-4A	D7-2-1A	D7-4-1A	D7-6-1A	D7-9-1A	D8-2A	D9-3-1A	D9-3-1B	D9-4A	D9-6-2A	D9-11-1A
SiO_2 wt%	49.8	42.9	46.4	46.2	45.4	38.3	39.5	46.8	48.2	59.5	63.6	45.8
Al_2O_3	14.0	8.52	13.1	18.8	13.6	11.3	0.67	13.7	16.4	15.5	13.2	12.2
FeO	2.0	3.5	6.4	2.5	6.3	--	1.4	<0.1	<0.1	4.0	4.2	0.1
Fe_2O_3	5.96	5.11	8.49	10.5	8.60	11.7	10.3	16.3	13.2	3.92	2.56	19.5
MgO	10.4	22.4	4.73	1.51	4.53	3.13	34.4	3.45	3.81	2.00	2.25	4.24
CaO	9.79	6.63	9.32	11.1	9.81	14.7	0.33	1.91	2.16	6.99	5.69	3.26
Na_2O	1.70	0.69	2.97	3.91	3.07	2.18	0.23	2.16	2.22	3.08	2.56	1.42
K_2O	0.52	0.19	0.52	0.46	0.41	2.34	0.04	3.79	2.62	0.90	0.77	3.66
TiO_2	0.372	0.200	3.179	1.511	3.319	2.081	0.018	1.065	0.820	0.598	0.509	1.154
P_2O_5	0.03	0.04	0.53	0.23	0.62	0.14	0.06	0.08	0.11	0.26	0.16	0.09
MnO	0.11	0.13	0.25	0.19	0.26	0.21	0.08	0.52	0.95	0.15	0.13	0.88
LOI[2]	2.25	6.35	0.80	1.70	0.55	12.9	12.3	8.00	8.50	0.35	2.70	7.40
Total	96.93	96.66	96.69	98.63	96.47	98.98	99.37	97.88	99.09	97.25	98.33	99.69
H_2O^+	1.8	6.3	1.5	1.7	1.3	3.2	11.3	7.6	6.8	0.9	3.1	--
H_2O^-	3.10	0.90	1.10	0.30	0.08	<0.01	1.30	5.70	6.10	0.30	0.40	--
CO_2	0.02	0.03	0.07	0.46	0.07	8.70	0.04	0.04	0.07	0.04	0.01	0.07
As ppm	<2	<2	--	--	--	--	23	7	9	<2	<2	6
Ba	<20	<20	22	41	70	48	<20	112	170	130	105	122
Cr	550	2390	68	270	68	68	3560	68	140	68	<68	140
Nb	6	5	15	8	19	10	6	12	11	8	6	14
Rb	<2	4	5	6	12	45	<2	64	37	6	7	82
Sb	<0.5	<0.5	--	--	--	--	1.4	4.0	3.2	<0.5	<0.5	5.3
Sr	37	29	167	298	184	228	12	104	138	319	250	130
W	<2	<2	--	--	--	--	<2	4	<2	<2	<2	<2
Y	11	2	66	24	71	26	<2	9	15	24	14	16
Zr	30	24	192	75	191	123	14	208	98	63	60	266
Au ppb	16	<5	--	--	--	--	<5	15	<5	<5	<5	26
Rock type	Breccia	Serpentinite	Basalt	Basalt	Basalt	Breccia	Serpentinite	Tuffaceous sandstone	Tuffaceous mudstone	Andesite	Andesite	Sandstone

[1]Duplicate analysis
[2]LOI = loss on ignition at 925° C; -- = not analyzed

Table 11. Calculated growth rates and ages of bulk Fe-Mn crusts and crust layers that have <2% P content, KODOS 98-3 cruise

Sample	Interval (mm)[1]	Type	Growth rate (mm/Ma)[2]	Crust age (Ma)	Growth rate (mm/Ma)[3]	Crust age (Ma)
Marshall Islands Fe-Mn crust cruise						
D1-1A	0-100	Bulk	9.3	10.8	3.5	28.6
D1-1A[4]	0-100	Bulk	8.4	11.9	3.3	30.3
D1-1B	0-7	Layer	2.8	2.5	1.2	5.8
D1-1C	7-37	Layer	6.7	7	2.8	16.5
D1-2B	0-10	Layer	4.2	2.4	1.9	5.3
D1-2C	10-25	Layer	6.6	4.7	2.8	10.7
D1-2D	25-55	Layer	7.5	8.7	3.0	20.7
D1-4A	0-45	Bulk	4.2	10.7	1.9	23.7
D2-1B	0-10	Layer	1.5	6.7	0.6	16.7
D2-1C	10-60	Layer	3.0	23.4	1.3	55.2
D2-1C[4]	10-60	Layer	3.3	21.9	1.5	50.0
D2-2B	0-30	Layer	1.8	16.7	0.7	42.8
D2-4A	0-25	Bulk	2.7	9.3	1.2	20.8
D2-5A	0-20	Layer	2.6	7.7	1.1	18.2
D2-6A	0-32	Bulk	4.5	7.1	2.0	16.0
FSM Hydrothermal cruise						
D5-2A	0-8	Bulk	8.0	1.0	3.1	2.6
D5-2A[4]	0-8	Bulk	8.5	0.9	3.3	2.4
D7-11A	0-5	Bulk	15.4	0.3	4.5	1.1
D9-5-1A	0-5	Bulk	12.0	0.4	4.0	1.3
D9-6-1A	0-9	Bulk	44.1	0.2	6.1	1.5
D8-1A	Stratabound Mn		--	--	38.3	0.4

[1]Intervals measured from the outer surface of crusts
[2]From equation of Puteanus and Halbach (1988); age of a layer is for the base of that layer
[3]From equation of Manheim and Lane-Bostwick (1988)
[4]Duplicate sample

Table 12. X-ray diffraction mineralogy of Fe-Mn crusts and hydrothermal deposits from Marshall Islands and FSM, KODOS 98-3 cruise

Sample	Type & Interval (mm)[1]	δ-MnO_2 (%)[2]	Others (%)
Marshall Islands Fe-Mn crust leg			
D1-1A	Bulk (0-100)	95	4-CFA, 1-goethite
D1-1B	Layer (0-7)	98	2-smectite
D1-1C	Layer (7-37)	99	1-goethite
D1-1D	Layer (37-102)	87	13-CFA, <1-quartz
D1-2A	Bulk (0-95)	91	6-CFA, 2-pyroxene , 1- smectite
D1-2B	Layer (0-10)	96	4-smectite
D1-2C	Layer (10-25)	94	2-plagioclase, 2-pyroxene, 1-quartz, 1-goethite
D1-2D	Layer (25-55)	95	2-goethite, 1-plagioclase, 1-quartz , <1- calcite
D1-2E	Layer (55-90)	85	12-CFA, 2-smectite, 1-goethite
D1-3A	Bulk (0-62)	94	6-CFA
D1-4A	Bulk (0-45)	97	3-K-feldspar
D2-1A	Bulk (0-142)	95	5-CFA
D2-1B	Layer (0-10)	99	1-calcite
D2-1C	Layer(10-60)	99	1-goethite
D2-1D	Layer (60-100)	82	16-CFA, 2-goethite
D2-1E	Layer (100-150)	93	5-CFA, 1-goethite, <1-quartz
D2-2A	Bulk (0-98)	90	10-CFA
D2-2B	Layer (0-30)	100	--
D2-2C	Layer (30-47)	88	8-CFA. 3-phillipsite, 1-goethite
D2-2D	Layer (47-82)	74	26-CFA
D2-3A	Bulk (0-110)	92	6-CFA, 2-smectite
D2-4A	Bulk (0-25)	99	1-plagioclase
D2-5A	Layer (0-20)	94	4-smectite, 1-plagioclase, 1-quartz
D2-5B	Layer (20-35)	69	14-CFA, 9-phillipsite, 7-plagioclase, 1-goethite
D2-6A	Bulk (0-32)	93	5-CFA, 1-plagioclase, 1-quartz
FSM Hydrothermal leg			
D5-2A	Bulk (0-8)	94	5-plagioclase, 1-calcite
D5-16A	Mn sandstone	?	25-birnessite, 50-plagioclase,12-serpentine, 6-pyroxene, 4-amphibole, 3-quartz
D7-11A	Bulk (0-5)	94	2-calcite, 2-plagioclase, 2-quartz
D8-1A	Stratabound Mn	?	78-birnessite, 17-smectite, 5-quartz
D9-5-1A	Bulk (0-5)	95	3-plagioclase, 1-calcite, 1-quartz
D9-6-1A	Bulk (0-9)	91	5-quartz, 2-calcite, 2-plagioclase

[1]Intervals measured from the outer surface of crusts;

[2]Percentages were determined by using the following weighting factors relative to quartz set at 1: δ-MnO_2 70; todorokite 10; birnessite 12 (Hein et al., 1988); carbonate fluorapatite (CFA) 3.1; plagioclase 2.8; calcite 1.65; smectite 3.0; goethite 7.0; phillipsite 17.0; illite 6.0; pyroxene 5.0; halite 2.0 (Cook et al., 1975); the limit of detection for each mineral falls between 0.2 and 1.0%, except the manganese minerals which are greater, perhaps as much as 10% for δ-MnO_2

Table 13. Chemical composition of Fe-Mn oxyhydroxide crusts from Marshall Islands Fe-Mn crust leg, KODOS 98-3 cruise

	D1-1A	D1-1A[1]	D1-1B	D1-1C	D1-1D	D1-2A	D1-2B	D1-2C	D1-2D	D1-2E	D1-3A	D1-4A	D2-1A	D2-1B
Fe wt%	18.5	18.5	18.9	20.7	15.7	18.1	20.7	19.4	21.0	15.3	18.0	19.5	17.3	16.5
Mn	23.7	23.5	26.5	21.7	18.4	19.7	24.4	20.9	21.3	15.3	18.4	22.8	22.3	30.1
Fe/Mn	0.8	0.8	0.7	1.0	0.9	0.9	0.8	0.9	1.0	1.0	1.0	0.9	0.8	0.5
Si	2.71	2.70	3.17	4.77	2.20	4.03	4.03	5.84	4.96	3.51	3.96	4.82	2.56	2.26
Na	1.08	1.08	1.30	1.25	0.84	1.07	1.31	1.39	1.21	1.02	1.02	1.19	1.02	1.23
Al	0.34	0.34	0.21	0.89	0.33	0.83	0.50	1.34	1.01	0.93	0.85	1.02	0.44	0.01
K	0.36	0.36	0.42	0.52	0.20	0.42	0.47	0.67	0.58	0.31	0.41	0.56	0.32	0.37
Mg	0.89	0.89	1.04	0.97	0.74	0.89	1.02	1.00	1.00	0.81	0.84	1.03	0.89	1.09
Ca	5.79	5.76	2.66	2.90	12.9	7.72	2.59	3.41	3.22	13.7	9.01	2.59	8.15	2.89
Ti	1.305	1.297	1.273	1.659	1.064	1.302	1.608	1.603	1.598	0.862	1.268	1.733	1.519	1.162
P	1.50	1.51	0.48	0.58	4.19	2.25	0.45	0.71	0.62	4.67	2.76	0.44	2.27	0.43
S	0.21	0.21	0.24	0.17	0.27	0.24	0.18	0.17	0.15	0.28	0.26	0.18	0.22	0.19
H_2O^-	16.6	16.3	13.9	17.6	15.0	6.90	10.5	11.3	9.40	6.30	8.60	8.60	18.7	8.60
LOI	18.7	18.6	20.1	17.9	16.5	16.2	17.9	16.3	17.0	14.7	16.3	18.2	17.7	19.8
As ppm	198	170	--	200	185	170	--	165	--	135	206	194	149	--
B	178	184	228	204	147	197	242	202	206	155	188	218	144	208
Ba	3140	3150	1970	2610	2800	2860	2200	3430	2560	2170	2500	2700	2900	1680
Be	9.9	10.7	7.5	9.6	9.4	11.1	9.3	10.1	11.4	10.0	10.1	10.0	10.1	6.9
Bi	47.0	45.0	42.0	37.8	58.5	45.8	34.6	39.7	33.6	44.2	50.1	38.2	48.8	38.1
Cd	0.7	1.2	0.7	0.2	<0.2	0.8	1.7	2.1	1.5	0.5	0.4	0.9	0.4	2.4
Cl	6560	6440	7230	7850	5330	6840	6950	7430	8250	5290	6650	7640	7660	7870
Co	3150	3290	6000	3560	2230	3320	4890	3850	3730	1780	3290	4970	4240	9790
Cr	189	171	--	182	183	<2	--	41	--	28	174	162	<2	--
Cu	1150	1180	370	872	1280	955	481	866	894	1170	1210	937	716	410
Ga	61	63	28	24	23	48	74	79	46	40	26	33	50	61
Hf	8	7	--	15	8	13	--	12	--	13	12	14	12	--
Li	3	3	2	2	<1	2	2	5	3	5	2	3	3	<1
Mo	497	515	492	344	423	362	424	307	342	281	398	383	379	583
Nb	37	36	40	57	31	43	45	55	64	27	45	55	57	39
Ni	2510	2700	2990	2300	1940	2840	3190	3250	3200	2880	2220	3470	2830	5020
Pb	1310	1360	1460	1090	1300	1130	1380	1070	1100	935	1170	1330	1390	1610
Rb	15	16	11	7	9	12	14	17	12	16	13	11	14	13
Sb	34.9	27.8	--	31.1	32.1	26.3	--	25.2	--	23.2	31.7	30.6	25.8	--
Sc	6.6	6.7	5.6	5.5	5.4	7.0	5.5	5.4	5.4	8.8	8.3	6.5	5.3	4.8
Sn	6	8	7	11	9	9	8	12	15	11	8	12	11	8
Sr	1440	1480	1400	1300	1500	1500	1340	1260	1260	1440	1480	1450	1230	1270
Te	65.3	69.8	56.4	64.3	74.0	71.8	56.6	80.1	76.6	57.4	91.5	78.8	118	85.7
Th	10.2	10.0	--	6.5	14.5	<0.5	--	<0.5	--	6.3	11.8	10.4	11.8	--
Tl	73.3	73.4	152	91.0	59.4	94.7	122	112	104	60.4	69.1	137	116	213
U	<0.5	<0.5	--	11.5	8.0	<0.5	--	<0.5	--	13.2	11.6	17.0	<0.5	--
V	646	727	648	556	610	676	704	624	705	552	607	662	576	666
W	<4	<4	--	74	<4	<4	--	<4	--	<4	<4	113	<4	--
Zn	576	612	528	635	549	719	626	708	741	679	627	800	520	611
Zr	499	502	513	652	367	524	481	585	685	442	488	581	471	391
Au ppb	<2	<2	5	<2	6	<2	--	<2	--	<2	<2	<2	<2	--
Hg	<5	<5	9	7	<5	6	16	9	8	6	9	<5	5	11
Ir	4	--	2	4	4	--	--	--	--	--	--	--	--	--
Os	2	--	2	--	--	--	--	--	--	--	--	--	--	--
Pd	4	--	6	4	8	--	--	--	--	--	--	--	--	--
Pt	470	--	130	320	410	--	--	--	--	--	--	--	--	--
Rh	22	--	12	21	19	--	--	--	--	--	--	--	--	--
Ru	20	--	20	18	10	--	--	--	--	--	--	--	--	--
Interval	0-100	0-100	0-7	7-37	37-102	0-95	0-10	10-25	25-55	55-90	0-62	0-45	0-142	0-10
Type	Bulk	Bulk	Layer	Layer	Layer	Bulk	Layer	Layer	Layer	Layer	Bulk	Bulk	Bulk	Layer

Table 13 continued

	D2-1C	D2-1C[1]	D2-1D	D2-1E	D2-2A	D2-2B	D2-2C	D2-2D	D2-3A	D2-4A	D2-5A	D2-5B	D2-6A
Fe wt%	19.3	19.2	14.5	18.4	15.0	18.0	14.5	14.6	16.2	18.0	18.2	15.7	18.4
Mn	25.6	25.4	17.1	22.1	21.4	28.2	24.6	16.1	23.0	26.3	26.5	10.2	20.7
Fe/Mn	0.8	0.8	0.8	0.8	0.7	0.6	0.6	0.9	0.7	0.7	0.7	1.5	0.9
Si	3.40	3.40	1.94	2.86	1.80	2.20	1.37	1.88	2.09	3.89	3.60	10.9	5.05
Na	1.22	1.22	0.82	0.96	0.91	1.25	0.91	0.79	0.93	1.27	1.29	1.60	1.20
Al	0.62	0.63	0.35	0.43	0.23	0.15	0.06	0.44	0.28	0.65	0.59	3.69	1.19
K	0.46	0.46	0.17	0.39	0.21	0.35	0.22	0.16	0.29	0.47	0.50	1.62	0.53
Mg	1.05	1.04	0.72	0.80	0.80	1.04	0.85	0.66	0.86	1.09	1.08	1.47	1.12
Ca	2.87	2.85	14.7	6.97	11.3	2.94	9.86	15.1	9.36	3.07	2.64	5.65	5.02
Ti	1.560	1.553	0.847	1.659	1.325	1.713	1.253	1.445	1.104	1.496	1.437	1.317	1.607
P	0.48	0.47	4.93	1.88	3.49	0.38	2.84	5.19	2.77	0.46	0.41	1.83	1.20
S	0.22	0.19	0.31	0.27	0.26	0.19	0.32	0.32	0.28	0.20	0.20	0.14	0.18
H_2O^-	12.2	12.3	6.30	9.40	14.1	17.1	10.0	7.30	15.7	8.80	9.70	6.30	12.9
LOI	18.7	18.8	16.0	17.1	17.5	20.4	18.8	14.9	17.7	18.5	18.5	13.2	17.4
As ppm	169	157	171	160	181	210	--	184	197	172	169	129	185
B	188	200	153	166	138	158	143	136	146	211	213	165	183
Ba	2270	2280	2140	4180	2730	2430	2810	3130	2920	1940	2000	1040	1780
Be	9.0	10.1	10.3	15.2	8.4	7.0	8.5	10.6	8.1	7.5	7.8	5.4	7.1
Bi	41.7	45.6	68.8	81.0	54.6	53.0	88.0	80.4	53.7	43.2	40.4	11.7	24.8
Cd	1.9	1.7	<0.2	<0.2	<0.2	1.4	<0.2	0.7	0.5	2.5	2.0	2.3	1.6
Cl	9770	9550	6120	9090	6670	9680	7120	5710	6520	7350	7540	5340	7880
Co	5850	5470	2420	3250	4200	8030	5430	2710	3600	6440	6640	2190	4580
Cr	<2	<2	<2	<2	163	158	--	140	145	<2	<2	58	136
Cu	917	940	914	730	700	993	947	535	914	434	381	685	607
Ga	58	47	51	55	25	31	34	27	29	51	64	49	27
Hf	11	10	9	11	8	11	--	8	8	5	<1	13	12
Li	2	2	3	2	<1	<1	<1	1	3	3	2	30	8
Mo	449	426	391	553	419	401	591	370	581	486	486	102	308
Nb	58	59	25	55	42	86	38	43	30	42	45	49	54
Ni	4260	4350	2430	2490	2300	3720	2990	1400	2650	5010	4690	4590	3100
Pb	1210	1100	1060	2170	1440	1450	1820	1880	1350	1430	1500	507	1170
Rb	19	20	12	19	17	15	10	14	15	15	16	37	19
Sb	23.1	22.6	21.5	32.7	31.0	35.8	--	37.0	28.5	23.1	25.7	28.1	30.8
Sc	5.7	5.4	10.2	5.7	5.0	5.5	6.6	4.2	6.0	4.6	4.4	10.8	7.3
Sn	12	13	9	9	10	16	9	8	6	8	8	7	7
Sr	1260	1270	1460	1550	1430	1280	1630	1750	1510	1210	1220	559	1130
Te	101	104	72.7	127	109	158	143	125	71.1	73.4	68.6	30.0	64.0
Th	<0.5	6.2	14.7	13.5	16.0	14.4	--	9.8	11.4	<0.5	5.0	<0.5	7.8
Tl	176	164	87.9	101	112	172	154	82.8	61.4	182	165	55.4	112
U	<0.5	<0.5	<0.5	10.6	15.4	<0.5	--	<0.5	12.7	<0.5	<0.5	<0.5	<0.5
V	615	659	644	814	563	541	611	545	617	631	646	420	490
W	<4	<4	<4	<4	<4	<4	--	<4	144	<4	<4	<4	<4
Zn	692	653	557	633	511	621	629	536	628	651	651	633	598
Zr	566	567	375	510	359	543	394	310	353	445	462	464	509
Au ppb	<2	<2	<2	<2	<2	45	--	<2	<2	<2	<2	<2	10
Hg	<5	<5	6	<5	<5	5	6	<5	<5	8	8	212	11
Ir	--	--	--	--	6	14	6	4	4	--	--	--	8
Os	--	--	--	--	2	2	2	--	--	--	--	--	2
Pd	--	--	--	--	6	10	4	4	6	--	--	--	14
Pt	--	--	--	--	620	1600	700	540	340	--	--	--	420
Rh	--	--	--	--	29	70	27	24	16	--	--	--	21
Ru	--	--	--	--	14	34	12	8	12	--	--	--	20
Interval	10-60	10-60	60-100	100-150	0-98	0-30	30-47	47-82	0-110	0-25	0-20	20-35	0-32
Type	Layer	Layer	Layer	Layer	Bulk	Layer	Layer	Layer	Bulk	Bulk	Layer	Layer	Bulk

All Ag contents <0.2ppm; Br <1ppm; Cs <3ppm; Ge <10ppm; In <0.5ppm; Se <5ppm; Ta <1ppm

[1]Duplicate analysis of sample

Table 14. Hygroscopic water-free (0% H_2O^-) composition of Fe-Mn crusts from Table 13

	D1-1A	D1-1A[1]	D1-1B	D1-1C	D1-1D	D1-2A	D1-2B	D1-2C	D1-2D	D1-2E	D1-3A	D1-4A	D2-1A	D2-1B
Fe wt%	22.1	22.1	21.9	25.1	18.4	19.5	23.1	21.8	23.2	16.3	19.7	21.3	21.2	18.1
Mn	28.4	28.1	30.8	26.3	21.6	21.2	27.3	23.6	23.5	16.4	20.1	24.9	27.4	32.9
Fe/Mn	0.8	0.9	0.7	1.0	0.9	0.9	0.8	0.9	1.0	1.0	1.0	0.9	0.8	0.5
Si	3.25	3.23	3.69	5.79	2.59	4.33	4.50	6.59	5.47	3.74	4.33	5.27	3.15	2.48
Na	1.29	1.29	1.51	1.51	0.99	1.15	1.46	1.56	1.33	1.08	1.12	1.31	1.25	1.35
Al	0.41	0.40	0.25	1.09	0.39	0.89	0.56	1.51	1.11	0.99	0.93	1.12	0.55	0.01
K	0.43	0.43	0.49	0.63	0.23	0.45	0.53	0.76	0.64	0.33	0.45	0.62	0.40	0.41
Mg	1.07	1.07	1.21	1.18	0.87	0.95	1.14	1.12	1.11	0.86	0.92	1.13	1.09	1.19
Ca	6.94	6.88	3.09	3.52	15.1	8.29	2.90	3.84	3.55	14.6	9.85	2.84	10.0	3.17
Ti	1.564	1.549	1.479	2.014	1.252	1.398	1.797	1.807	1.764	0.920	1.387	1.896	1.868	1.271
P	1.80	1.80	0.55	0.70	4.93	2.42	0.51	0.80	0.68	4.98	3.02	0.48	2.80	0.47
S	0.25	0.25	0.28	0.21	0.32	0.26	0.20	0.19	0.17	0.30	0.28	0.20	0.27	0.21
As ppm	237	203	--	243	218	183	--	186	--	144	225	212	183	--
B	213	220	265	248	173	212	270	228	227	165	206	239	177	228
Ba	3765	3763	2288	3167	3294	3072	2458	3867	2826	2316	2735	2954	3567	1838
Be	11.9	12.8	8.7	11.7	11.1	11.9	10.4	11.4	12.6	10.7	11.1	10.9	12.4	7.5
Bi	56.4	53.8	48.8	45.9	68.8	49.2	38.7	44.8	37.1	47.2	54.8	41.8	60.0	41.7
Cd	0.8	1.4	0.8	0.2	<0.2	0.9	1.9	2.4	1.7	0.5	0.4	1.0	0.5	2.6
Cl	7866	7694	8397	9527	6271	7347	7765	8377	9106	5646	7276	8359	9422	8611
Co	3777	3931	6969	4320	2624	3566	5464	4340	4117	1900	3600	5438	5215	10711
Cr	227	204	--	221	215	<2	--	46	--	30	190	177	<2	--
Cu	1379	1410	430	1058	1506	1026	537	976	987	1249	1324	1025	881	449
Ga	73	75	33	29	27	52	83	89	51	43	28	36	62	67
Hf	10	8	--	18	9	14	--	14	--	14	13	15	15	--
Li	4	4	2	2	<1	2	2	6	3	5	2	3	4	<1
Mo	596	615	571	417	498	389	474	346	377	300	435	419	466	638
Nb	44	43	46	69	36	46	50	62	71	29	49	60	70	43
Ni	3010	3226	3473	2791	2282	3050	3564	3664	3532	3074	2429	3796	3481	5492
Pb	1571	1625	1696	1323	1529	1214	1542	1206	1214	998	1280	1455	1710	1761
Rb	18	19	13	8	11	13	16	19	13	17	14	12	17	14
Sb	41.8	33.2	--	37.7	37.8	28.2	--	28.4	--	24.8	34.7	33.5	31.7	--
Sc	7.9	8.0	6.5	6.7	6.4	7.5	6.1	6.1	6.0	9.4	9.1	7.1	6.5	5.3
Sn	7	10	8	13	11	10	9	14	17	12	9	13	14	9
Sr	1727	1768	1626	1578	1765	1611	1497	1421	1391	1537	1619	1586	1513	1389
Te	78.3	83.4	65.5	78.0	87.1	77.1	63.2	90.3	84.5	61.3	100	86.2	145	93.8
Th	12.2	11.9	--	7.9	17.1	<0.5	--	<0.6	--	6.7	12.9	11.4	14.5	--
Tl	87.9	87.7	177	110	69.9	102	136	126	115	64.5	75.6	150	143	233
U	<0.6	<0.6	--	14.0	9.4	<0.5	--	<0.6	--	14.1	12.7	18.6	<0.6	--
V	775	869	753	675	718	726	787	703	778	589	664	724	708	729
W	<5	<5	--	90	<5	<4	--	<5	--	<4	<4	124	<5	--
Zn	691	731	613	771	646	772	699	798	818	725	686	875	640	668
Zr	598	600	596	791	432	563	537	660	756	472	534	636	579	428
Au ppb	<2	<2	6	<2	7	<2	--	<2	--	<2	<2	<2	<2	--
Hg	<6	<6	10	8	<6	6	18	10	9	6	10	<5	6	12
Ir	5	--	2	5	5	--	--	--	--	--	--	--	--	--
Os	2	--	2	--	--	--	--	--	--	--	--	--	--	--
Pd	5	--	7	5	9	--	--	--	--	--	--	--	--	--
Pt	564	--	151	388	482	--	--	--	--	--	--	--	--	--
Rh	26	--	14	25	22	--	--	--	--	--	--	--	--	--
Ru	24	--	23	22	12	--	--	--	--	--	--	--	--	--
Interval	0-100	0-100	0-7	7-37	37-102	0-95	0-10	10-25	25-55	55-90	0-62	0-45	0-142	0-10
Type	Bulk	Bulk	Layer	Layer	Layer	Bulk	Layer	Layer	Layer	Layer	Bulk	Bulk	Bulk	Layer

Table 14 continued

	D2-1C	D2-1C[1]	D2-1D	D2-1E	D2-2A	D2-2B	D2-2C	D2-2D	D2-3A	D2-4A	D2-5A	D2-5B	D2-6A
Fe wt%	22.0	21.9	15.5	22.2	17.4	21.8	16.1	15.8	19.2	19.7	20.1	16.7	21.1
Mn	29.1	29.0	18.3	26.6	24.9	34.0	27.3	17.4	27.3	28.8	29.3	10.9	23.7
Fe/Mn	0.9	0.9	0.9	1.0	0.8	0.8	0.7	1.0	0.8	0.8	0.8	1.6	1.0
Si	3.87	3.88	2.08	3.45	2.10	2.65	1.52	2.03	2.47	4.26	3.99	11.7	5.80
Na	1.39	1.40	0.88	1.15	1.06	1.50	1.01	0.85	1.11	1.39	1.43	1.70	1.38
Al	0.71	0.72	0.38	0.52	0.27	0.18	0.07	0.48	0.33	0.71	0.66	3.94	1.36
K	0.53	0.53	0.18	0.47	0.24	0.42	0.24	0.17	0.34	0.52	0.55	1.73	0.61
Mg	1.20	1.19	0.77	0.97	0.93	1.26	0.94	0.71	1.02	1.19	1.20	1.57	1.29
Ca	3.27	3.25	15.6	8.41	13.1	3.54	11.0	16.3	11.1	3.37	2.93	6.03	5.77
Ti	1.777	1.770	0.904	2.002	1.543	2.067	1.392	1.559	1.309	1.640	1.591	1.405	1.845
P	0.54	0.54	5.26	2.26	4.06	0.46	3.16	5.60	3.28	0.51	0.46	1.95	1.37
S	0.25	0.22	0.33	0.33	0.30	0.23	0.36	0.35	0.33	0.22	0.22	0.15	0.21
As ppm	192	179	182	193	211	253	--	198	234	189	187	138	212
B	214	228	163	200	161	191	159	147	173	231	236	176	210
Ba	2585	2600	2284	5042	3178	2931	3122	3376	3464	2127	2215	1110	2044
Be	10.3	11.5	11.0	18.3	9.8	8.4	9.4	11.4	9.6	8.2	8.6	5.8	8.2
Bi	47.5	52.0	73.4	97.7	63.6	63.9	97.8	86.7	63.7	47.4	44.7	12.5	28.5
Cd	2.2	1.9	<0.2	<0.2	<0.2	1.7	<0.2	0.8	0.6	2.7	2.2	2.5	1.9
Cl	11128	10889	6531	10965	7765	11677	7911	6160	7734	8059	8350	5699	9047
Co	6663	6237	2583	3920	4889	9686	6033	2923	4270	7061	7353	2337	5258
Cr	<2	<2	<2	<2	190	191	--	151	172	<2	<2	62	156
Cu	1044	1072	975	881	815	1198	1052	577	1084	476	422	731	697
Ga	66	54	54	66	29	37	38	29	34	56	71	52	31
Hf	14	12	11	13	10	14	--	9	10	6	<1	15	15
Li	2	2	3	2	<1	<1	<1	1	4	3	2	32	9
Mo	511	486	417	667	488	484	657	399	689	533	538	109	354
Nb	66	67	27	66	49	104	42	46	36	46	50	52	62
Ni	4852	4960	2593	3004	2678	4487	3322	1510	3144	5493	5194	4899	3559
Pb	1378	1254	1131	2618	1676	1749	2022	2028	1601	1568	1661	541	1343
Rb	22	23	13	23	20	18	11	15	18	16	18	39	22
Sb	26.3	25.8	22.9	39.4	36.1	43.2	--	39.9	33.8	25.3	28.5	30.0	35.4
Sc	6.5	6.2	10.9	6.9	5.8	6.6	7.3	4.5	7.1	5.0	4.9	11.5	8.4
Sn	14	15	10	11	12	19	10	9	7	9	9	7	8
Sr	1435	1448	1558	1870	1665	1544	1811	1888	1791	1327	1351	597	1297
Te	115	119	77.6	153	127	191	159	135	84.3	80.5	76.0	32.0	73.5
Th	<0.6	7.1	15.7	16.3	18.6	17.4	--	10.6	13.5	<0.6	6.1	<0.6	9.4
Tl	200	187	94	122	130	207	171	89	73	200	183	59	129
U	<0.6	<0.6	<0.5	12.8	17.9	<0.6	--	<0.5	15.1	<0.6	<0.6	<0.5	<0.6
V	700	751	687	982	655	653	679	588	732	692	715	448	563
W	<5	<5	<4	<5	<5	<5	--	<4	171	<4	<4	<4	<5
Zn	788	745	594	764	595	749	699	578	745	714	721	676	687
Zr	645	647	400	615	418	655	438	334	419	488	512	495	584
Au ppb	<2	<2	<2	<2	<2	54	--	<2	<2	<2	<2	<2	11
Hg	<6	<6	6	<6	<6	6	7	<5	<6	9	9	226	13
Ir	--	--	--	--	7	17	7	4	5	--	--	--	9
Os	--	--	--	--	2	2	2	--	--	--	--	--	2
Pd	--	--	--	--	7	12	4	4	7	--	--	--	16
Pt	--	--	--	--	722	1930	778	583	403	--	--	--	482
Rh	--	--	--	--	34	84	30	26	19	--	--	--	24
Ru	--	--	--	--	16	41	13	9	14	--	--	--	23
Interval	10-60	10-60	60-100	100-150	0-98	0-30	30-47	47-82	0-110	0-25	0-20	20-35	0-32
Type	Layer	Layer	Layer	Layer	Bulk	Layer	Layer	Layer	Bulk	Bulk	Layer	Layer	Bulk

All Ag contents <0.2ppm; Br <1ppm; Cs <3ppm; Ge <10ppm; In <0.5ppm; Se <5ppm; Ta <1ppm

[1]Duplicate analysis of sample

Table 15 Statistics for 25 bulk Fe-Mn crusts and crust layers from Marshall Islands Fe-Mn crust leg KODOS 98-3 cruise; hygroscopic water-free data from Table 14

	N	Mean	Median	SD[1]	Min[2]	Max[3]
Fe wt. %	25	20.0	20.1	2.6	15.5	25.1
Mn	25	24.9	26.3	5.4	10.9	34.0
Fe/Mn[4]	25	0.8	0.8	0.5	1.4	0.7
Si	25	4.04	3.74	2.08	1.52	11.68
Na	25	1.27	1.31	0.22	0.85	1.70
Al	25	0.78	0.56	0.77	0.01	3.94
K	25	0.49	0.45	0.30	0.17	1.73
Mg	25	1.08	1.11	0.19	0.71	1.57
Ca	25	7.53	6.03	4.68	2.84	16.27
Ti	25	1.578	1.564	0.313	0.904	2.067
P	25	2.12	1.80	1.75	0.46	5.60
S	25	0.26	0.25	0.06	0.15	0.36
H_2O^-	25	11.3	10.0	3.86	6.30	18.7
LOI	25	17.4	17.7	1.70	13.2	20.4
As ppm	20	201	196	30	138	253
B	25	204	210	35	147	270
Ba	25	2865	2931	795	1110	5042
Be	25	10.5	10.7	2.4	5.8	18.3
Bi	25	54.5	48.8	19.8	12.5	97.8
Cd	25	~1.2	~0.8	0.9	<0.2	2.7
Cl	25	8200	8059	1571	5646	11677
Co	25	5001	4340	2179	1900	10711
Cr	20	~102	~107	92	<2	227
Cu	25	911	976	308	422	1506
Ga	25	49	51	19	27	89
Hf	20	~12	~13	4	<1	18
Li	25	~4	~2	6	<1	32
Mo	25	471	474	130	109	689
Nb	25	53	49	16	27	104
Ni	25	3535	3473	1026	1510	5493
Pb	25	1513	1542	396	541	2618
Rb	25	17	16	6	8	39
Sb	20	33.0	33.6	6.0	22.9	43.2
Sc	25	7.0	6.6	1.7	4.5	11.5
Sn	25	11	10	3	7	19
Sr	25	1536	1558	258	597	1888
Te	25	96.6	84.5	36.3	32.0	191
Th	20	~9.7	~11.0	6.4	<0.5	18.6
Tl	25	130	126	50	59	233
U	20	~6.1	~0.6	7.1	<0.5	18.6
V	25	697	703	95	448	982
W	20	~23.1	~5	47	<4	171
Y	25	287	271	69	195	393
Zn	25	708	699	75	578	875
Zr	25	543	537	114	334	791
Au ppb	21	~5	~2	11	<2	54
Hg	25	~17	~6	44	<5	226
Ir	10	7	5	4	2	17
Os	6	2	2	0.1	2	2
Pd	10	8	7	4	4	16
Pt	10	648	523	484	151	1930
Rh	10	31	26	20	14	84
Ru	10	20	19	9	9	41
Depth[5]	25	1878	1805	84	1805	1970
Thickness[6]	25	47	35	37	7	142

[1]Standard deviation; [2]Minimum; [3]Maximum; [4]Ratio of means, not a mean of the summation of ratios; [5]Water depth in meters; [6]Crust thickness in millimeters

Table 16. Statistics for 9 bulk Fe-Mn crusts from Marshall Islands Fe-Mn crust leg KODOS 98-3 cruise; hygroscopic water-free data from Table 14

	N	Mean	Median	SD[1]	Min[2]	Max[3]
Fe wt.%	9	20.1	19.7	1.5	17.4	22.1
Mn	9	25.2	24.9	3.1	20.1	28.8
Fe/Mn[4]	9	0.8	0.8	0.5	0.9	0.8
Si	9	3.88	4.26	1.24	2.10	5.80
Na	9	1.23	1.25	0.12	1.06	1.39
Al	9	0.73	0.71	0.37	0.27	1.36
K	9	0.45	0.45	0.12	0.24	0.62
Mg	9	1.07	1.07	0.12	0.92	1.29
Ca	9	7.93	8.29	3.50	2.84	13.1
Ti	9	1.606	1.564	0.222	1.309	1.896
P	9	2.19	2.42	1.24	0.48	4.06
S	9	0.26	0.26	0.05	0.20	0.33
H_2O^-	9	12.3	12.9	4.23	6.90	18.7
LOI	9	17.6	17.7	0.9	16.2	18.7
As ppm	9	210	212	21	183	237
B	9	202	210	27	161	239
Ba	9	2990	3072	603	2044	3765
Be	9	10.4	10.9	1.6	8.2	12.4
Bi	9	51.7	54.8	11.4	28.5	63.7
Cd	9	~1.0	~0.8	0.8	<0.2	2.7
Cl	9	8097	7866	730	7276	9422
Co	9	4786	4889	1129	3566	7061
Cr	9	~124	~172	94	<2	227
Cu	9	967	1025	288	476	1379
Ga	9	45	36	16	28	73
Hf	9	12	13	3	6	15
Li	9	~4	~3	2	<1	9
Mo	9	485	466	106	354	689
Nb	9	51	49	11	36	70
Ni	9	3404	3144	893	2429	5493
Pb	9	1491	1568	177	1214	1710
Rb	9	17	17	3	12	22
Sb	9	33.4	33.8	4.7	25.3	41.8
Sc	9	7.2	7.1	1.3	5.0	9.1
Sn	9	10	9	2	7	14
Sr	9	1571	1611	167	1297	1791
Te	9	94.7	84.3	25.0	73.5	145
Th	9	~10.4	~12.2	6.1	<0.5	18.6
Tl	9	121	129	41	73	200
U	9	~7.5	~0.6	8.3	<0.5	18.6
V	9	693	708	61	563	775
W	9	~36	~5	64	<4	171
Y	9	288	304	58	205	366
Zn	9	712	691	81	595	875
Zr	9	535	563	78	418	636
Au ppb	9	~3	~2	3	<2	11
Hg	9	~8	~6	2	<5	13
Ir	4	6	6	2	5	9
Os	3	2	2	0.1	2	2
Pd	4	9	7	5	5	16
Pt	4	543	523	136	403	722
Rh	4	26	25	6	19	34
Ru	4	19	20	5	14	24
Depth[5]	9	1878	1805	87	1805	1970
Thickness[6]	9	79	95	40	25	142

[1]Standard Deviation; [2]Minimum; [3]Maximum; [4]Ratio of means, not a mean of the summation of ratios; [5]Water depth in meters; [6]Crust thickness in millimeters

Table 17. Statistics for 16 Fe-Mn crust layers from Fe-Mn crust leg KODOS 98-3 cruise; hygroscopic water-free data from Table 14

	N	Mean	Median	SD[1]	Min[2]	Max[3]
Fe wt. %	16	19.9	21.0	3.1	15.5	25.1
Mn	16	24.7	26.5	6.4	10.9	34.0
Fe/Mn[4]	16	0.9	0.8	0.5	1.4	0.7
Si	16	4.13	3.71	2.47	1.52	11.68
Na	16	1.30	1.37	0.26	0.85	1.70
Al	16	0.80	0.54	0.93	0.01	3.94
K	16	0.52	0.48	0.37	0.17	1.73
Mg	16	1.08	1.13	0.22	0.71	1.57
Ca	16	7.31	3.70	5.33	2.90	16.27
Ti	16	1.563	1.575	0.360	0.904	2.067
P	16	2.08	0.75	2.01	0.46	5.60
S	16	0.25	0.24	0.07	0.15	0.36
H_2O^-	16	10.7	9.85	3.64	6.30	17.6
LOI	16	17.4	17.5	2.0	13.2	20.4
As ppm	11	194	192	35	138	253
B	16	206	207	39	147	270
Ba	16	2795	2706	896	1110	5042
Be	16	10.5	10.5	2.7	5.8	18.3
Bi	16	56.1	47.3	23.5	12.5	97.8
Cd	16	~1.3	~1.2	1.0	<0.2	2.6
Cl	16	8257	8363	1912	5646	11677
Co	16	5122	4330	2622	1900	10711
Cr	11	~84	~46	91	<2	221
Cu	16	880	976	324	422	1506
Ga	16	52	52	20	27	89
Hf	11	~12	~14	4	<1	18
Li	16	~4	~2	8	<1	32
Mo	16	463	479	144	109	667
Nb	16	54	50	19	27	104
Ni	16	3608	3502	1116	1510	5492
Pb	16	1525	1536	484	541	2618
Rb	16	17	15	7	8	39
Sb	11	32.6	30.0	7.1	22.9	43.2
Sc	16	7.0	6.5	2.0	4.5	11.5
Sn	16	11	10	3	7	19
Sr	16	1516	1540	300	597	1888
Te	16	97.6	85.8	42.1	32.0	191
Th	11	~9.0	~7.9	6.8	<0.6	17.4
Tl	16	135	124	54	59	233
U	11	~4.9	~0.6	6.2	<0.5	14.1
V	16	699	702	112	448	982
W	11	~12	~5	26	<4	90
Y	16	286	263	76	195	393
Zn	16	707	710	74	578	818
Zr	16	548	525	132	334	791
Au ppb	12	~7	~2	15	<2	54
Hg	16	~22	~8	55	<5	226
Ir	6	7	5	5	2	17
Os	3	2	2	0.1	2	2
Pd	6	7	6	3	4	12
Pt	6	719	532	629	151	1930
Rh	6	34	26	25	14	84
Ru	6	20	18	12	9	41
Depth[5]	16	1877	1805	85	1805	1970
Thickness[6]	16	29	30	17	7	65

[1]Standard Deviation; [2]Minimum; [3]Maximum; [4]Ratio of means, not a mean of the summation of ratios; [5]Water depth in meters; [6]Crust thickness in millimeters

Table 18. Concentrations of yttrium and rare earth elements (ppm) in Fe-Mn crusts from Marshall Islands (D1, D2) and Fe-Mn crusts and Mn stratabound deposits from FSM (D5–D9), KODOS 98-3 cruise

	D1-1A	D1-1A[1]	D1-1B	D1-1C	D1-1D	D1-3A	D1-4A	D2-1C	D2-2A	D2-2B
Y	264	280	233	177	248	220	187	210	313	175
La	345	359	281	248	352	271	279	318	373	253
Ce	1450	1510	755	841	1560	1240	1030	1170	1470	1420
Pr	54.0	57.4	44.8	41.9	55.5	46.5	48.2	52.9	52.9	39.6
Nd	240	247	199	179	221	193	207	232	216	164
Sm	43.1	43.3	37.1	34.4	40.3	36.4	40.1	43.1	37.0	30.4
Eu	10.1	10.7	9.80	8.67	9.51	9.28	10.3	10.1	9.04	7.63
Gd	52.2	56.4	50.6	42.2	47.4	44.8	49.4	51.2	46.7	37.7
Tb	7.9	8.2	7.7	6.5	7.2	6.7	7.5	8.0	7.0	5.9
Dy	46.2	47.0	47.5	36.5	39.9	37.6	42.5	46.3	40.8	34.1
Ho	9.80	9.94	10.7	7.79	8.36	8.20	8.87	9.37	9.03	7.57
Er	29.6	30.8	32.3	23.7	24.6	23.6	25.8	29.3	27.9	22.4
Tm	4.3	4.5	4.8	3.4	3.8	3.5	3.7	4.2	4.0	3.3
Yb	28.6	28.5	31.3	20.3	24.4	23.7	25.1	29.3	27.1	21.3
Lu	4.54	4.66	4.98	3.34	3.91	3.82	3.95	4.34	4.24	3.41
Σ REE	2325	2417	1517	1497	2398	1948	1781	2008	2325	2050
Ce*	2.3	2.3	1.5	1.8	2.4	2.5	2.0	2.0	2.2	3.1
Interval[2]	B 0-85	B 0-85	L 0-7	L 7-37	L 37-102	B 0-62	B 0-45	B 0-9	B 0-98	L 0-30

	D2-2C	D2-2D	D2-3A	D2-6A	D5-2A	D5-2A[1]	D5-16A	D7-11A	D8-1A	D9-5-1A
Y	343	344	256	319	204	192	24	207	10	224
La	359	398	333	273	299	298	23.1	290	9.4	307
Ce	1790	1750	1230	710	718	663	55.1	594	6.3	673
Pr	57.0	52.2	56.2	46.7	62.1	58.8	5.1	58.8	1.7	63.9
Nd	231	208	233	209	258	247	21.5	247	7.1	271
Sm	40.2	32.5	41.1	40.5	53.8	51.3	4.8	52.9	1.9	55.6
Eu	9.68	8.16	9.96	10.6	13.0	12.6	1.30	11.1	0.86	13.6
Gd	51.3	45.9	50.8	53.7	61.9	58.9	5.8	58.6	2.1	65.4
Tb	7.8	6.6	7.6	8.0	9.4	9.0	0.9	9.1	0.3	9.8
Dy	44.3	37.6	43.1	47.0	50.4	48.1	4.9	50.2	1.7	54.1
Ho	9.66	8.96	9.44	10.4	10.2	9.54	1.10	10.1	0.44	11.0
Er	30.0	26.9	27.8	30.2	28.8	28.0	3.0	27.9	1.3	31
Tm	4.5	3.7	4.0	4.1	3.6	3.9	0.4	3.4	0.2	3.7
Yb	30.0	24.6	27.2	26.7	27.6	25.8	2.0	30.5	0.6	32.2
Lu	4.43	4.19	4.06	4.59	4.10	3.90	0.51	4.06	0.22	4.47
Σ REE	2669	2607	2077	1474	1600	1518	130	1448	34	1596
Ce*	2.7	2.6	2.0	1.4	1.2	1.1	1.2	1.0	0.4	1.1
Interval	L 30-47	L 47-82	B 0-110	B 0-32	B 0-8	B 0-8	Mn SS	B 0-5	Strat. Mn	B 0-5

[1]Duplicate analysis of sample

[2]Intervals measured from the outer surface of the crust; B = bulk, L = layer; Ce* = 2Ce/La+Pr from chondrite-normalized data

Table 19. Correlation coefficient matrix for 9 bulk crusts listed in Table 14; n=9, except for Cd, Li = 8; Th = 7; Cr, Hg = 6; Ir, Pd, Pt, Rh, Ru, and U = 4; the zero correlations for 9 points, 8 points, 7 points, 6 points, and 4 points at the 95% confidence level are |0.665|, |0.706|, |0.753|, |0.813|, |0.962|, respectively; statistically significant correlations are in bold; -- = insufficient correlation pairs

	Fe	Mn	Fe/Mn	Si	Na	Al	K	Mg	Ca	Ti	P	S	LOI	As	B	Ba	Be	Bi	Cd	Cl	Co	Cr	Cu	Ga	Hf
Mn	0.25																								
Fe/Mn	0.161	**-0.812**																							
Si	0.509	-0.371	**0.751**																						
Na	0.66	0.507	0	0.546																					
Al	0.363	-0.537	**0.853**	**0.968**	0.403																				
K	0.633	-0.167	0.546	**0.953**	0.643	**0.871**																			
Mg	0.62	0.404	0.109	0.615	**0.929**	0.509	**0.714**																		
Ca	-0.602	-0.193	-0.208	**-0.777**	**-0.76**	-0.608	**-0.871**	**-0.721**																	
Ti	0.636	0.269	0.065	0.468	**0.761**	0.408	0.549	0.634	-0.525																
P	-0.62	-0.243	-0.174	**-0.76**	**-0.796**	-0.586	**-0.864**	**-0.758**	**0.997**	-0.542															
S	-0.558	-0.144	-0.3	**-0.837**	**-0.847**	**-0.714**	**-0.892**	**-0.832**	**0.954**	-0.631	**0.958**														
LOI	0.369	**0.889**	**-0.68**	-0.417	0.445	-0.527	-0.266	0.334	0.008	0.383	-0.039	0.005													
As	0.097	0.057	0.081	-0.193	-0.217	-0.202	-0.295	-0.216	0.169	-0.324	0.187	0.253	0.262												
B	0.539	-0.072	0.371	**0.801**	0.539	0.648	**0.848**	0.495	**-0.934**	0.32	**-0.915**	**-0.844**	-0.269	-0.112											
Ba	0.095	0.267	-0.564	**-0.697**	-0.437	**-0.716**	-0.563	-0.498	0.505	-0.142	0.501	0.647	0.445	0.27	-0.48										
Be	0.311	-0.17	-0.116	-0.231	-0.343	-0.248	-0.134	-0.441	0.249	0.06	0.26	0.381	-0.002	-0.078	-0.092	**0.754**									
Bi	-0.439	0.252	-0.664	**-0.944**	-0.631	**-0.932**	**-0.899**	**-0.745**	**0.741**	-0.49	**0.732**	**0.865**	0.281	0.18	**-0.691**	**0.75**	0.422								
Cd	-0.062	0.305	-0.02	0.483	**0.712**	0.36	0.558	**0.763**	**-0.718**	0.213	**-0.751**	**-0.785**	0.025	-0.334	0.548	**-0.781**	**-0.793**	-0.613							
Cl	0.511	0.39	-0.046	0.257	**0.705**	0.24	0.345	**0.684**	-0.244	**0.86**	-0.287	-0.407	0.525	-0.33	-0.039	-0.107	-0.085	-0.352	0.199						
Co	0.015	0.529	-0.255	0.234	**0.702**	0.142	0.302	0.596	-0.527	0.517	-0.556	-0.611	0.287	-0.435	0.274	-0.549	-0.609	-0.329	**0.793**	0.512					
Cr	0.202	0.362	-0.488	-0.445	-0.134	-0.569	-0.371	-0.351	0.117	-0.207	0.117	0.285	0.436	0.566	0.038	0.742	**0.846**	0.524	-0.522	-0.544	-0.641				
Cu	0.258	-0.283	0.145	-0.19	-0.499	-0.198	-0.22	-0.531	0.275	-0.322	0.304	0.448	-0.053	0.624	-0.044	0.64	**0.685**	0.364	**-0.833**	-0.453	**-0.858**	0.739			
Ga	0.535	0.563	-0.536	-0.143	0.391	-0.322	0.093	0.295	-0.251	0.22	-0.291	-0.154	0.478	-0.258	0.209	0.405	0.457	0.163	0.051	0.187	0.049	0.798	0.09		
Hf	0.384	-0.555	0.593	0.456	-0.03	0.567	0.418	0.06	-0.003	0.46	0.016	-0.085	-0.28	-0.164	0.042	0.065	0.441	-0.372	-0.481	0.399	-0.342	-0.584	0.244	-0.213	
Li	0.393	0.143	0.271	0.368	0.562	0.407	0.339	**0.764**	-0.131	0.411	-0.166	-0.376	0.345	0.151	-0.134	-0.351	-0.521	-0.594	0.346	0.642	0.225	-0.504	-0.367	-0.196	0.239
Mo	-0.117	**0.673**	**-0.717**	**-0.695**	-0.18	**-0.799**	-0.583	-0.202	0.262	-0.443	0.237	0.423	0.585	0.504	-0.337	0.513	-0.049	0.662	-0.144	-0.253	-0.046	0.407	0.226	0.259	**-0.677**
Nb	0.44	-0.07	0.273	0.425	0.501	0.461	0.429	0.411	-0.217	**0.883**	-0.23	-0.378	0.117	-0.464	0.081	-0.162	0.172	-0.409	0.008	**0.831**	0.324	-0.432	-0.287	0.025	**0.684**
Ni	0.184	0.548	-0.259	0.342	**0.728**	0.181	0.481	**0.679**	**-0.717**	0.368	**-0.747**	**-0.714**	0.195	-0.456	0.526	-0.526	-0.51	-0.386	**0.865**	0.339	**0.888**	-0.463	**-0.732**	0.306	-0.424
Pb	-0.083	**0.821**	**-0.839**	**-0.679**	0.168	**-0.739**	-0.559	0	0.265	0.225	0.224	0.26	**0.848**	0.048	-0.511	0.446	-0.03	0.568	0.001	0.385	0.403	0.343	-0.227	0.285	-0.418
Rb	-0.104	0.321	-0.132	-0.251	0.231	-0.172	-0.317	0.317	0.325	0.051	0.287	0.113	0.512	0.251	-0.524	-0.091	-0.492	-0.03	0.277	0.384	0.137	-0.171	-0.316	-0.105	-0.181
Sb	0.281	0.044	0.048	-0.218	-0.091	-0.19	-0.297	-0.146	0.269	0.037	0.279	0.259	0.429	**0.789**	-0.248	0.463	0.232	0.154	-0.47	-0.006	-0.509	**0.827**	0.628	-0.029	0.148
Sc	0.38	-0.624	**0.757**	0.389	-0.198	0.456	0.248	-0.084	0.058	-0.119	0.084	0.062	-0.346	0.487	0.142	0.022	0.282	-0.28	-0.53	-0.158	**-0.716**	-0.011	**0.682**	-0.234	0.575
Sn	-0.057	-0.039	-0.144	-0.026	0.033	0.016	0.018	-0.148	0.02	0.583	0.03	-0.027	0.012	-0.555	-0.096	0.145	0.351	0.092	-0.17	0.407	0.299	-0.129	-0.236	-0.034	0.409
Sr	-0.211	-0.017	-0.341	-0.664	**-0.748**	-0.641	-0.638	**-0.756**	0.562	-0.537	0.586	**0.745**	0.11	0.555	-0.427	**0.831**	0.534	**0.739**	**-0.795**	-0.554	**-0.706**	0.587	**0.766**	-0.003	-0.071
Te	-0.252	0.085	-0.331	-0.534	-0.207	-0.45	-0.548	-0.392	0.589	0.238	0.572	0.513	0.255	-0.295	-0.659	0.392	0.368	0.566	-0.453	0.346	0.062	0.138	-0.071	0	0.168
Th	**-0.762**	0.132	-0.613	**-0.842**	-0.671	**-0.755**	**-0.883**	-0.748	**0.81**	-0.353	**0.824**	**0.788**	0.123	-0.209	**-0.781**	0.479	0.194	**0.796**	**-0.922**	-0.283	-0.049	0.282	-0.114	-0.067	-0.523
Tl	0.037	0.403	-0.231	0.289	**0.678**	0.201	0.375	0.541	-0.563	0.588	-0.584	-0.647	0.159	-0.641	0.362	-0.509	-0.407	-0.358	**0.763**	0.478	**0.937**	-0.352	**-0.836**	0.177	-0.229
U	0.025	0.564	-0.543	0.022	0.621	-0.001	0.171	0.523	-0.364	0.721	-0.364	-0.478	0.612	-0.749	0.117	0.256	-0.229	-0.303	0.997	0.881	**0.984**	-0.205	-0.852	0.515	0.125
V	0.211	0.388	-0.605	-0.414	-0.217	-0.566	-0.201	-0.308	-0.029	-0.192	-0.027	0.237	0.276	0.119	0.096	**0.736**	0.621	0.55	-0.42	-0.329	-0.272	0.682	0.512	0.619	-0.243
Y	-0.151	0.145	-0.131	-0.375	-0.014	-0.247	-0.436	0.089	0.542	0	0.514	0.335	0.427	0.208	**-0.683**	0.162	-0.187	0.113	-0.042	0.313	-0.149	-0.059	-0.116	-0.081	0.032
Zn	0.335	-0.117	0.22	0.533	0.088	0.441	0.634	0.169	-0.644	0.12	-0.61	-0.477	-0.29	0.021	**0.689**	-0.094	0.071	-0.402	0.015	-0.146	0.025	-0.234	0.155	-0.05	0.241
Zr	**0.858**	-0.15	0.412	**0.692**	0.505	0.608	**0.763**	0.456	-0.619	**0.677**	-0.61	-0.603	-0.027	-0.145	0.651	-0.026	0.44	-0.579	-0.1	0.394	-0.068	0.12	0.242	0.365	0.638
Hg	-0.085	-0.168	0.584	0.465	0.303	0.519	0.146	0.416	0.01	-0.158	-0.01	-0.227	-0.069	0.475	-0.044	-0.793	-0.729	-0.542	0.436	0.073	0.082	-0.493	-0.263	-0.518	-0.167
Ir	-0.042	-0.957	0.87	0.718	0.522	0.845	0.561	0.561	-0.3	0.753	-0.289	-0.636	-0.812	-0.888	0.176	-0.96	-0.781	-0.803	0.99	0.854	0.933	-0.648	-0.885	-0.57	0.87
Pd	0.197	-0.818	**0.982**	0.882	0.643	0.961	0.783	0.783	-0.514	0.699	-0.511	-0.76	-0.738	-0.635	0.36	**-0.984**	-0.848	-0.922	0.951	0.961	0.818	-0.785	-0.767	-0.515	**0.982**
Pt	-0.442	-0.213	-0.297	-0.376	-0.228	-0.295	-0.487	-0.487	0.419	0.139	0.438	0.256	-0.04	-0.478	-0.331	0.135	0.272	0.287	0.132	-0.276	0.151	0.43	-0.148	0.013	-0.297
Rh	-0.448	-0.328	-0.187	-0.286	-0.169	-0.19	-0.415	-0.415	0.383	0.218	0.403	0.181	-0.145	-0.578	-0.314	0.014	0.164	0.188	0.376	-0.17	0.265	0.333	-0.258	-0.067	-0.187
Ru	0.858	-0.015	0.501	0.703	0.924	0.574	0.753	0.753	-0.897	0.85	-0.889	-0.854	0.308	0.031	0.938	-0.263	0.22	-0.664	0.545	0.576	-0.066	0.312	0.181	0.607	0.501
Depth	0.342	-0.471	0.365	0.309	-0.239	0.254	0.299	-0.299	-0.257	-0.106	-0.209	-0.082	-0.424	0.215	0.537	0.223	0.605	-0.096	-0.436	-0.501	-0.58	0.577	**0.729**	0.155	0.3
Thick	-0.081	0.177	-0.527	**-0.752**	-0.478	**-0.704**	-0.64	-0.476	**0.72**	-0.165	**0.699**	**0.769**	0.355	-0.013	**-0.727**	**0.884**	**0.677**	**0.768**	**-0.739**	0.05	-0.488	0.545	0.396	0.341	0.143

Table 19 continued

	Li	Mo	Nb	Ni	Pb	Rb	Sb	Sc	Sn	Sr	Te	Th	Tl	U	V	Y	Zn	Zr	Hg	Ir	Pd	Pt	Rh	Ru	Depth
Mo	-0.195																								
Nb	0.373	-0.658																							
Ni	0.073	0.048	0.107																						
Pb	0.063	0.601	0.07	0.198																					
Rb	**0.874**	0.175	0.05	-0.075	0.398																				
Sb	0.33	0.207	-0.039	-0.636	0.162	0.414																			
Sc	0.207	-0.291	0.039	-0.628	-0.663	-0.058	0.506																		
Sn	-0.245	-0.422	**0.681**	0.045	0.293	-0.309	-0.223	-0.392																	
Sr	-0.487	0.568	-0.54	**-0.669**	0.175	-0.193	0.479	0.18	-0.104																
Te	-0.172	-0.034	0.473	-0.255	0.581	0.114	0.031	-0.311	**0.7**	0.118															
Th	-0.688	0.291	-0.204	-0.527	0.677	0.108	-0.077	**-0.725**	0.401	0.48	**0.744**														
Tl	0.088	-0.255	0.427	**0.849**	0.296	-0.022	-0.571	**-0.73**	0.474	**-0.729**	0.119	0.049													
U	0.404	-0.189	0.507	0.657	0.599	0.067	0.042	-0.823	0.805	-0.229	0.183	0.237	0.918												
V	-0.69	0.578	-0.398	-0.017	0.256	-0.526	0.051	-0.171	0.01	0.653	-0.037	0.161	-0.207	0.212											
Y	**0.803**	0.082	0.092	-0.374	0.341	**0.921**	0.517	0.049	-0.169	0.026	0.26	0.271	-0.222	0.126	-0.42										
Zn	-0.304	-0.094	-0.08	0.256	-0.426	**-0.684**	-0.247	0.139	0.025	0.066	-0.587	-0.574	0.045	0.266	0.356	**-0.715**									
Zr	0.142	-0.542	0.593	0.061	-0.378	-0.354	0.147	0.438	0.225	-0.274	-0.199	**-0.691**	0.097	0.185	0.092	-0.295	0.442								
Hg	0.673	-0.237	-0.089	0.004	-0.279	0.765	0.328	0.39	**-0.818**	-0.654	-0.362	-0.602	-0.115	-1	**-0.94**	0.579	-0.514	-0.366							
Ir	1	**-0.964**	0.95	0.48	-0.683	**1**	-0.342	0.215	0.35	-0.945	0.023	-0.26	0.878	1	**-0.982**	0.903	-0.389	0.25	--						
Pd	0.985	-0.811	0.843	0.803	-0.891	0.901	-0.435	0.519	-0.065	-0.954	-0.36	-0.594	0.585	--	-0.91	0.627	0.048	0.357	--	0.901					
Pt	-0.011	-0.299	0.206	-0.748	0.485	0.147	0.34	-0.636	0.877	0.067	0.814	0.721	0.602	1	-0.069	0.556	**-0.963**	-0.157	--	0.147	-0.292				
Rh	0.24	-0.406	0.312	-0.675	0.396	0.265	0.279	-0.603	0.903	-0.046	0.804	0.679	0.694	1	-0.189	0.652	**-0.987**	-0.135	--	0.265	-0.176	**0.993**			
Ru	0.419	-0.484	0.571	0.446	-0.63	0.296	0.7	0.759	-0.33	-0.527	-0.565	-0.661	0.22	1	-0.128	0.208	0.014	**0.986**	--	0.296	0.329	0.012	0.035		
Depth	-0.539	-0.23	-0.142	-0.354	-0.594	-0.699	0.233	0.556	-0.043	0.369	-0.35	-0.34	-0.399	-0.181	0.452	-0.541	0.522	0.576	-0.418	-0.522	-0.508	0.104	0.027	0.634	
Thick	-0.227	0.376	-0.015	-0.522	0.456	0.081	0.245	-0.052	0.21	0.634	0.605	0.617	-0.446	-0.097	0.481	0.353	-0.362	-0.18	-0.539	-0.906	-0.961	0.162	0.052	-0.563	-0.078

Table 20. Correlation coefficient matrix for 5 bulk crusts ≥85mm listed in Table 14; n=5, except for Cd, Li, and Th = 4; the zero correlations for 5 and 4 points at the 95% confidence level are |0.883| and |0.962|, respectively; statistically significant correlations are in bold; -- = insufficient correlation pairs

	Fe	Mn	Fe/Mn	Si	Na	Al	K	Mg	Ca	Ti	P	S	LOI	As	B	Ba	Be	Bi	Cd	Cl	Co
Mn	0.511																				
Fe/Mn	-0.116	**-0.896**																			
Si	0.486	-0.495	0.808																		
Na	0.882	0.649	-0.408	0.184																	
Al	0.141	-0.768	**0.943**	**0.926**	-0.11																
K	0.629	-0.32	0.686	**0.977**	0.32	0.845															
Mg	**0.982**	0.522	-0.134	0.467	0.873	0.144	0.629														
Ca	-0.83	-0.049	-0.366	-0.79	-0.541	-0.509	-0.84	-0.754													
Ti	0.548	0.395	-0.34	0.082	0.833	-0.026	0.171	0.597	-0.151												
P	-0.877	-0.118	-0.306	-0.769	-0.605	-0.472	-0.836	-0.812	**0.996**	-0.218											
S	-0.803	0.041	-0.389	-0.816	-0.634	-0.584	-0.838	-0.727	**0.94**	-0.387	**0.937**										
LOI	0.493	**0.981**	**-0.92**	-0.518	0.704	-0.775	-0.361	0.492	-0.017	0.503	-0.085	0.011									
As	0.082	0.612	-0.566	-0.509	0.014	-0.708	-0.449	-0.007	-0.034	-0.418	-0.03	0.203	0.548								
B	0.624	-0.221	0.582	0.853	0.299	0.649	0.841	0.524	**-0.953**	-0.052	**-0.921**	**-0.9**	-0.246	-0.026							
Ba	0.8	**0.919**	-0.665	-0.125	0.827	-0.479	0.054	0.785	-0.434	0.465	-0.497	-0.346	**0.896**	0.521	0.166						
Be	0.772	-0.04	0.332	0.778	0.715	0.613	0.824	0.769	-0.75	0.674	-0.775	**-0.897**	0.01	-0.524	0.659	0.294					
Bi	-0.346	0.613	-0.867	**-0.963**	-0.057	**-0.924**	**-0.89**	-0.286	0.753	0.047	0.709	0.793	0.613	0.447	-0.881	0.252	-0.68				
Cd	-0.066	-0.628	0.73	0.739	-0.316	0.625	0.671	-0.316	-0.749	-0.483	-0.662	-0.592	-0.603	0.018	0.925	-0.432	0.189	-0.853			
Cl	0.44	0.508	-0.472	-0.1	0.7	-0.181	0.037	0.556	0.067	**0.902**	-0.019	-0.089	0.559	-0.366	-0.316	0.479	0.454	0.303	-0.803		
Co	-0.216	0.355	-0.616	-0.614	0.198	-0.497	-0.558	-0.102	0.69	0.592	0.628	0.512	0.433	-0.257	-0.834	0.085	-0.146	0.711	-0.943	0.756	
Cu	0.669	0.378	-0.028	0.315	0.387	-0.016	0.385	0.555	-0.792	-0.18	-0.783	-0.592	0.308	0.634	0.73	0.621	0.243	-0.327	0.511	-0.312	-0.72
Ga	**0.95**	0.301	0.06	0.62	0.862	0.32	0.71	**0.903**	-0.881	0.592	**-0.91**	**-0.932**	0.327	-0.083	0.735	0.637	**0.892**	-0.534	0.209	0.367	-0.276
Hf	0.278	-0.373	0.494	0.652	0.257	0.718	0.669	0.384	-0.238	0.541	-0.266	-0.41	-0.351	**-0.915**	0.203	-0.198	0.727	-0.505	-0.139	0.531	0.178
Li	0.482	**0.989**	**-1**	-0.877	0.577	-0.951	-0.816	0.577	0.279	0.378	0.184	0.309	**0.967**	0.577	-0.56	0.904	-0.239	0.876	-0.73	0.544	0.582
Mo	0.13	0.731	-0.65	-0.545	0.042	-0.742	-0.419	0.123	0.068	-0.331	0.041	0.345	0.618	**0.897**	-0.205	0.595	-0.529	0.595	-0.338	-0.105	-0.055
Nb	0.286	0.101	-0.132	0.124	0.576	0.15	0.173	0.377	0.051	**0.924**	-0.007	-0.223	0.209	-0.699	-0.193	0.127	0.606	0.007	-0.498	0.88	0.683
Ni	0.634	0.317	-0.044	0.363	0.548	0.216	0.529	0.768	-0.328	0.547	-0.402	-0.31	0.249	-0.356	0.109	0.444	0.574	-0.099	-0.85	0.731	0.232
Pb	0.026	0.792	**-0.96**	-0.805	0.396	-0.868	-0.697	0.076	0.5	0.485	0.433	0.445	0.843	0.32	-0.711	0.532	-0.273	0.881	-0.867	0.627	0.811
Rb	-0.231	0.659	**-0.907**	**-0.936**	0.106	**-0.962**	**-0.898**	-0.254	0.57	0.109	0.543	0.562	0.715	0.597	-0.673	0.363	-0.575	**0.887**	-0.614	0.178	0.563
Sb	0.306	0.696	-0.672	-0.441	0.436	-0.68	-0.394	0.181	-0.16	0.089	-0.167	-0.108	0.741	0.798	0.059	0.67	-0.144	0.355	0.032	-0.062	-0.052
Sc	0.667	0.05	0.364	0.667	0.264	0.395	0.719	0.591	**-0.909**	-0.225	**-0.893**	-0.717	-0.047	0.292	**0.894**	0.378	0.432	-0.642	0.856	-0.336	-0.854
Sn	-0.209	-0.197	-0.035	-0.081	0.149	0.121	-0.117	-0.123	0.433	0.67	0.404	0.123	-0.066	-0.768	-0.456	-0.297	0.263	0.123	-0.446	0.636	0.762
Sr	-0.164	0.288	-0.264	-0.398	-0.354	-0.501	-0.384	-0.242	0.035	-0.749	0.064	0.324	0.183	**0.913**	0.002	0.191	-0.676	0.31	0.195	-0.646	-0.448
Te	-0.156	0.2	-0.448	-0.419	0.271	-0.287	-0.392	-0.055	0.572	0.718	0.517	0.32	0.313	-0.462	-0.689	0.001	0.068	0.5	-0.792	0.784	**0.959**
Th	-0.842	**-0.984**	--	-0.777	-0.564	-0.365	-0.831	-0.831	0.862	-0.043	0.873	0.645	-0.822	-0.419	-0.795	-0.931	-0.466	0.646	-0.993	-0.08	0.65
Tl	-0.128	-0.119	-0.104	-0.094	0.26	0.069	-0.13	-0.067	0.366	0.739	0.336	0.039	0.032	-0.7	-0.401	-0.2	0.315	0.119	-0.409	0.649	0.748
V	0.806	0.343	0.087	0.509	0.468	0.171	0.617	0.747	-0.881	-0.053	**-0.89**	-0.68	0.246	0.409	0.777	0.635	0.436	-0.435	0.508	-0.115	-0.673
Y	-0.346	0.453	-0.776	-0.874	0.063	-0.826	**-0.889**	-0.383	0.625	0.19	0.611	0.52	0.56	0.386	-0.674	0.165	-0.496	0.779	-0.612	0.168	0.615
Zn	0.193	-0.339	0.639	0.632	-0.289	0.559	0.644	0.194	-0.537	-0.578	-0.506	-0.298	-0.493	0.05	0.615	-0.123	0.111	-0.589	0.654	-0.498	-0.796
Zr	0.85	0.039	0.298	0.78	0.747	0.557	0.832	0.815	-0.865	0.586	**-0.884**	**-0.966**	0.077	-0.339	0.773	0.401	**0.976**	-0.703	0.328	0.337	-0.295
Depth	0.458	-0.328	0.612	0.779	0.167	0.623	0.721	0.327	-0.863	-0.159	-0.813	-0.833	-0.329	0.014	**0.969**	0.03	0.542	-0.873	0.949	-0.477	-0.87
Thick	0.393	0.471	-0.406	-0.075	0.568	-0.141	0.08	0.542	0.101	0.76	0.012	0.011	0.472	-0.366	-0.349	0.426	0.368	0.317	-0.9	**0.96**	0.711

Table 20 continued

	Cu	Ga	Hf	Li	Mo	Nb	Ni	Pb	Rb	Sb	Sc	Sn	Sr	Te	Th	Tl	V	Y	Zn	Zr	Depth
Ga	0.607																				
Hf	-0.377	0.368																			
Li	0.212	0.131	-0.444																		
Mo	0.493	-0.137	-0.721	0.729																	
Nb	-0.499	0.36	0.736	0.137	-0.556																
Ni	0.024	0.494	0.68	0.378	0.006	0.549															
Pb	-0.228	-0.118	-0.295	0.961	0.444	0.358	0.112														
Rb	-0.102	-0.334	-0.69	**0.98**	0.548	-0.046	-0.364	0.872													
Sb	0.585	0.263	-0.741	0.656	0.571	-0.26	-0.365	0.493	0.698												
Sc	**0.894**	0.639	-0.017	-0.279	0.221	-0.423	0.218	-0.569	-0.531	0.165											
Sn	-0.825	-0.08	0.607	-0.077	-0.688	0.872	0.183	0.308	0.051	-0.395	-0.748										
Sr	0.548	-0.318	**-0.887**	0.267	0.824	**-0.918**	-0.453	0.019	0.368	0.518	0.329	-0.87									
Te	-0.756	-0.136	0.36	0.389	-0.315	0.831	0.236	0.68	0.406	-0.131	-0.831	**0.904**	-0.661								
Th	-0.83	-0.692	-0.048	--	-0.592	0.198	-0.562	0.646	0.766	-0.294	-0.939	0.643	-0.279	0.626							
Tl	-0.737	0.018	0.544	-0.008	-0.674	**0.887**	0.132	0.359	0.124	-0.247	-0.715	**0.985**	-0.857	**0.904**	0.62						
V	**0.932**	0.715	-0.066	0.217	0.399	-0.317	0.36	-0.3	-0.336	0.321	**0.953**	-0.728	0.345	-0.693	**-0.971**	-0.678					
Y	-0.276	-0.355	-0.576	**0.979**	0.262	0.093	-0.492	0.799	**0.948**	0.614	-0.675	0.273	0.164	0.533	0.878	0.355	-0.532				
Zn	0.483	0.13	0.125	-0.682	0.129	-0.545	0.227	-0.772	-0.736	-0.378	0.769	-0.665	0.325	-0.822	-0.799	-0.745	0.629	-0.877			
Zr	0.445	**0.958**	0.571	-0.19	-0.394	0.448	0.498	-0.3	-0.537	0.02	0.586	0.07	-0.505	-0.1	-0.592	0.143	0.594	-0.492	0.183		
Depth	0.688	0.616	0.073	-0.577	-0.257	-0.288	-0.135	-0.745	-0.6	0.122	0.814	-0.454	0.065	-0.714	-0.603	-0.387	0.657	-0.554	0.537	0.665	
Thick	-0.33	0.263	0.567	0.529	-0.012	0.784	0.844	0.553	0.075	-0.225	-0.286	0.54	-0.569	0.696	-0.167	0.509	-0.074	0.011	-0.303	0.241	-0.544

Table 21. Correlation coefficient matrix for 4 bulk crusts ≤62mm listed in Table 14; n=4; the zero correlation for 4 points at the 95% confidence level is |0.962|; statistically significant correlations are in bold

	Fe	Mn	Fe/Mn	Si	Na	Al	K	Mg	Ca	Ti	P	S	LOI	As	B	Ba	Be	Bi	Cd	Cl	Co
Mn	-0.011																				
Fe/Mn	0.26	-0.91																			
Si	0.932	-0.06	0.406																		
Na	0.379	0.808	-0.492	0.471																	
Al	0.828	-0.348	0.67	0.949	0.237																
K	0.901	0.4	-0.091	0.87	0.739	0.67															
Mg	0.46	0.633	-0.255	0.618	**0.966**	0.441	0.764														
Ca	-0.455	-0.857	0.737	-0.302	-0.775	0.015	-0.732	-0.622													
Ti	0.925	0.368	-0.118	0.827	0.638	0.617	**0.981**	0.638	-0.757												
P	-0.419	-0.89	0.753	-0.292	-0.82	0.024	-0.723	-0.67	**0.996**	-0.733											
S	-0.575	-0.795	0.522	-0.556	-0.943	-0.279	-0.87	-0.878	0.916	-0.827	0.933										
LOI	0.448	0.866	-0.608	0.446	**0.967**	0.166	0.79	0.886	-0.911	0.735	-0.937	**-0.989**									
As	0.192	**-0.976**	0.895	0.185	-0.771	0.436	-0.244	-0.606	0.727	-0.186	0.774	0.69	-0.787								
B	0.285	0.727	-0.794	0.007	0.427	-0.289	0.468	0.213	-0.897	0.568	-0.867	-0.645	0.639	-0.584							
Ba	0.165	-0.437	0.145	-0.141	-0.683	-0.112	-0.157	-0.748	0.104	0.028	0.187	0.401	-0.483	0.56	0.279						
Be	0.028	-0.63	0.323	-0.22	-0.845	-0.11	-0.344	-0.868	0.359	-0.176	0.435	0.618	-0.692	0.711	0.03	**0.966**					
Bi	-0.779	-0.183	-0.226	-0.931	-0.715	-0.847	-0.866	-0.849	0.387	-0.766	0.408	0.701	-0.635	0.107	0.009	0.483	0.561				
Cd	-0.091	0.872	-0.655	0.044	0.887	-0.155	0.345	0.812	-0.603	0.223	-0.669	-0.726	0.815	-0.923	0.311	-0.821	-0.926	-0.383			
Cl	0.775	0.359	0.037	0.888	0.82	0.747	0.923	0.909	-0.556	0.832	-0.577	-0.826	0.771	-0.27	0.171	-0.487	-0.608	**-0.981**	0.498		
Co	0.012	**0.996**	-0.872	-0.007	0.853	-0.288	0.432	0.695	-0.845	0.384	-0.883	-0.819	0.891	**-0.979**	0.677	-0.509	-0.695	-0.252	0.909	0.421	
Cu	-0.026	-0.871	0.622	-0.156	-0.935	0.054	-0.452	-0.87	0.655	-0.332	0.717	0.795	-0.869	0.902	-0.34	0.808	0.928	0.479	-0.993	-0.593	-0.911
Ga	-0.372	0.93	-0.96	-0.419	0.58	-0.653	0.035	0.375	-0.644	0.009	-0.683	-0.516	0.625	**-0.965**	0.614	-0.402	-0.539	0.155	0.806	0.016	0.911
Hf	0.74	-0.68	0.795	0.715	-0.276	0.83	0.387	-0.103	0.238	0.431	0.288	0.117	-0.259	0.8	-0.266	0.435	0.463	-0.434	-0.664	0.314	-0.663
Li	0.557	0.007	0.408	0.816	0.589	0.828	0.625	0.777	-0.08	0.481	-0.119	-0.469	0.427	-0.003	-0.348	-0.649	-0.637	-0.932	0.361	0.863	0.092
Mo	-0.724	0.603	-0.844	-0.83	0.054	-0.957	-0.458	-0.17	-0.261	-0.428	-0.282	-0.002	0.124	-0.677	0.445	-0.069	-0.124	0.659	0.416	-0.522	0.553
Nb	**0.969**	-0.191	0.472	**0.974**	0.297	0.939	0.823	0.437	-0.247	0.82	-0.219	-0.441	0.312	0.341	0.038	0.086	0.008	-0.823	-0.162	0.773	-0.153
Ni	-0.122	**0.993**	-0.915	-0.145	0.781	-0.414	0.305	0.607	-0.789	0.26	-0.829	-0.733	0.819	**-0.995**	0.659	-0.495	-0.666	-0.124	0.899	0.296	**0.99**
Pb	-0.079	**0.969**	**-0.977**	-0.207	0.652	-0.5	0.292	0.434	-0.852	0.304	-0.869	-0.69	0.76	-0.931	0.832	-0.224	-0.428	0.018	0.736	0.173	0.943
Rb	0.177	0.052	0.322	0.514	0.546	0.568	0.322	0.723	0.091	0.139	0.026	-0.309	0.323	-0.134	-0.52	-0.864	-0.791	-0.735	0.504	0.662	0.142
Sb	0.531	-0.847	0.935	0.573	-0.438	0.769	0.147	-0.23	0.507	0.168	0.546	0.352	-0.475	0.91	-0.526	0.364	0.467	-0.313	-0.733	0.153	-0.823
Sc	0.196	**-0.966**	**0.985**	0.296	-0.628	0.57	-0.193	-0.412	0.783	-0.192	0.808	0.629	-0.715	0.955	-0.761	0.29	0.471	-0.077	-0.769	-0.109	-0.941
Sn	0.499	0.149	-0.293	0.153	-0.062	-0.021	0.391	-0.198	-0.55	0.559	-0.477	-0.269	0.188	0.045	0.785	0.769	0.578	0.09	-0.321	0.006	0.086
Sr	-0.042	-0.602	0.272	-0.294	-0.858	-0.187	-0.399	-0.896	0.361	-0.23	0.436	0.639	-0.703	0.673	0.043	0.961	**0.997**	0.623	-0.905	-0.663	-0.67
Te	-0.489	-0.627	0.248	-0.64	**-0.965**	-0.46	-0.786	**-0.999**	0.635	-0.664	0.68	0.888	-0.89	0.593	-0.228	0.726	0.851	0.861	-0.796	-0.92	-0.688
Tl	0.034	**0.999**	-0.906	-0.027	0.814	-0.321	0.437	0.637	-0.883	0.41	-0.912	-0.816	0.881	**-0.964**	0.755	-0.407	-0.609	-0.203	0.855	0.381	**0.993**
V	-0.196	0.298	-0.629	-0.532	-0.247	-0.681	-0.189	-0.479	-0.374	-0.026	-0.324	0.031	-0.017	-0.216	0.741	0.666	0.533	0.654	-0.174	-0.523	0.211
Y	0.314	-0.196	0.564	0.635	0.374	0.741	0.336	0.596	0.23	0.175	0.182	-0.181	0.159	0.139	-0.629	-0.687	-0.591	-0.762	0.251	0.65	-0.107
Zn	0.593	0.228	-0.313	0.266	0.075	0.067	0.521	-0.053	-0.643	0.673	-0.575	-0.401	0.316	-0.024	0.819	0.677	0.466	-0.048	-0.22	0.151	0.174
Zr	0.923	-0.268	0.379	0.772	0.015	0.723	0.685	0.084	-0.261	0.769	-0.2	-0.277	0.132	0.462	0.252	0.517	0.41	-0.5	-0.446	0.474	-0.27
Hg	-0.18	-0.255	0.501	0.185	0.143	0.363	-0.132	0.34	0.514	-0.307	0.449	0.151	-0.114	0.104	-0.829	-0.758	-0.58	-0.377	0.25	0.253	-0.175
Depth	0.066	-0.604	0.302	-0.192	-0.816	-0.097	-0.302	-0.845	0.314	-0.13	0.392	0.577	-0.655	0.694	0.072	**0.977**	**0.999**	0.538	-0.915	-0.579	-0.669
Thick	-0.146	-0.871	0.599	-0.26	**-0.971**	-0.034	-0.556	-0.912	0.715	-0.444	0.772	0.861	-0.919	0.877	-0.389	0.769	0.908	0.559	**-0.972**	-0.674	-0.912

Table 21 continued

	Cu	Ga	Hf	Li	Mo	Nb	Ni	Pb	Rb	Sb	Sc	Sn	Sr	Te	Tl	V	Y	Zn	Zr	Hg	Depth
Ga	-0.762																				
Hf	0.578	-0.896																			
Li	-0.432	-0.254	0.384																		
Mo	-0.328	0.845	-0.927	-0.686																	
Nb	0.047	-0.539	0.834	0.679	-0.868																
Ni	-0.885	0.959	-0.758	-0.014	0.66	-0.288															
Pb	-0.725	0.942	-0.704	-0.229	0.716	-0.292	0.958														
Rb	-0.532	-0.086	0.072	0.916	-0.44	0.331	0.08	-0.196													
Sb	0.67	**-0.983**	0.956	0.369	-0.92	0.683	-0.894	-0.881	0.148												
Sc	0.745	**-0.977**	0.788	0.248	-0.779	0.394	**-0.97**	**-0.992**	0.163	0.933											
Sn	0.269	0.018	0.285	-0.428	0.029	0.31	0.051	0.313	-0.741	0.048	-0.208										
Sr	0.916	-0.486	0.393	-0.693	-0.049	-0.069	-0.631	-0.39	-0.823	0.404	0.426	0.566									
Te	0.858	-0.36	0.077	-0.779	0.188	-0.463	-0.597	-0.43	-0.711	0.212	0.403	0.17	0.88								
Tl	-0.859	0.914	-0.646	0.011	0.579	-0.151	**0.985**	**0.971**	0.035	-0.825	-0.961	0.193	-0.583	-0.633							
V	0.204	0.413	-0.322	-0.882	0.645	-0.404	0.272	0.524	-0.937	-0.448	-0.495	0.745	0.575	0.47	0.313						
Y	-0.295	-0.361	0.34	0.944	-0.667	0.498	-0.184	-0.432	0.959	0.423	0.417	-0.666	-0.638	-0.59	-0.206	**-0.988**					
Zn	0.156	0.051	0.299	-0.306	-0.021	0.401	0.123	0.363	-0.639	0.039	-0.251	**0.989**	0.448	0.024	0.274	0.673	-0.575				
Zr	0.34	-0.562	0.863	0.273	-0.721	0.892	-0.381	-0.255	-0.131	0.678	0.376	0.664	0.344	-0.117	-0.219	0.009	0.074	0.707			
Hg	-0.236	-0.238	0.018	0.685	-0.355	0.035	-0.186	-0.46	0.887	0.217	0.386	-0.939	-0.595	-0.32	-0.287	-0.928	0.876	-0.898	-0.371		
Depth	0.913	-0.527	0.473	-0.631	-0.129	0.036	-0.645	-0.4	-0.802	0.462	0.449	0.617	**0.994**	0.826	-0.58	0.551	-0.602	0.51	0.443	-0.612	
Thick	**0.993**	-0.72	0.489	-0.48	-0.25	-0.065	-0.87	-0.722	-0.531	0.609	0.727	0.19	0.903	0.903	-0.865	0.206	-0.311	0.068	0.223	-0.192	0.887

Table 22. Chemical composition of Fe-Mn oxyhydroxide crusts and stratabound Mn deposits from FSM hydrothermal leg, KODOS 98-3 cruise

	D5-2A	D5-2A[1]	D5-16A	D7-11A	D8-1A	D9-5-1A	D9-6-1A
Fe wt.%	19.0	19.0	7.90	23.8	1.50	19.9	18.7
Mn	21.1	21.1	6.97	20.3	43.1	20.9	20.4
Fe/Mn	0.9	0.9	1.1	1.2	0.03	0.9	0.9
Si	6.40	6.40	17.1	5.89	2.76	6.40	7.01
Na	1.19	1.19	1.05	1.36	0.98	1.29	1.36
Al	1.49	1.49	3.34	<0.01	2.35	1.28	1.54
K	0.48	0.48	0.41	0.67	0.67	0.60	0.64
Mg	1.50	1.49	11.2	1.24	2.55	1.16	1.18
Ca	3.22	3.21	2.94	2.83	1.02	2.81	3.14
Ti	0.933	0.930	0.282	0.752	0.036	0.895	0.900
P	0.41	0.41	0.06	0.46	0.06	0.45	0.61
S	0.17	--	0.04	0.20	0.06	0.19	0.20
H_2O^-	7.70	--	2.10	8.70	2.00	10.2	7.80
LOI	17.2	17.5	9.90	16.6	19.2	16.9	16.9
B ppm	213	225	59	222	56	222	219
Ba	1420	1420	267	1180	11520	1420	1300
Be	6.2	7.2	1.7	6.7	0.6	7.0	6.8
Bi	11.1	9.6	2.1	12.1	<0.5	15.4	14.1
Cd	1.8	1.5	2.7	1.4	15.3	1.1	0.9
Cl	9090	--	5630	9310	7160	8400	7940
Co	3700	3600	309	2950	889	3110	2480
Cu	763	749	873	541	1970	620	507
Ga	51	54	18	28	58	28	40
Li	8	8	85	5	175	3	5
Mo	364	361	59	352	359	337	277
Nb	44	44	5	68	2	39	37
Ni	3530	3980	1520	2900	6280	2570	3370
Pb	1080	1100	80	1010	54	1020	863
Rb	19	20	4	40	11	21	21
Sc	10.8	9.2	19.9	7.2	3.7	8.3	6.7
Sn	6	6	<2	5	<2	5	4
Sr	1160	1090	149	1150	639	1140	882
Te	39.5	--	2.2	31.1	0.8	34.0	28.9
Tl	117	111	37.6	80.7	57.7	86.9	72.0
V	531	586	217	568	506	523	552
Zn	619	607	353	505	1610	493	452
Zr	480	480	84	578	25	504	462
Hg ppb	15	15	16	16	18	9	24
Interval	0-8	0-8	Mn	0-5	Stratabound	0-5	0-9
Type	Bulk	Bulk	Sandstone	Bulk	Mn	Bulk	Bulk

All Ag contents <0.2ppm; Ge <10ppm; In <0.5ppm

[1]Duplicate analysis of sample

Table 23. Hygroscopic water-free (0% H_2O^-) composition of Fe-Mn crusts and stratabound Mn deposits from Table 22

	D5-2A	D5-2A[1]	D5-16A	D7-11A	D8-1A	D9-5-1A	D9-6-1A
Fe wt.%	20.5	20.5	8.07	26.0	1.53	22.1	20.3
Mn	22.8	22.8	7.12	22.2	44.0	23.3	22.2
Fe/Mn	0.9	0.9	1.1	1.2	0.03	0.9	0.9
Si	6.94	6.94	17.4	6.45	2.81	7.13	7.61
Na	1.29	1.29	1.08	1.49	1.00	1.44	1.47
Al	1.61	1.61	3.42	<0.01	2.40	1.43	1.67
K	0.52	0.52	0.42	0.74	0.69	0.67	0.69
Mg	1.63	1.61	11.5	1.35	2.60	1.29	1.28
Ca	3.48	3.48	3.01	3.10	1.04	3.13	3.40
Ti	1.011	1.007	0.288	0.823	0.037	0.997	0.977
P	0.44	0.44	0.06	0.50	0.06	0.51	0.66
S	0.18	--	0.04	0.22	0.06	0.21	0.22
B ppm	231	244	60	243	57	247	238
Ba	1538	1538	273	1292	11755	1581	1410
Be	6.7	7.8	1.7	7.3	0.6	7.8	7.4
Bi	12.0	10.4	2.1	13.3	<0.5	17.1	15.3
Cd	2.0	1.6	2.8	1.5	15.6	1.2	1.0
Cl	9848	--	5751	10197	7306	9354	8612
Co	4009	3900	316	3231	907	3463	2690
Cu	827	811	892	593	2010	690	550
Ga	55	59	18	31	59	31	43
Li	9	9	87	5	179	3	5
Mo	394	391	60	386	366	375	300
Nb	48	48	5	74	2	43	40
Ni	3824	4312	1553	3176	6408	2862	3655
Pb	1170	1192	82	1106	55	1136	936
Rb	21	22	4	44	11	23	23
Sc	11.7	10.0	20.3	7.9	3.8	9.2	7.3
Sn	7	7	<2	5	<2	6	4
Sr	1257	1181	152	1260	652	1269	957
Te	42.8	--	2.2	34.1	0.8	37.9	31.3
Tl	127	120	38.4	88.4	58.9	96.8	78.1
V	575	635	222	622	516	582	599
Y	221	208	25	227	10	249	249
Zn	671	658	361	553	1643	549	490
Zr	520	520	86	633	26	561	501
Hg ppb	16	16	16	18	18	10	26
Interval	0-8	0-8	Mn	0-5	Stratabound	0-5	0-9
Type	Bulk	Bulk	Sandstone	Bulk	Mn	Bulk	Bulk

All Ag contents <0.2ppm; Ge <10ppm; In <0.5ppm

[1]Duplicate analysis of sample

Table 24. Statistics for 4 bulk Fe-Mn crusts from the Yap convergent margin hydrothermal leg KODOS 98-3 cruise; data from Table 23

	N	Mean	Median	SD[1]	Min[2]	Max[3]
Fe wt.%	4	22.2	20.5	10.2	20.3	26.0
Mn	4	22.6	22.2	10.1	22.2	23.3
Fe/Mn[4]	4	1.0	0.9	1.0	0.9	1.1
Si	4	7.03	6.94	3.17	6.45	7.61
Na	4	1.42	1.44	0.64	1.29	1.49
Al	4	~1.18	~1.43	0.86	<0.01	1.67
K	4	0.65	0.67	0.30	0.52	0.74
Mg	4	1.39	1.29	0.64	1.28	1.63
Ca	4	3.28	3.13	1.48	3.10	3.48
Ti	4	0.952	0.977	0.432	0.823	1.011
P	4	0.53	0.50	0.25	0.44	0.66
S	4	0.21	0.21	0.09	0.18	0.22
H_2O^-	4	8.60	7.80	3.97	7.70	10.2
LOI	4	16.9	16.9	7.6	16.6	17.2
B ppm	4	240	238	107	231	247
Ba	4	1456	1410	661	1292	1581
Be	4	7.31	7.34	3.29	6.72	7.80
Bi	4	14.43	13.25	6.74	12.03	17.15
Cd	4	1.42	1.22	0.73	0.98	1.95
Cl	4	9503	9354	4291	8612	10197
Co	4	3348	3231	1570	2690	4009
Cu	4	665	593	316	550	827
Ga	4	40	31	21	31	55
Li	4	6	5	3	3	9
Mo	4	364	375	167	300	394
Nb	4	51	43	27	40	74
Ni	4	3379	3176	1559	2862	3824
Pb	4	1087	1106	494	936	1170
Rb	4	28	23	16	21	44
Sc	4	9.0	7.9	4.4	7.3	11.7
Sn	4	5	5	3	4	7
Sr	4	1186	1257	546	957	1269
Te	4	36.5	34.1	16.9	31.3	42.8
Tl	4	98	88	47	78	127
V	4	595	582	267	575	622
Y	4	237	227	107	221	249
Zn	4	566	549	261	490	671
Zr	4	554	520	253	501	633
Hg ppb	4	17	16	10	10	26
Depth[5]	4	2408	2504	1099	2029	2550
Thickness[6]	4	7	5	4	5	9

[1]Standard deviation; [2]Minimum; [3]Maximum; [4]Ratio of means, not a mean of the summation of ratios; [5]Water depth in meters; [6]Crust thickness in millimeters; LOI and H_2O^- from Table 22

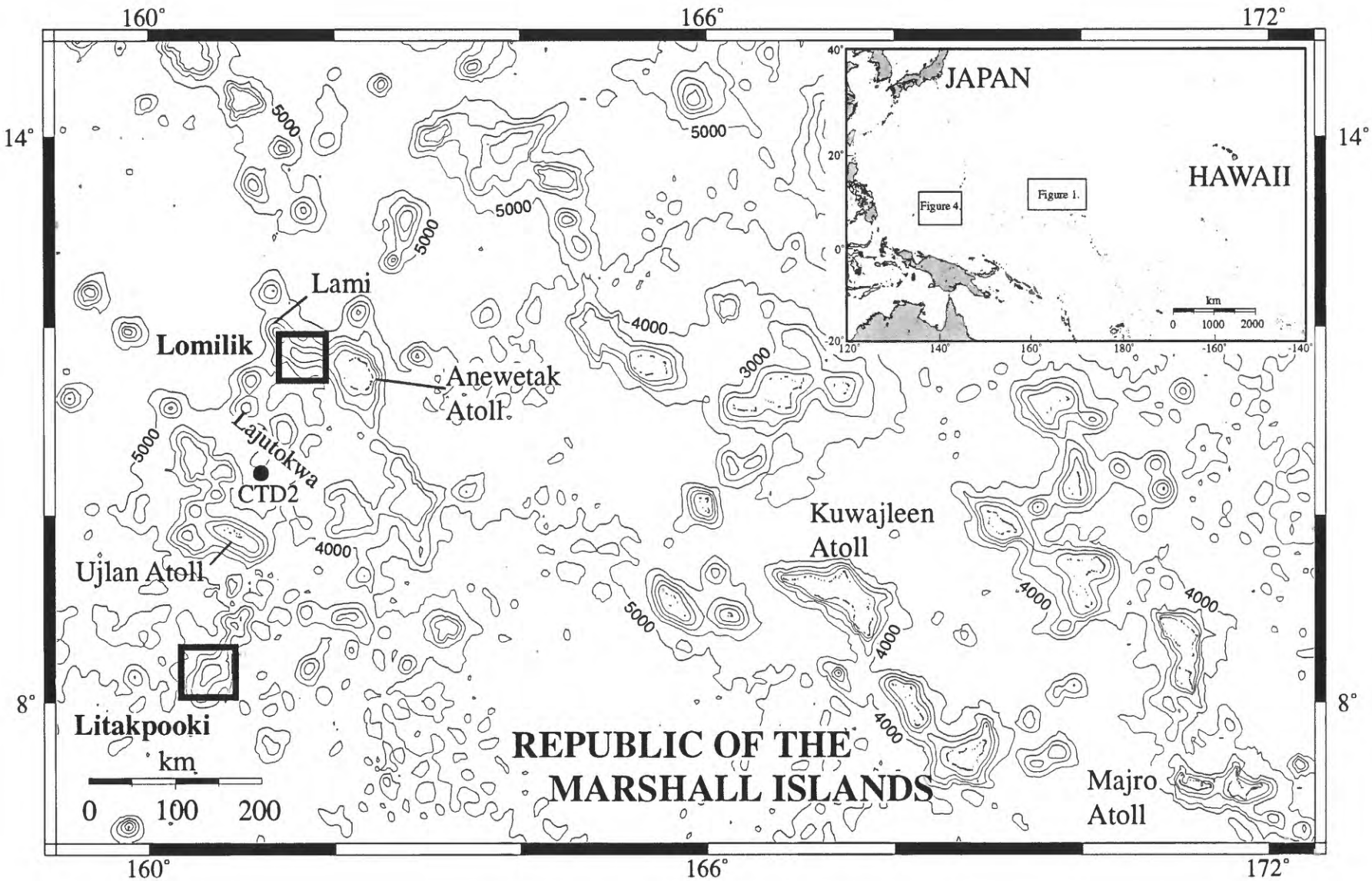

Figure 1. Atolls and seamounts comprising the Marshall Islands with the two boxed areas enclosing Lomilik Seamount and Litakpooki Ridge, which were studied during cruise KODOS 98-3; note the location of CTD 2 between Lomilik and Litakpooki seamounts. The boxed regions in the inset map show locations in Figures 1 and 4

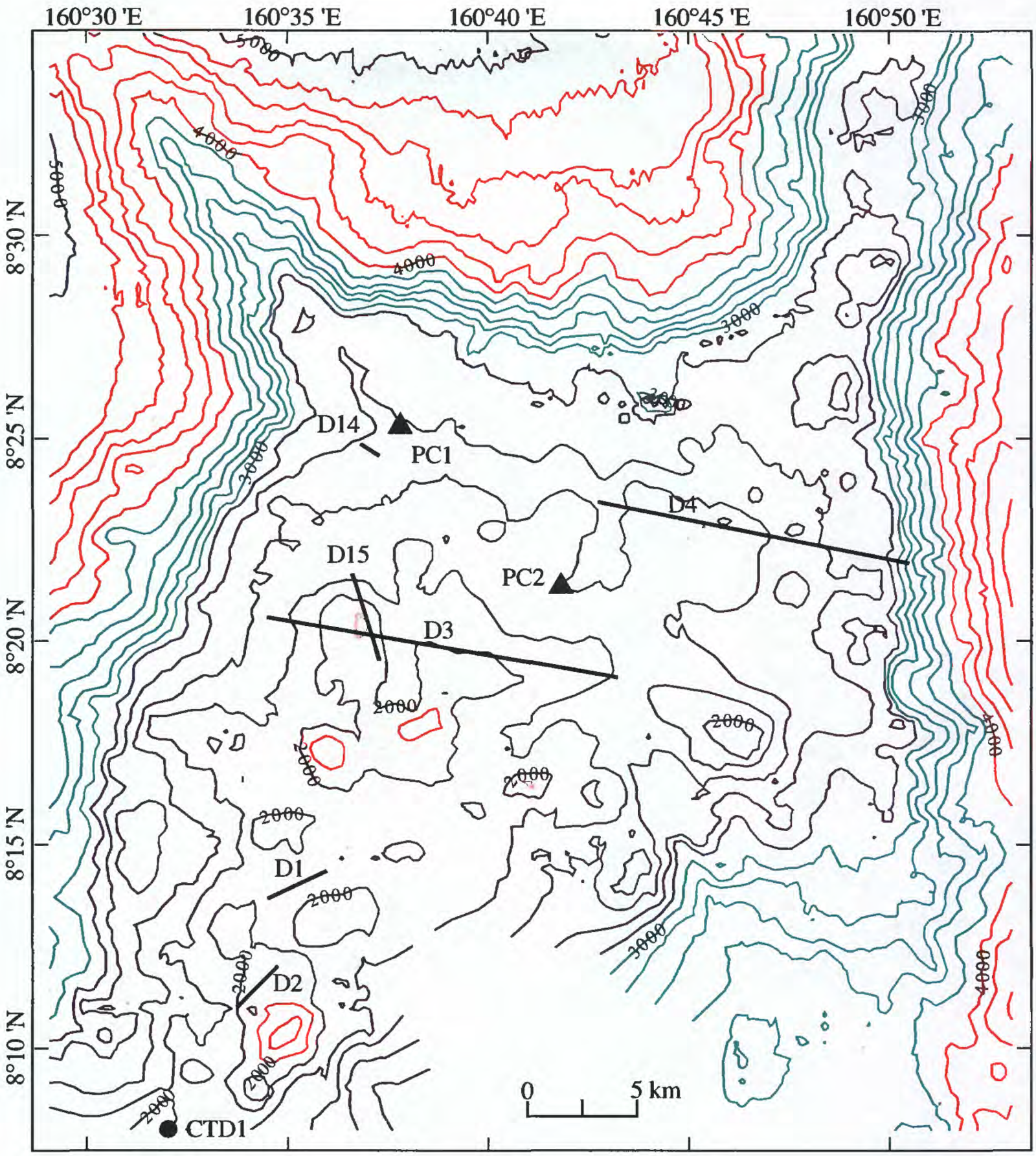

Figure 2. SeaBeam bathymetry, dredge (D), CTD, and piston core (PC) locations for Litakpooki Ridge, located south of Ujlan Atoll in the Marshall Islands group; D14 and D15 from KODOS 97-4 (Hein, Moon, et al., 1998); contour interval is 200m

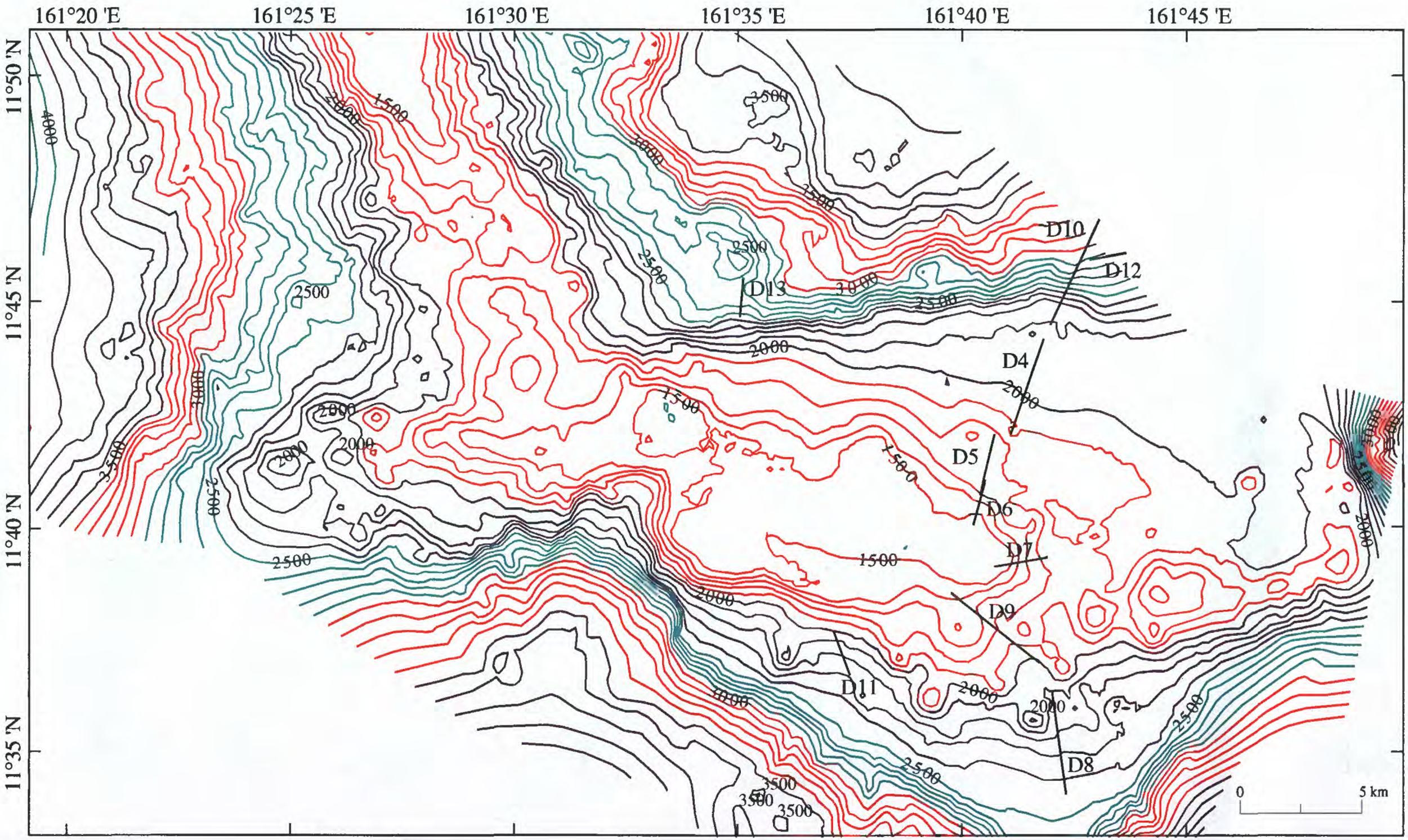

Figure 3. SeaBeam bathymetry for Lomilik Seamount, located west of Anewetak Atoll; D4-D13 from KODOS 97-4 (Hein, Moon, et al., 1998); contour interval is 100m

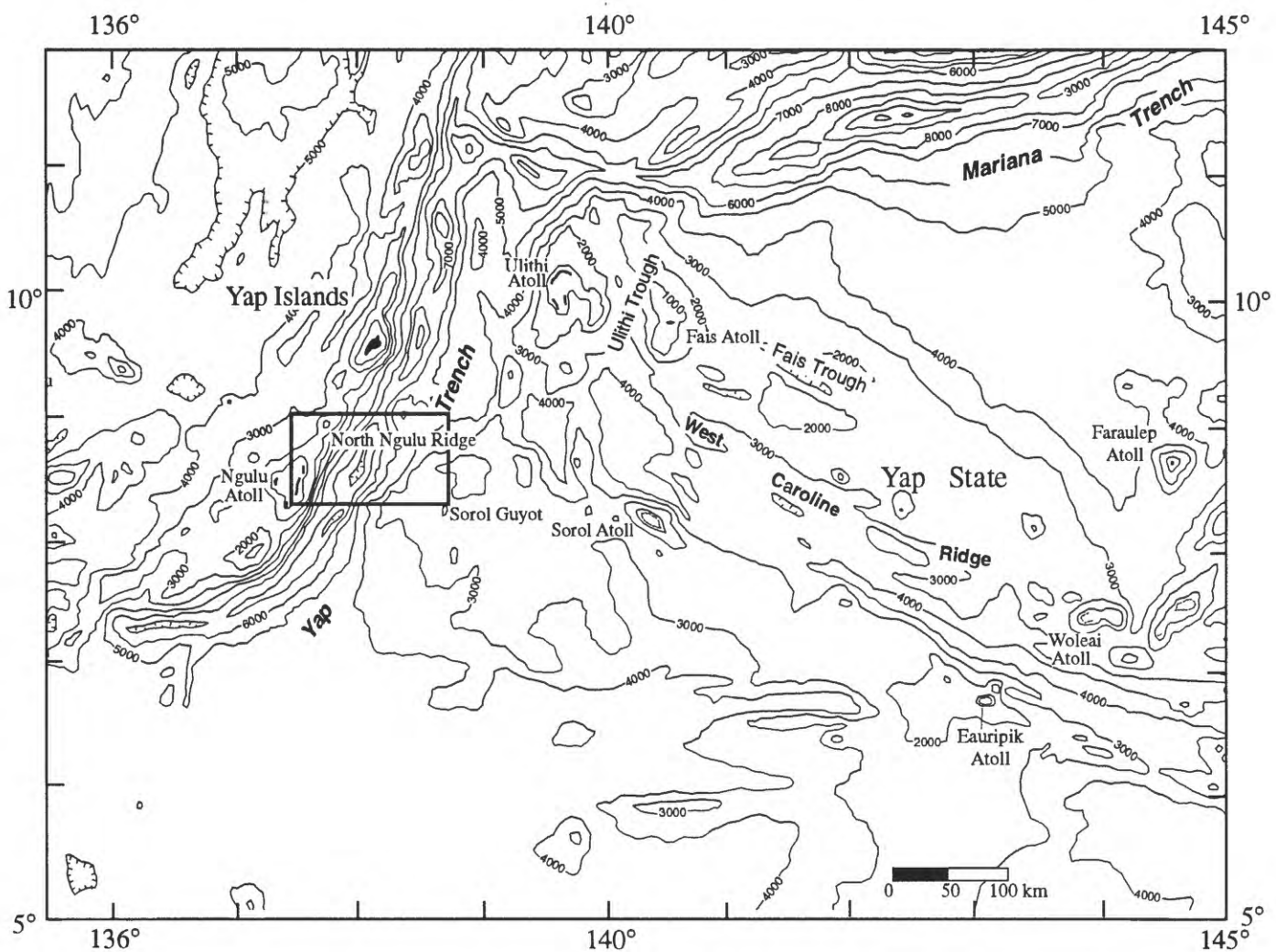

Figure 4. Atoll and island names within the Exclusive Economic Zone of the western Federated States of Micronesia, including the Yap convergent margin and the western edge of Caroline Ridge; hatchured lines are basins; boxed area was surveyed during KODOS 98-3; contour interval is 1000 m; modified from Chase et al. (1988).

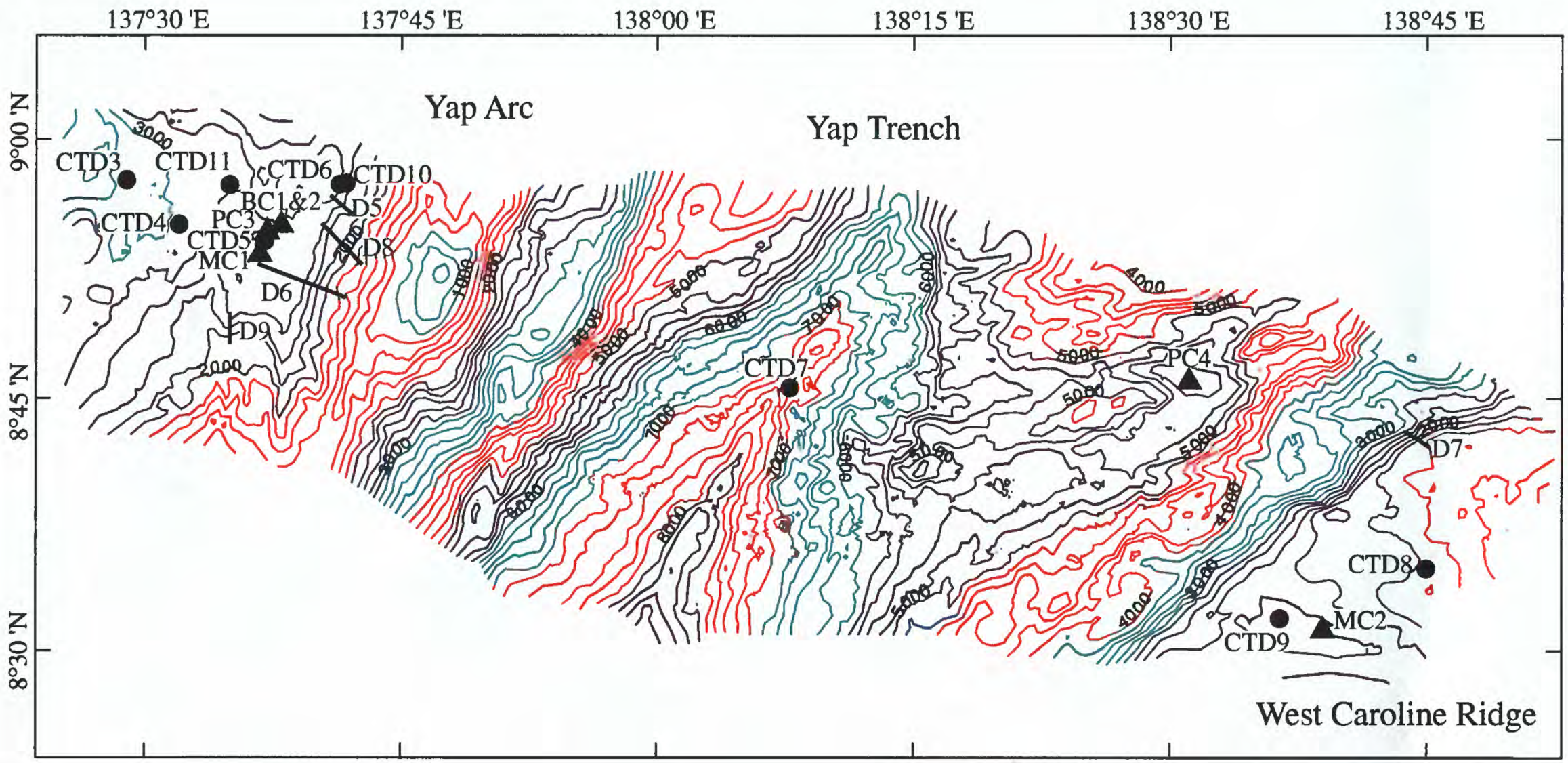

Figure 5. SeaBeam bathymetry, dredge (D), CTD, piston core (PC), box core (BC), and multiple core (MC) locations for Yap-Caroline Ridge convergent margin; contour interval is 200 m

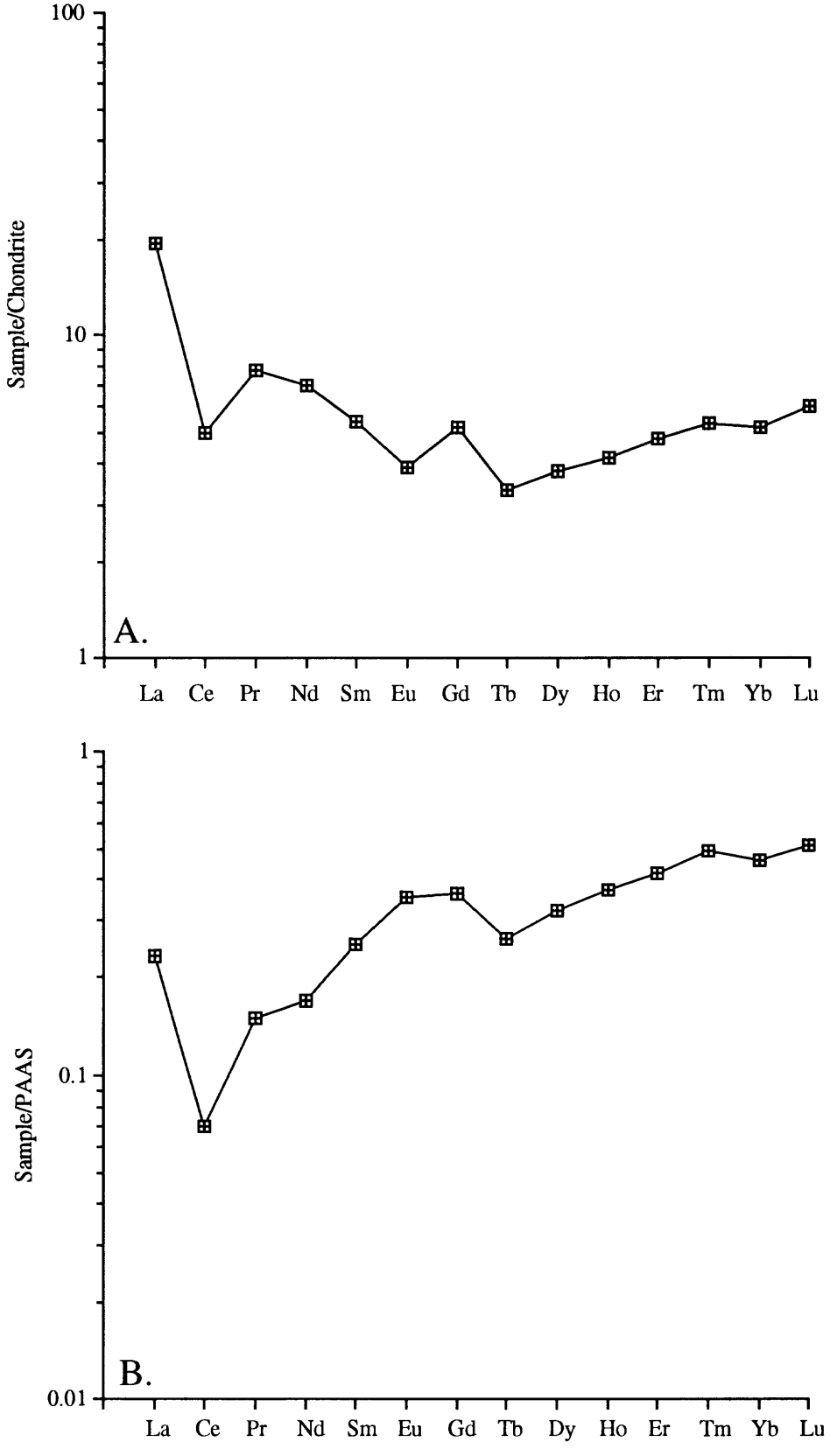

Figure 6. REE plots of phosphatized limestone sample D1-10A, Litakpooki Ridge: (A) Chondrite (Anders and Grevesse, 1989) normalized, and (B) Post Archean Australian Shale (PAAS, McLennan,1989) normalized

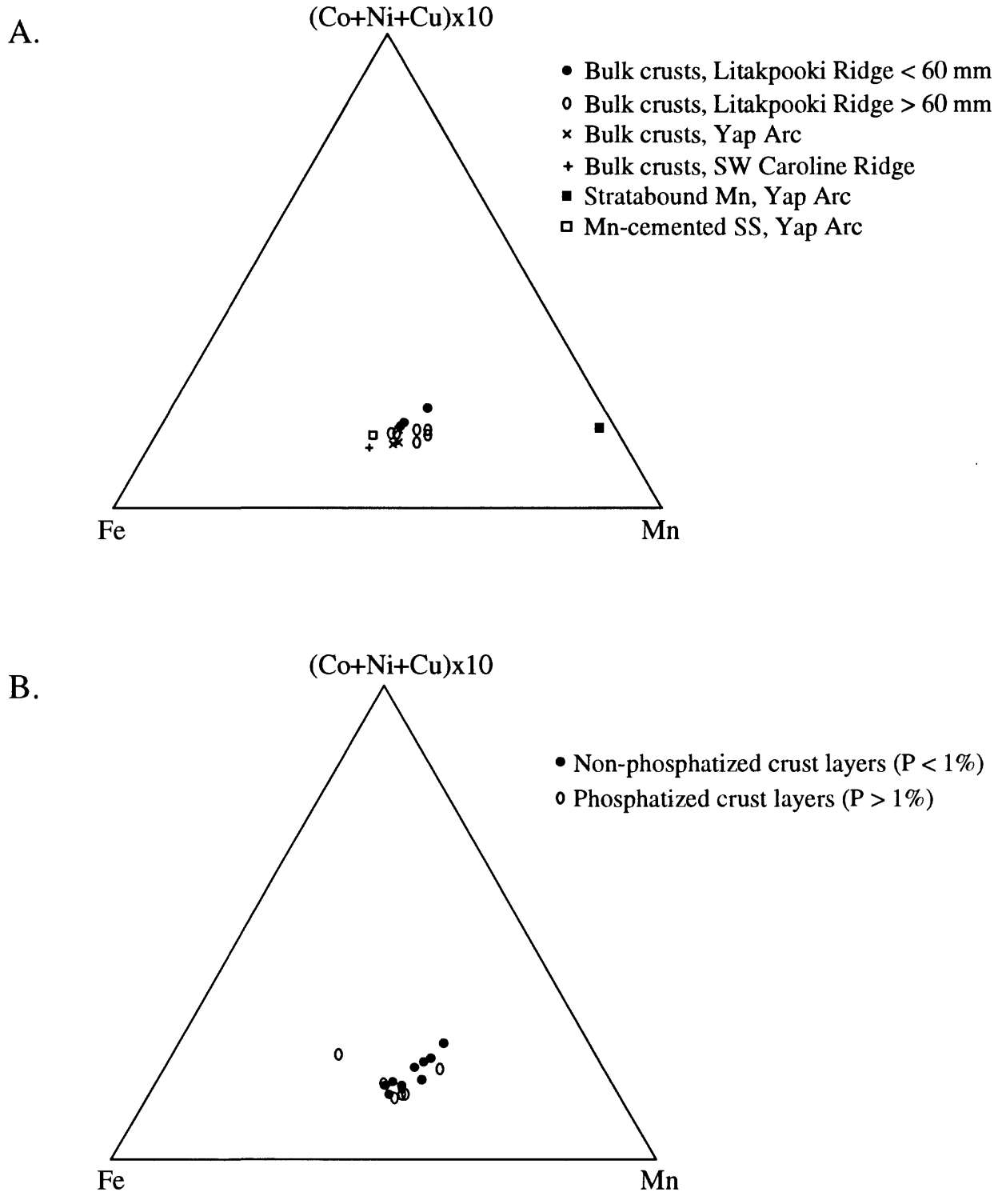

Figure 7. Mn-Fe-(Co+Ni+Cu)x10 ternary diagram after Bonatti et al. (1972) for: (A) bulk crusts, and (B) crust layers

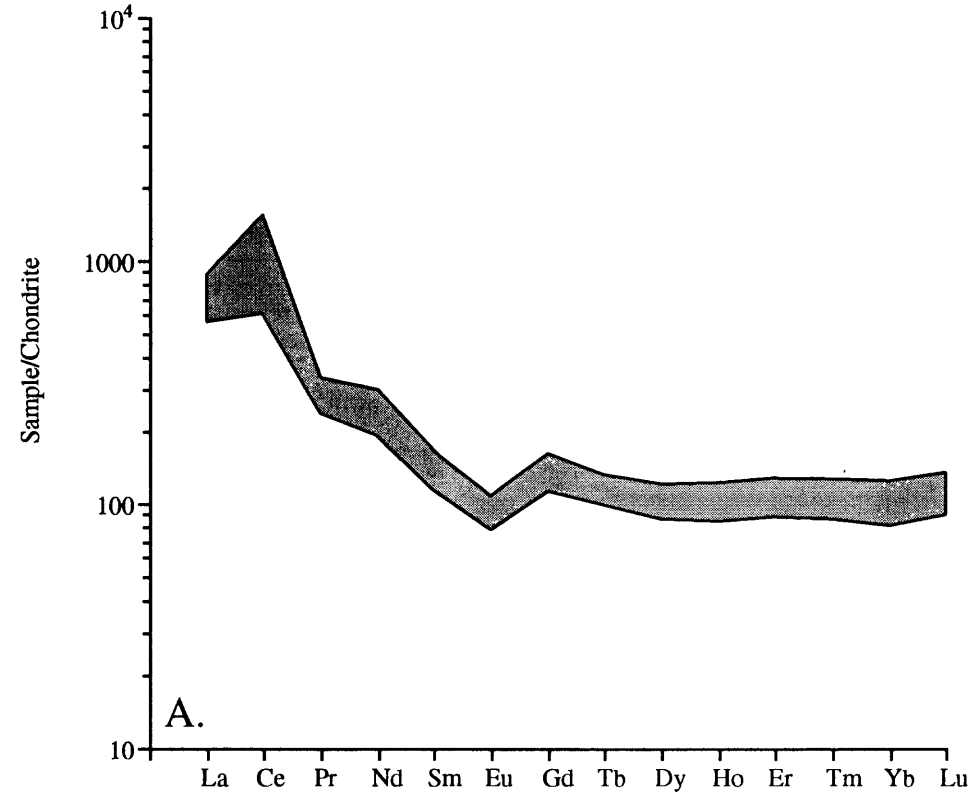

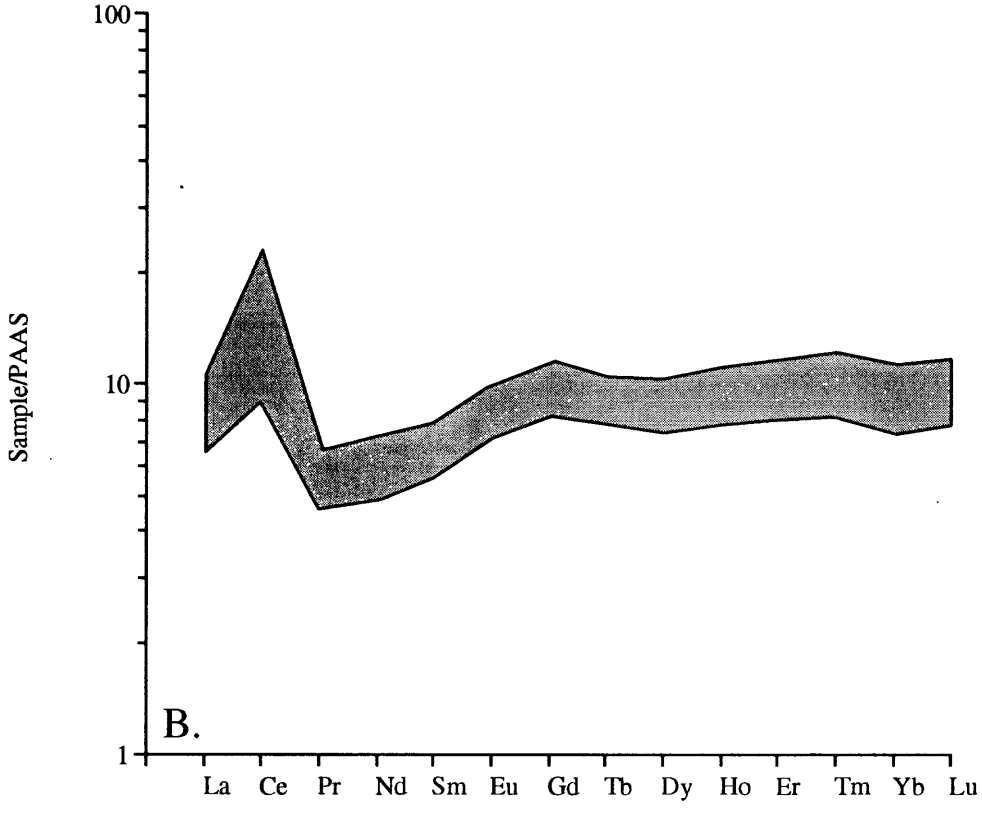

Figure 8. Range of REE plots for 13 Fe-Mn samples from Litakpooki Ridge: (A) Chondrite normalized, and (B) PAAS normalized

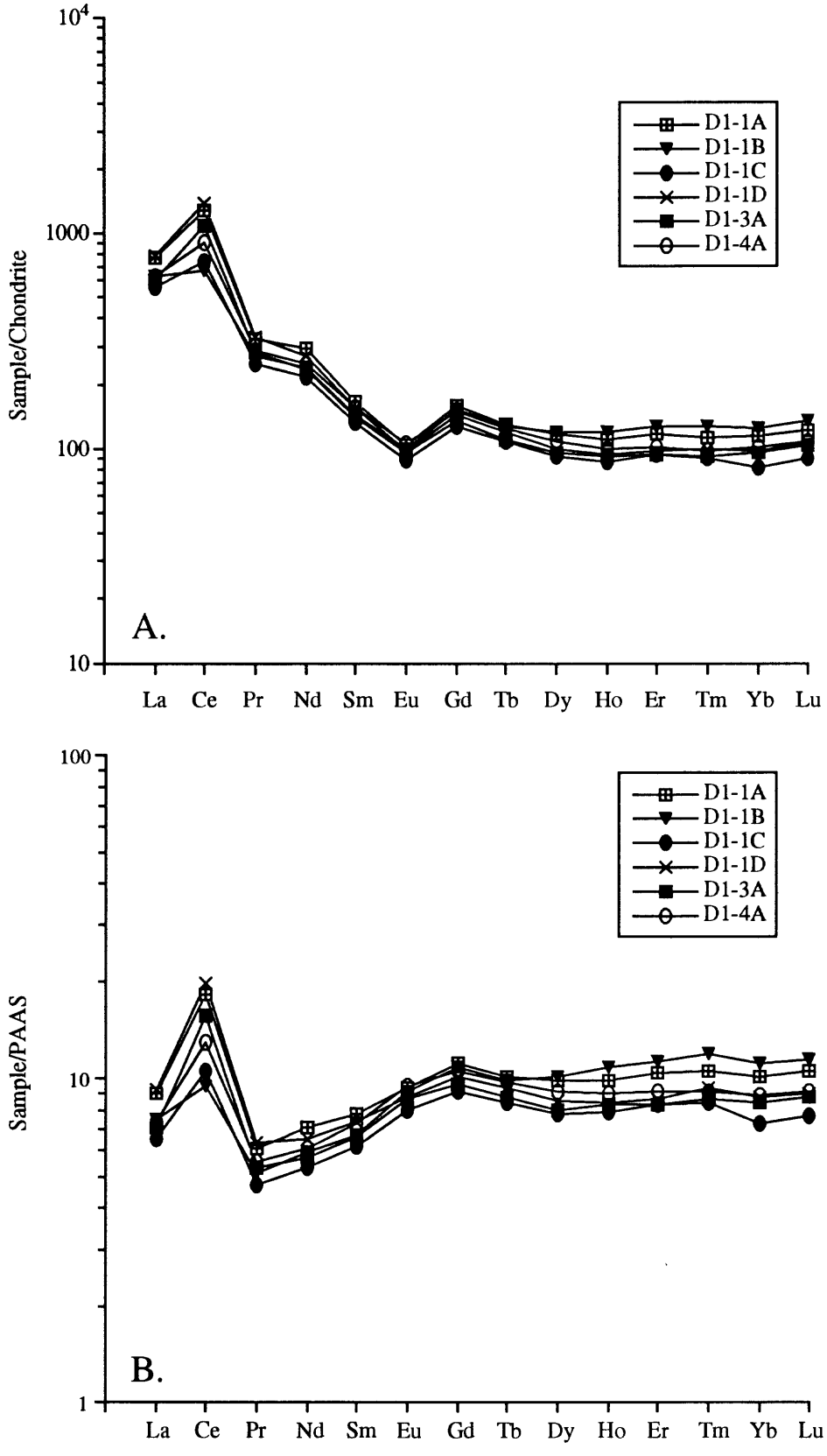

Figure 9. REE plots of bulk crusts and layers from dredge D1, Litakpooki Ridge: (A) Chondrite normalized, and (B) PAAS normalized

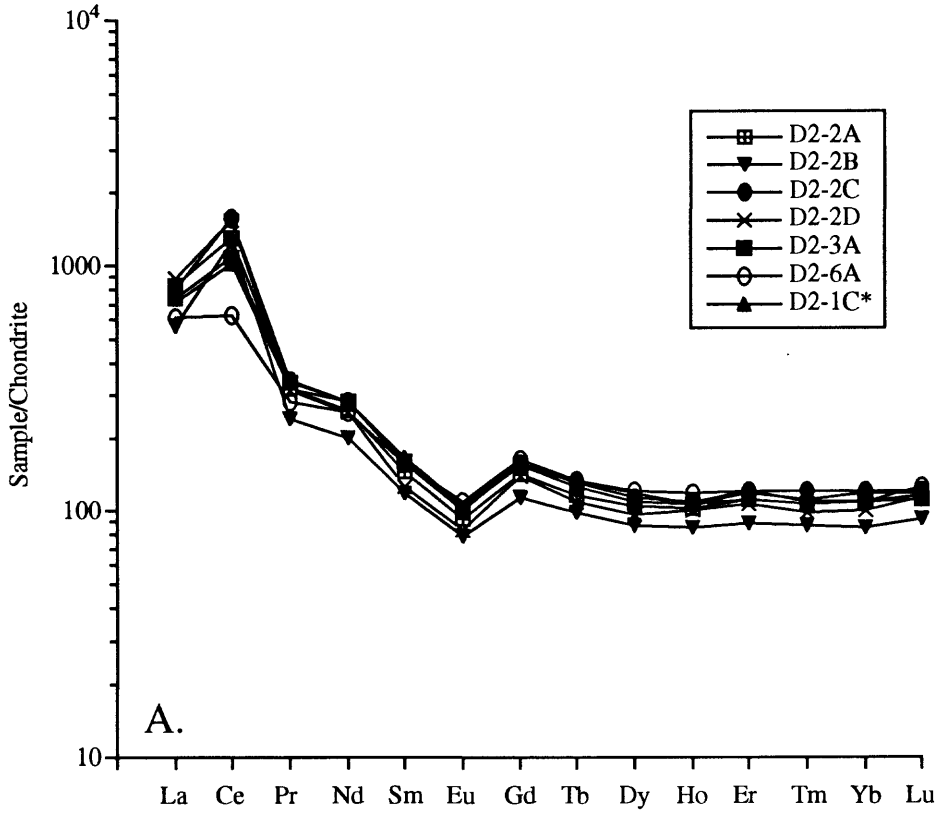

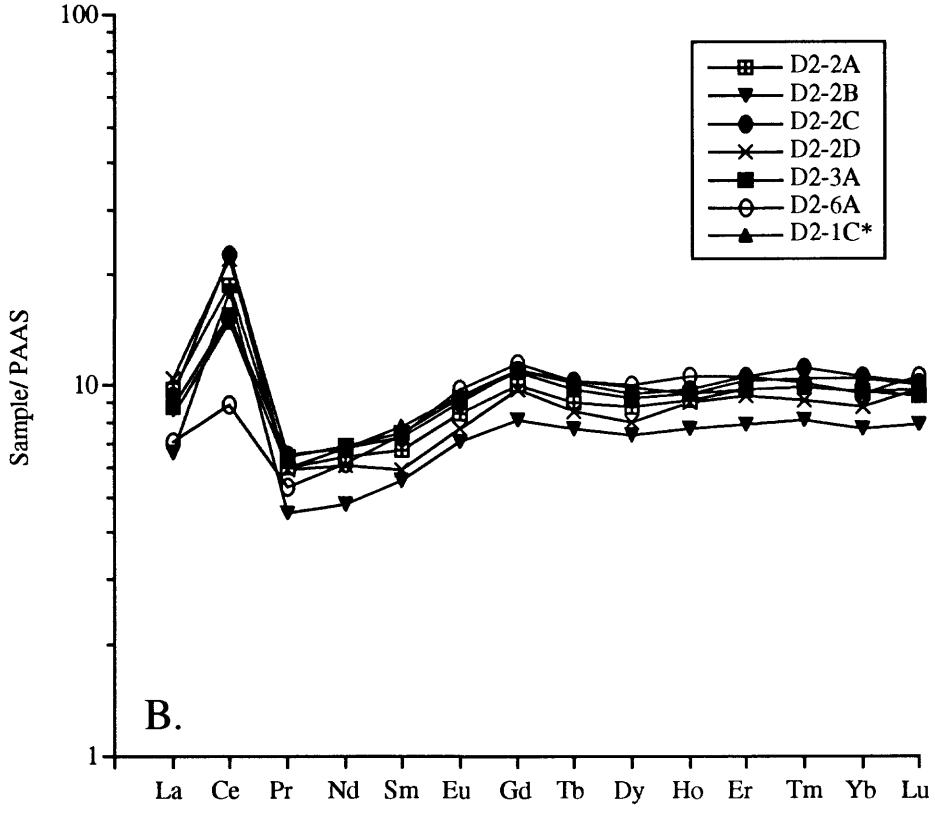

Figure 10. REE plots of bulk crusts and layers from dredge D2, Litakpooki Ridge: (A) Chondrite normalized, and (B) PAAS normalized

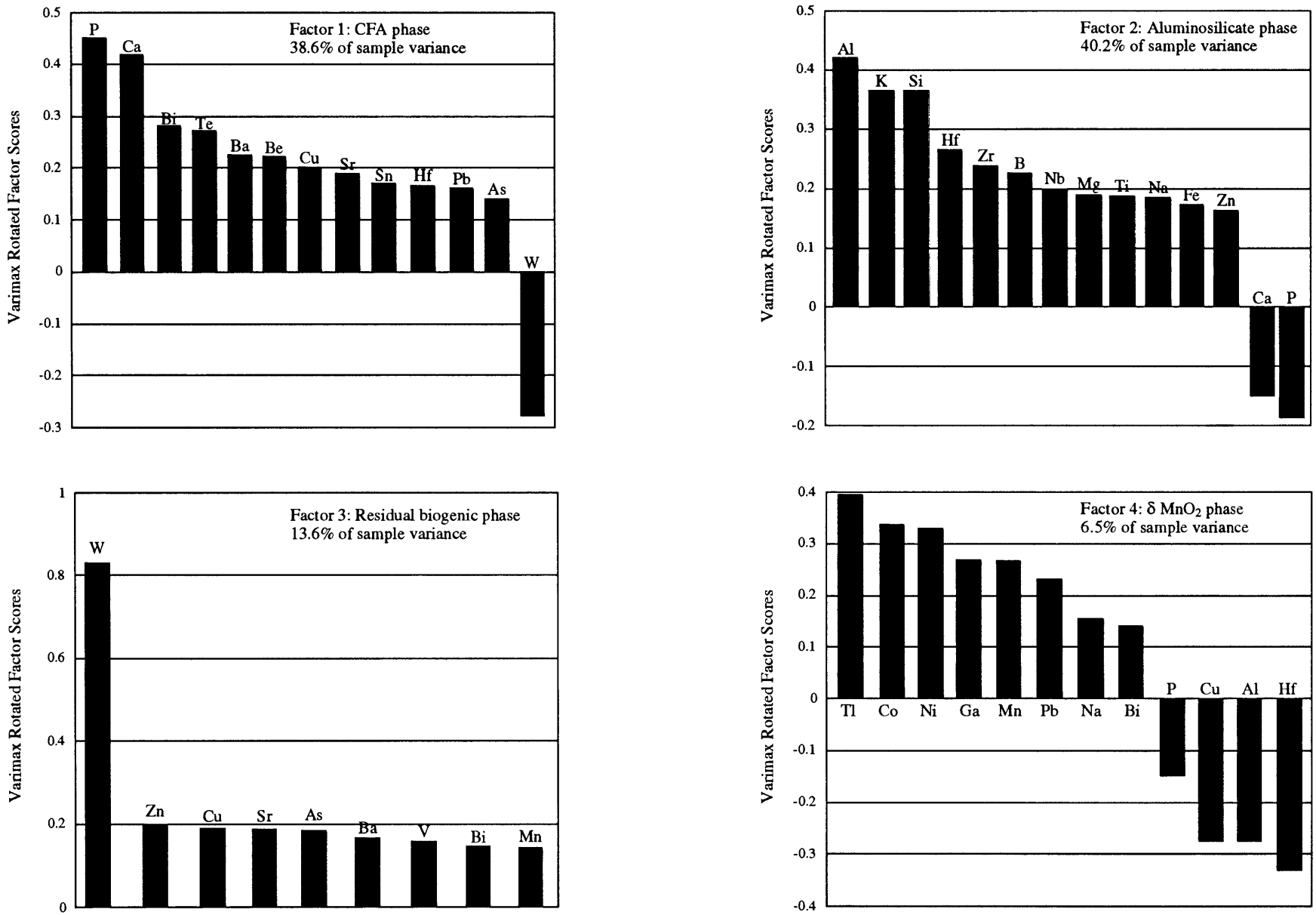

Figure 11. Four Q-mode factors for 9 bulk crusts from Litakpooki Ridge. The four factors account for 98.9% of the variance. Factor scores between 0 and |0.14| are not included because random noise makes it difficult to resolve the orientation of the factor to within 10° of an absolute direction in variable space.

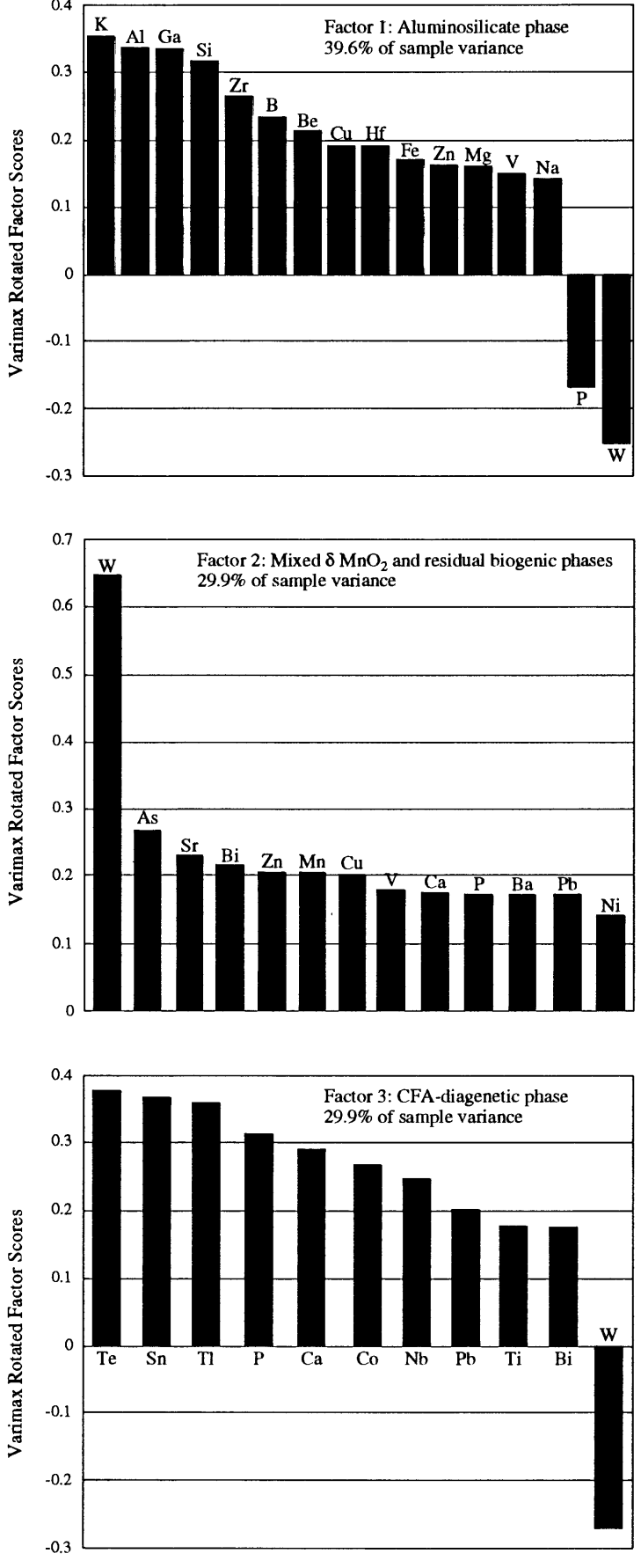

Figure 12. Three Q-mode factors for 5 bulk crusts >85mm from Litakpooki Ridge. The three factors account for 99.4% of the variance. Factor scores between 0 and |0.14| are not included because random noise makes it difficult to resolve the orientation of the factor to within 10° of an absolute direction in variable space.

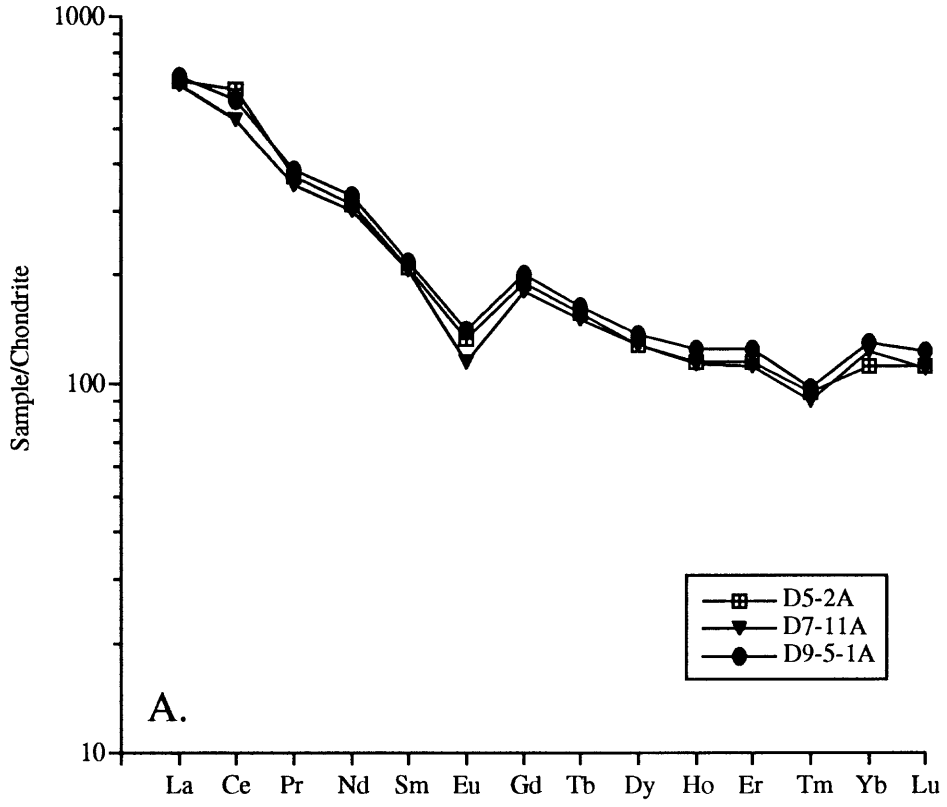

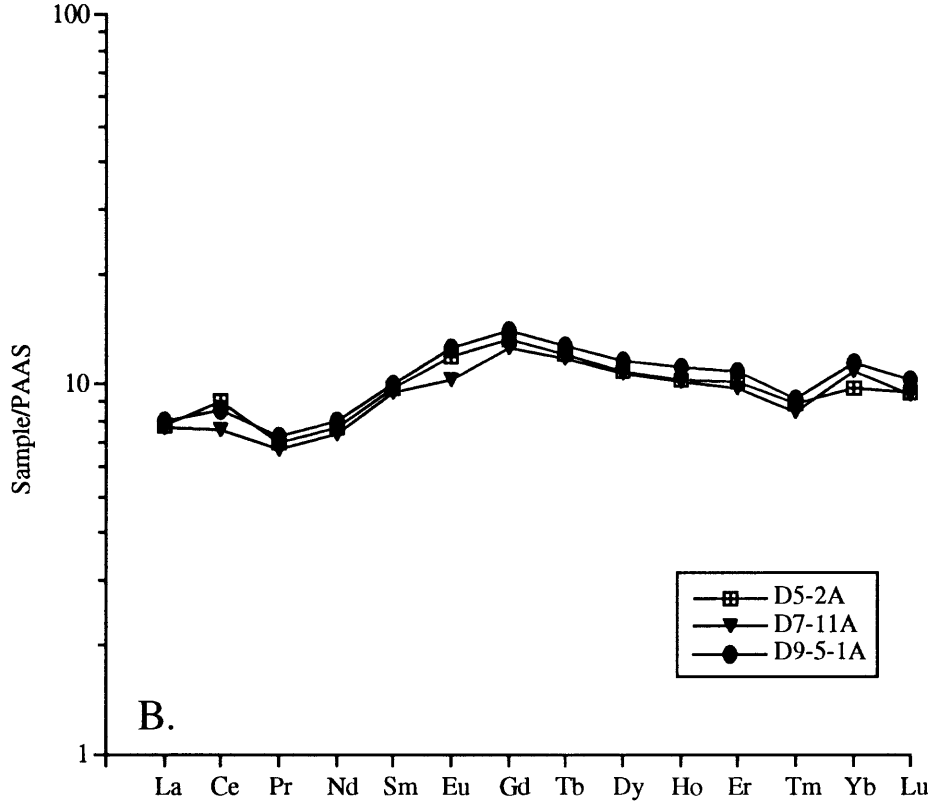

Figure 13. REE plots of bulk crusts from dredges D5, D7, and D9, FSM: (A) Chondrite normalized, and (B) PAAS normalized

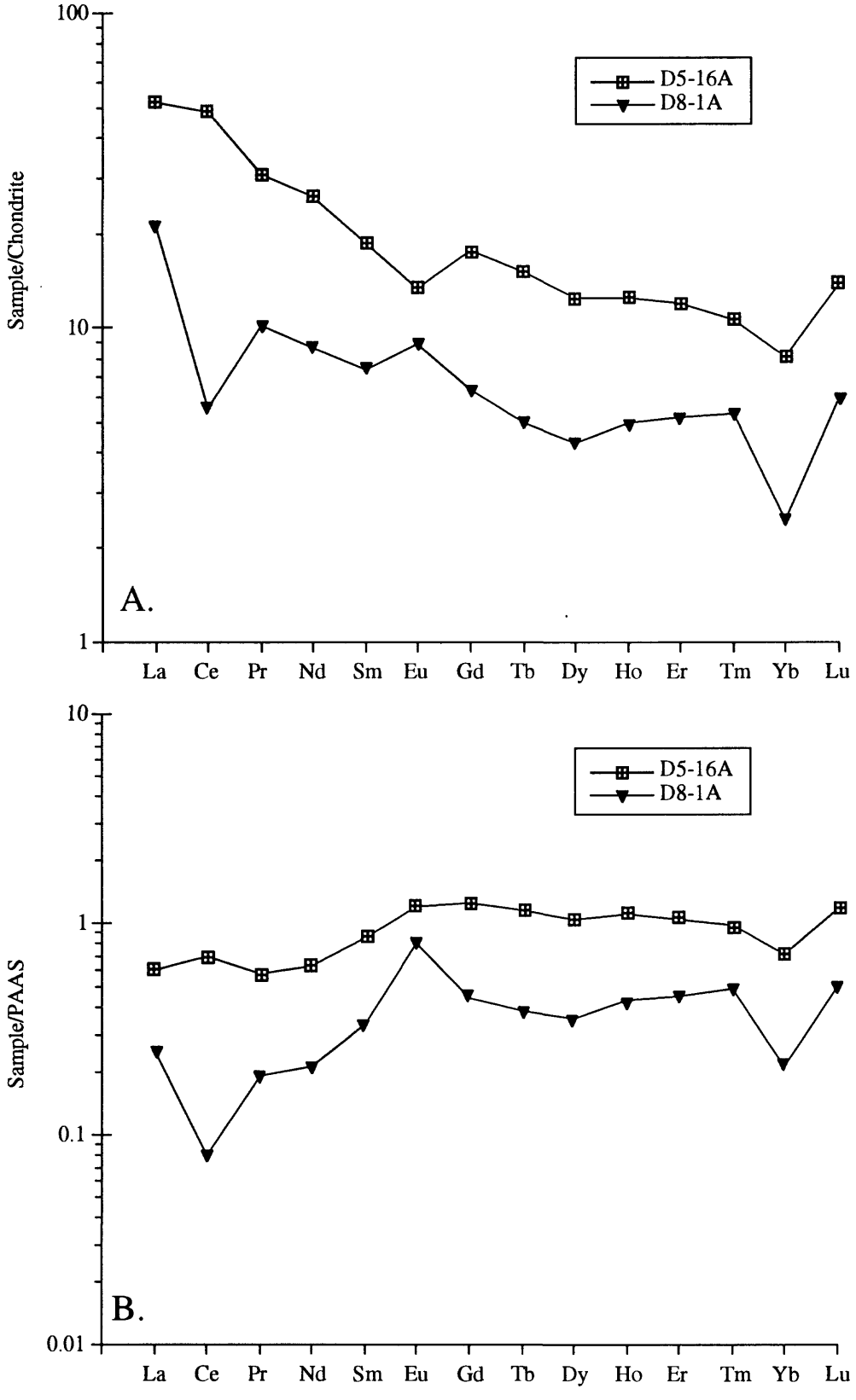

Figure 14. REE plots of hydrothermal Mn-cemented sandstone (D5) and stratabound Mn layer (D8) from Yap Arc: (A) Chondrite normalized, and (B) PAAS normalized